ACID DECOMPOSITION REACTIONS ON COMPOUNDS AND MINERALS IN THE Fe-Ni-SULPHIDE SYSTEM

by

KYOSUKE JIBIKI

B.A.Sc. Hokkaido Univ. Sapporo, 1966
M.A.Sc. U.B.C., 1971

A THESIS SUBMITTED IN PARTIAL FULFILMENT OF THE REQUIREMENTS FOR THE DEGREE OF DOCTOR OF PHILOSOPHY

in the Department

of

Metallurgy

We accept this thesis as conforming to the required standard

THE UNIVERSITY OF BRITISH COLUMBIA

May, 1974

In presenting this thesis in partial fulfilment of the requirements for an advanced degree at the University of British Columbia, I agree that the Library shall make it freely available for reference and study. I further agree that permission for extensive copying of this thesis for scholarly purposes may be granted by the Head of my Department or by his representatives. It is understood that copying or publication of this thesis for financial gain shall not be allowed without my written permission.

Department of Metallurgy

The University of British Columbia
Vancouver 8, Canada

Date June 18, 1974

ABSTRACT

A recent awareness of sulphur dioxide air pollution encourages the sulphide treating metallurgical plants to recover SO_2 from exhaust gases. Although manufacture of sulphuric acid is probably the most economical way of recovering SO_2, the limited market for acid and the difficulties involved in handling it could make elemental sulphur a more desirable end-product.

Hydrometallurgical oxidative treatment of sulphide ores has commonly been considered and practiced to be an option for the direct recovery of sulphur as elemental sulphur. Acid decomposition of sulphides has also been considered to be an alternative way to recover sulphur as elemental form via H_2S.

In this study, the acid decomposition of natural and synthesized pyrrhotites was investigated kinetically choosing temperature and the compositions of the various phases as independent parameters.

Comparison of the acid decomposition reaction rates was made for various compositions of synthesized sulphides in the Fe-Ni-S system. These results indicated that virtually quantitative separation of pentlandite from pyrrhotite can be achieved.

The results obtained in above studies were not directly applicable to nickel concentrates due to interference by the products of air oxidation of pyrrhotite during milling and flotation. Methods of overcoming the inhibiting effect of air oxidation in the dissolution of pyrrhotite

were separately studied.

Reduction of the nickel concentrate by hydrogen at 500~800°C prior to leaching was found to be a suitable way to activate the pyrrhotite in the nickel concentrate. It was found that by appropriate control of reduction and leaching conditions a satisfactory separation of pyrrhotite and pentlandite in the nickel concentrate was obtained and the acid decomposition of the pentlandite was also achieved.

A conceptual flowsheet is proposed for the treatment of pyrrhotite and nickel concentrates in a hydrometallurgical plant. Firstly, the pyrrhotite and secondly, the pentlandite are leached for iron rejection and nickel recovery, leaving a residue that constitutes a copper concentrate. Sulphur is recovered as elemental sulphur via H_2S.

TABLE OF CONTENTS

TABLE OF CONTENTS - Continued

TABLE OF CONTENTS - Continued

LIST OF TABLES

LIST OF FIGURES

LIST OF FIGURES - Continued

LIST OF FIGURES - Continued

LIST OF FIGURES - Continued

LIST OF FIGURES - Continued

LIST OF FIGURES - Continued

ACKNOWLEDGEMENTS

The author expresses his sincere thanks to Dr. E. Peters for his encouragement and advice throughout this study.

Many discussions with Dr. E. Devuyst (former graduate student) and Mr. D. Jones were helpful in the course of this study.

Numerous contributions from other members of faculty, staff, and fellow students are gratefully acknowledged.

Also, the author is grateful to his wife Mary for her patience and affection during this study.

Financial support from the National Research Council of Canada in the form of a Research Assistantship is appreciated.

CHAPTER I

INTRODUCTION

Pyrrhotite is one of the most common iron minerals occurring in sulphide ores, and with some exceptions is considered of little significance as an ore mineral. In the Sudbury district of Canada, pyrrhotite coexists with pentlandite, which is an important nickel mineral, and bears nickel in solid solution up to a maximum composition of about 0.5%. In spite of its low content, the nickel recovery from this pyrrhotite is an important part of the nickel industry because of its extensive occurrence.

1. Extractive Metallurgy of Pyrrhotite

1.1 Extractive metallurgy of nickeliferrous pyrrhotite ore

Most of the pyrrhotite in the Sudbury district bears nickel and cobalt; therefore, by leaving the pyrrhotite in the nickel extraction circuit, these metal values are recovered. Large amounts of pyrrhotite have thus been smelted with pentlandite, the contained iron being discarded as slag. However, about 15 years ago, a separate treatment for pyrrhotite was developed, which yields iron ore after extraction of the nickel, cobalt and copper. At present, this process is practiced by two companies: the International Nickel Company of Canada Ltd. and Falconbridge Nickel Mining Ltd. (1)

The pyrrhotite ore processed by INCO* at Sudbury, Ontario,

* The International Nickel Company of Canada Ltd.

analyses approximately 0.75% Ni,** 0.05% Cu, 58% Fe, 35% S and 2% SiO_2. This ore is first roasted in a fluid bed roaster at about 750°C to eliminate sulphur and oxidize sulphides to oxides. The calcine is then reduced in rotary kilns with natural gas at about 850°C to convert the nonferrous values to a leachable low iron alloy. The reduced calcine is leached at atmospheric pressure in aerated ammoniacal ammonium carbonate solution to extract nickel, cobalt and copper. The leach residue consists mainly of magnetite and silica which are separated from each other by a magnetic separator. The magnetite slurry is then dewatered, pelletized and fired to form solid pellets, which are marketed as a high grade iron ore. This iron ore analyses 68% Fe, 0.15% Ni, 0.01% Co, 0.01% Cu, 0.003% P, 1.5% SiO_2 and 0.005% S. Meanwhile, non-ferrous metals brought into solution are recovered, firstly by precipitation as sulphides of the copper and cobalt (together with some of the nickel), which are sent to a smelter. Then the bulk of the nickel remaining in solution is recovered by boiling as a basic carbonate which is calcined to oxide in an externally heated rotary kiln and marketed as oxide.

In the Falconbridge pyrrhotite plant, the mill concentrate analyzes approximately 1.1% Ni, 0.03% Cu, 0.1% Cu, 57% Fe, 36% S and 1.8% SiO_2. The first step consists of roasting the ore in a fluid bed roaster. During roasting, non-ferrous metal values are solubilized by a careful sulphate roasting operation at a temperature not greater than 680°C with excess oxygen in the gas phase. The calcine is leached with water to dissolve soluble sulphates. Ferric iron in the

** The nickel in excess of 0.5% is probably present as traces of pentlandite.

pregnant solution is reduced by ground pyrrhotite concentrate. Nickel, cobalt and copper in solution are cemented on iron turnings with addition of elemental sulphur. The final cake, which includes undissolved constituents of the pyrrhotite concentrate, analyses approximately 10.9% Ni, 0.3% Co, 1.6% Cu, 30% Fe, 26% S and 2.1% SiO_2 and is sent to a nickel smelter. The iron oxide in the leach residue is filtered, washed and dried in a long rotary kiln. During the drying process, balling is promoted, yielding a practically dust-free product analysing 66% Fe, 0.13% Ni, 0.003% Co, 0.01% Cu, 2.2% SiO_2 and 0.47% S.

1.2 Extractive metallurgy of pyrrhotite-bearing nickel ores

The pyrrhotite content of nickel concentrates was lowered as a result of the development of the above new processes for treating pyrrhotite ores separately for the recovery of nickel and cobalt. However, due to mineralogical and flotation difficulties in separating pentlandite from pyrrhotite, nickel sulphide concentrates still contain over 50% pyrrhotite compared to about 25% pentlandite. This means that a great quantity of pyrrhotite must still be processed for nickel extraction in the main nickel recovery circuit.

To process nickel concentrates both pyro- and hydro-metallurgical processes oxidize iron sulphide to oxide at high temperature and during subsequent smelting forms slag which is eliminated as waste. These steps are usually carried out in such unit operations as multiple

hearth roasters, fluid bed roasters, sintering roasters, rotary kilns, blast furnaces, reverberatory furnaces, flash smelting furnaces, electric furnaces and/or converters. Through this process the sulphur initially combined with iron is oxidized to sulphur dioxide, which in general is not recovered, although a modest fraction is converted to sulphuric acid, - liquid sulphur dioxide or sulphur.

The hydrometallurgical method, which was developed by Sherritt Gordon Mines Ltd., oxidizes iron sulphides to hydrated ferric oxide in ammonia solution under an air pressure of 100～150 psig at 70～90°C, while sulphur in the nickel concentrate is converted to sulphate and recovered as ammonium salts to be marketed for fertilizer.

In addition, Republic Steel Corporation recently proposed a new hydrometallurgical process for nickel concentrate. (2) In this process, the concentrate is oxidized in an acid medium at 250°C and 700 psi of oxygen pressure to oxidize both metal and sulphur and form metal sulphates. The pregnant solution is then neutralized with raw low grade nickel oxide ore of high magnesia content to precipitate iron as hydrous ferric oxide. Then nickel is recovered by cementation under hydrogen pressure using iron powder as a reducing agent. The resulting metallic phase of nickel and iron is magnetically separated from the solution and refined.

1.3 The oxidative leaching of pyrrhotite and nickel concentrate: Laboratory and academic studies

K. W. Downes et al. studied the pressure oxidation leaching

of pyrrhotite in an autoclave. (3) Natural and synthetic pyrrhotite, which was prepared by thermal decomposition of pyrite, were used in their work. Oxidation of pyrrhotite produced iron oxide, elemental sulphur and sulphate. The yield of elemental sulphur was found to be up to 80% under 150 psi air pressure at 110°C after 1.5 hrs. The rest of the sulphur in pyrrhotite was oxidized to sulphate. The ferric oxide residue from such a process is a potential iron ore depending on contaminating elements.

J. Gerlach et al. carried out a kinetic study of the pressure leaching of pyrrhotite in sulphuric acid solution under 1 to 50 atmospheres of oxygen at 30 to 80°C. (4) In order to account for the results obtained in their work, they proposed the following collection of leaching reaction steps:

$$FeS + 2H^{+} = Fe^{++} + H_2S \quad (1.1)$$

$$2H_2S + O_2 = 2S^{o} + 2H_2O \quad (1.2)$$

$$H_2S + 2O_2 = SO_4^{=} + 2H^{+} \quad (1.3)$$

$$H_2S + 2Fe^{+++} = S^{o} + 2Fe^{++} + 2H^{+} \quad (1.4)$$

$$H_2S + 8Fe^{+++} + 4H_2O = SO_4^{=} + 8Fe^{++} + 10H^{+} \quad (1.5)$$

$$S^{o} + \frac{3}{2} O_2 + H_2O = SO_4^{=} + 2H^{+} \quad (1.6)$$

In these reaction steps, (1.4) and (1.5) were considered to play a small role, because the oxidation of ferrous to ferric ion proceeds slowly in sulphuric acid media. On the average, 30% of sulphur was formed as sulphate and attributed to reactions (1.3) and (1.6).

W. Kunda et al. carried out leaching experiments on a pyrrhotite from thermally decomposed pyrite. They proposed a conceptual flow sheet to process pyrite and obtain elemental sulphur and iron metal. The process involves:

(1) Thermal decomposition of pyrite to artificial pyrrhotite by treatment at about 660°C for 15 ~ 30 minutes,

(2) Aqueous oxidation of pyrrhotite to hydrated iron oxide and elemental sulphur at 110°C, 150 psi O_2 for 90 minutes,

(3) Separation of elemental sulphur in the residue from the remaining solids,

(4) Dissolution of leach slurry with H_2SO_4 - SO_2 at 95°C for 60 minutes to obtain $FeSO_4$ solution,

(5) H_2S stripping of non-ferrous impurities in the leach solution,

(6) Oxidation and hydrolysis of the ferrous sulphate solution to produce basic sulphate precipitate at 205°C and 20 psi of oxygen for 60 minutes,

(7) Calcining of the iron oxide to iron metal by hydrogen at 900°C.

The iron produced here is very pure and suitable for direct moulding and powder metallurgy. The recoveries of each element are +98% for Fe, 90% for S^o, +95% for Cu, Zu, Ni and Co, 100% for Pb and precious metals.

The oxidative leaching of pyrrhotite was undertaken on a pilot plant scale by P.G. Thornhill. (6) In this study, a nickeliferrous

pyrrhotite from the Sudbury Basin was oxidized to Fe_2O_3 and elemental sulphur in an autoclave under 80 ~ 100 psi air at 110°C. The unreacted pyrrhotite in the leach liquor was magnetically separated from the non-magnetic solid, which consists mainly of Fe_2O_3 and sulphur, and recycled to the autoclave with fresh pyrrhotite feed. The non-magnetic solid was further treated by flotation to separate sulphur containing nickel from Fe_2O_3. Most of the nickel in the pyrrhotite was supposed to be recovered from the flotation concentrate, while 23% and 10% of the total nickel were lost into the discarded leach solution and the flotation tailing, respectively. The sulphur was obtained as a flotation concentrate at 60% recovery.

J.A. Vezina leached a pentlandite pyrrhotite-chalcopyrite concentrate in an autoclave under oxygen pressure at elevated temperature. (7) 98% extraction of nickel and cobalt and 90% of copper were achieved at 400 psig of oxygen and 110°C after 14 hrs of retention time with a 30% pulp density. Further grinding of the concentrate from 100% minus 325 mesh to minus 20 micron resulted in the same extraction at oxygen pressures as low as 80 psig under the same conditions.

Leaching of pyrrhotite ore in nitric acid was carried out by F. Habashi. (8) Maximum recoveries of Ni and Cu in the ore were attained using 45% HNO_3 at 100°C. The sulphur recovery was 65% using 30% HNO_3 in an open vessel.

In an autoclave under 100 psi oxygen pressure the same recoveries of Ni, Cu and S were achieved at half of the HNO_3 concentra-

tion used above because the NO reaction product was recycled after being oxidized by oxygen. In both operations, iron in the ore was oxidized to ferric oxide and precipitated.

It is evident that the treatment of pyrrhotite may be considered either for the purpose of recovering one of its primary components, iron or sulphur, or for the recovery of impurities such as copper, nickel and cobalt. Alternatively, a combination of both may be required to make a process viable.

The nickel industries, INCO, Falconbridge and Sherritt Gordon historically have been concerned mainly with nickel and copper recovery, restricting their scope of studies relating to iron and sulphur recoveries until recent times.

2. Acid Decomposition Reactions

An objective of oxidative decomposition of sulphide minerals is to yield sulphur from the minerals as elemental sulphur, which is a more acceptable form of sulphur than sulphur dioxide from the pyrometallurgical processes. Sulphur recovery from sulphides via the intermediate step of generating hydrogen sulphide is also being considered, because hydrogen sulphide is readily oxidized with a stoichiometric amount of oxygen according to the Claus reaction;

$$2H_2S + O_2 = 2H_2O + 2S \qquad (1.7)$$

Furthermore, hydrogen sulphide may be used to reduce SO_2

gas, which is abundant in pyrometallurgical plants for sulphide ores, to elemental sulphur by the following stoichiometry;

$$2H_2S + SO_2 = 2H_2O + 3S \qquad (1.8)$$

The technology for these reactions is well known and established. (9)

2.1 Acid decomposition of sulphides

When sulphides contact acid without oxidant, they may be attacked producing hydrogen sulphide and metal salts according to the reaction;

$$MS\frac{n}{2} + nHX = \frac{n}{2}H_2S(aq) + MXn \qquad (1.9)$$

In the case of soluble ionized salts, the equilibrium constant for this reaction is defined as;

$$K = \frac{a_{H_2S\,(aq)}^{n/2} \cdot a_{M^{n+}}}{a_{H+}^{n}} \qquad (1.10)$$

where a_Y refers to the activity of component Y, and the activity of the sulphide is considered unity. The values of K in equation (1.10) for each sulphide can be calculated from thermodynamic data. In Table 1-1, the room temperature K values for common sulphides are summarized as calculated from the Latimer's thermodynamic data. (10)

TABLE 1-I

CALCULATED K(1.10) VALUE FOR COMMON SULPHIDES AT 25°C

Sulphide	K	Sulphide	K
MnS	9.95×10^{7}	PbS	7.95×10^{-8}
FeS	3.91×10^{2}	CuS	1×10^{-15}
CoS	2.30	Cu_2S	3.16×10^{-28}
NiS(α)	1.75		
(γ)	1.12×10^{-7}	Ag_2S	1.26×10^{-29}
ZnS (wur)	1.55×10^{-2}		
(spal)	7.4×10^{-5}	HgS	6.3×10^{-33}
CdS	7.08×10^{-7}		

The K values vary through a wide range from one sulphide to another. Large values of K suggest that the sulphide is dissolved into acid with a decrease in standard Gibbs free energy. For example, the value for iron sulphide, FeS, is large and the reaction of iron sulphide to produce hydrogen sulphide for analytical chemical laboratories is well known. On the other hand, small values of K mean that such sulphides do not readily dissolve in acid. The extremely small value for copper sulphide, CuS, and silver sulphide, Ag_2S, are widely applied in analytical chemistry and industry in the precipitation of copper and silver from acid solution by hydrogen sulphide. In addition, the relatively small value of K (1-10) for NiS can be utilized in weak acid (pH = 2.4) to precipitate nickel from the leach liquor, as in the "Moa Bay" process. (11) An extensive literature survey on the acid decomposition of sulphides was made by T.R. Ingraham, et al. (12)

In the Falconbridge matte leach plant, Kristiansand, Norway, a copper-nickel converter matte containing about 48% Ni, 28% Cu and 21% S is leached in strong hydrochloric acid (280 grms $HC\ell/\ell$) at 70°C. (13). After 12 hrs of leaching, 98% of the nickel, but only 2% of the copper are dissolved. After filtering the leach solution containing Ni^{++}, Fe^{++}, Co^{++} and Cu^{++} is sent to a solvent extraction plant to remove Fe^{++}, Co^{++} and Cu^{++}. Nickel in the final solution is crystallized as $NiC\ell_2 \cdot 4H_2O$ utilizing the salting out properties of stronger $HC\ell$ solutions, and separated. The nickel chloride crystals are then dried and calcined to nickel oxide, the reaction being;

$$NiCl_2 + H_2O \rightarrow NiO + 2HCl \qquad (1.11)$$

The HCl gas from the drier-calciner is recycled to the crystallization plant and the nickel oxide is reduced to metal by hydrogen.

K.N. Subramanian, et al. studied hydrometallurgical processes to yield sulphur from pyrrhotite which was produced by the thermal decomposition of pyrite concentrate. They carried out leaching experiments in ferric sulphate, ferric chloride, hydrochloric acid, sulphuric acid and oxygen pressurized weak sulphuric acid. As a result, only sulphuric acid leaching of hydrogen activated pyrrhotite and oxygen pressure leaching were found feasible. Hydrogen activation of pyrrhotite for sulphuric acid leaching was essential to lower the sulphur to iron ratio of pyrrhotite from 1.18, which was the lowest ratio attainable by thermal decomposition, to 1.06, as also suggested by McGauley. (73) After leaching for 20 minutes at 60°C, it was possible to extract about 90% of the iron, not more than 0.4% of the copper, and about 2% of the zinc, using the stoichiometric amount of acid. Oxygen pressure leaching conditions were similar to those recommended by Sherritt Gordon Mines Ltd. (14)

Recently, nickeliferrous pyrrhotite from the Falconbridge Mines was tested for leachability in strong hydrochloric acid. (15) At 70°C after 3 hrs of leaching in 8N hydrochloric acid with 10 ~ 50% of excess acid, 97% of the iron, 10% of the copper and about 65% of the nickel in pyrrhotite dissolved. With constant acid addition rates at 60°C,

an incubation period was observed in the initial stages of leaching. After the incubation period, the leaching rate was proportional to the acid addition rate. An increase in the excess amount of HCl added resulted in an increase in the iron extraction. Furthermore, an increase in the rate of acid addition yielded more complete dissolution of both iron and nickel. An increase in leaching temperature from 60°C to 90°C lowered the iron dissolution from 96% to 87% under the same conditions, the unleached iron being found in the form of marcasite at higher temperature.

2.2 Thermodynamics of acid decomposition of sulphides

The thermodynamic driving force for acid decomposition reaction is simply referred to the K value in equation (1.10) or the standard Gibbs free energy change for the reaction, which is related to the K value in the following equation;

$$\Delta F = - RT \ln K \qquad (1.12)$$

In reality, data for the thermodynamic properties for the applicable aqueous species under applicable conditions are rarely available. From a hydrometallurgical point of view, data for the thermodynamic properties are needed at elevated temperatures ($\leq$ 200°C) and in strong solutions and solutions containing complexing agents. In recent years, several attempts were made to estimate the heat capacity of aqueous ionic species at elevated temperature. (16), (17), (18) Based on these methods,

several workers have tried to summarize the thermodynamic data in the form of pH-potential diagrams for the metal-water and the metal-water-sulphur systems. These diagrams call for many tedious calculations, and to expedite these as well as the subsequent drafting, a computer method is being tried by P. Duby. (19)

The equilibrium constants of the acid decomposition reaction, K in equation (1.10), for CuS, NiS and FeS at elevated temperature were calculated using the Criss and Cobble method and are shown in Figure 1-1. These data indicate that as the temperature increases, FeS and NiS become more insoluble, while CuS becomes more soluble in acid solution.

In concentrated solutions at elevated temperature, there are no theoretical data available for the temperature dependence of the thermodynamic functions. However, a leading work by H. C. Helgeson presents methods of estimating the high temperature properties of ions in concentrated media empirically. (20) Nevertheless, thermodynamic properties of concentrated solutions at elevated temperature are not generally available and await further work.

2.3 Kinetics of acid decomposition of sulphides

T.R. Ingraham, et al. surveyed the literature concerning the acid decomposition reactions of sulphides and proposed a reaction model as follows (12);

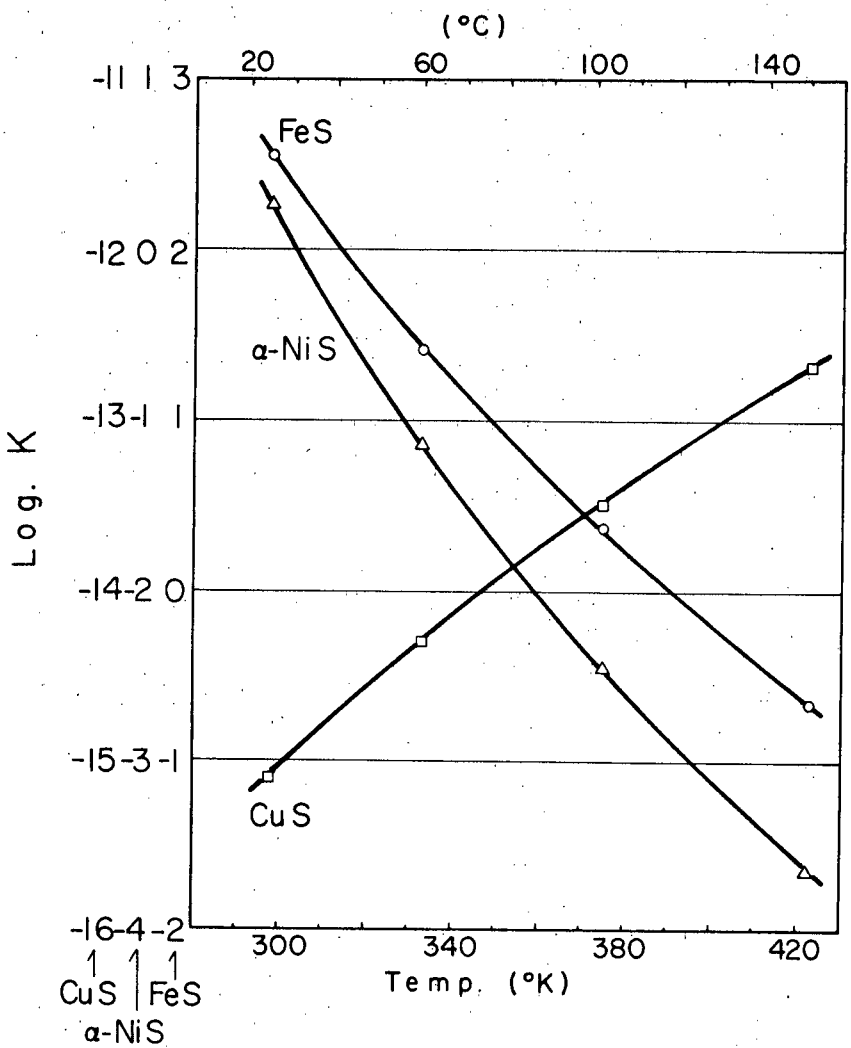

Figure 1-1. Calculated K(1-10) values for CuS, α -NiS and FeS at elevated temperatures.

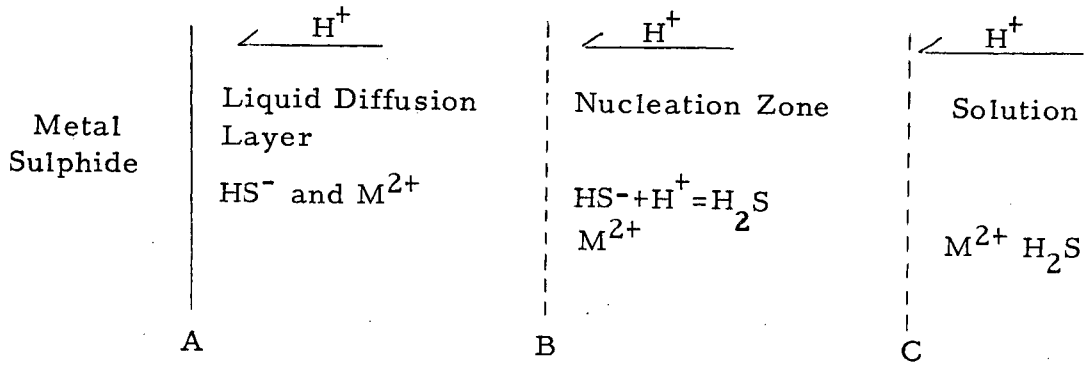

This model accounts for the fact that the rate of leaching of very finely divided FeS, CdS and ZnS is directly proportional to the concentration of the hydrogen ion, therefore the possible reaction at the sulphide surface would be;

$$MS + H^+ \longrightarrow M^{2+} + HS^- \qquad (1.13)$$

HS^- would be stable in the vicinity of the surface where H^+ is consumed by the above reaction and as a result the pH value is higher than in the bulk of the solution. Moreover, additional experimental data showed that the dissolution is controlled by a diffusion process. In this model, they claimed that the chemical reaction at interface A is normally fast, but rate-controlling only when the interfacial area is very large and the diffusion layer is thin. In general, the diffusion of H^+, M^{2+} and HS^- in the layer A-B will be rate-controlling. In the nucleation zone B-C, excess hydrogen ions react with migrating HS^- ions to produce dissolved H_2S, which above the solubility limit is expelled from the solution. There is no strong evidence to suggest that the nucleation or evolution of H_2S is

rate-controlling.

Meanwhile, L.D. Locker, et al. studied the dissolution of ZnS, CdS, ZnSe and Zn 0.85 Cd 0.15 S. (21) According to their leaching models, when the diffusion process is a rate-controlling step, the dissolution rate must be of an order of 10^{-5} moles/sec.cm^2. However, most of the rates were experimentally found to be smaller than 10^{-9} moles/sec. cm^2. In addition, the surface reaction is much slower for dissolution of ZnS in aqueous H_2SO_4 than in aqueous HCl or alcoholic H_2SO_4. These facts were used as evidence that a slow adsorption step of H^+ ion on the surface is a plausible mechanism for the dissolution of the compounds, which were investigated, in acid solution. If the rate of the dissolution reaction is controlled by the adsorption of hydrogen ions or the protonated solvent onto the surface, then the rate is expressed by the following equation;

$$R_o = k_t \quad A_o \left[H^+\right]_o \exp \left\{ - \frac{E_A}{RT} \right\} \qquad (1.14)$$

where k_t is the rate constant for dissolution

A_o is the surface area

$\left[H^+\right]_o$ is the hydrogen ion concentration in the bulk of solution

and E_A is the activation energy for adsorption

The activation energy E_A is made up of a chemical and an electrochemical contribution, i.e.,

$$E_A = F(\bar{\Phi} + \psi_o) \qquad (1.15)$$

where F is the Faraday constant, $\bar{\Phi}$ is the change in chemical potential during proton adsorption, and ψ_o is the electrostatic potential of the proton on the solid surface relative to that in the solution. The first term can be related to the bonding surface energy, and other solid properties that may effect $\bar{\Phi}$. The second term depends on the interaction between the charged solid surface and the ions in solution.

Although the experimental data for the kinetics of the reaction are limited, the available data are summarized in Table 1-II, with regard to the acid concentration dependence and the activation energy. According to this table, most of the rates of acid decomposition are first order with respect to hydrogen ion concentration. This means that the reaction, $H^+ + S^= = HS^-$, is involved in the dissolution process, as previously stated. The activation energies are generally small.

According to Locker, et al. the small difference of the activation energy between β-ZnS and ZnS (0.1% Fe) is due to the small change in $\bar{\Phi}$ due to compositional or structural change of the solid. On the other hand, the maximum different of about 5 K cal/mole in the activation energy for the dissolution of ZnS and CdS is due primarily to the electrostatic interaction at the solid-liquid interface, which is expressed by ψ_o in equation (1.15). This most probably accounts for the changes in the activation energy when the same solid ZnS was dissolved in different solutions. In hydrochloric acid, specific interactions

TABLE 1-II

KINETIC DATA FOR ACID DECOMPOSITION OF SULPHIDES

Sulphide	Sample Preparation	Acid Type	Acid Effect	Temperature	Activation Energy	Reference
CdS	precipitate	HCℓ (0.1～5M)	$[HCℓ]^1$	25°C	- (Kcal/mole)	(22)
	annealed precipitate	H_2SO_4 (0.5～5M)	$[H^+]^1$	0～50°C	14.2	(21)
ZnS	precipitate	HCℓ (0.015～1M)	$[HCℓ]^1$	25°C	-	(22)
	coarsened precipitate	H_2SO_4 (0.65～12.5M)	$[H^+]^1$	0.6～65°C	11.11	(23)
	annealed precipitate	HCℓ (0.5～5M)	$[H^+]^1$	0～50°C	9.5	(21)
	"	H_2SO_4 (0.5～5M)	$[H^+]^1$	0～50°C	9.9	(21)
	" (+ 0.1% Fe)	HCℓ (0.5～5M)	$[H^+]^1$	0～50°C	4.5	(21)
	precipitate	HCℓ (pH1～3)	$[H^+]^{0.6\sim1.0}$	25～60°C	5.6	(24)
(ZnCd)S	annealed precipitate	H_2SO_4 (0.5～5M)	$[H^+]^1$	0～50°C	5.7	(21)

TABLE 1-II - Continued

KINETIC DATA FOR ACID DECOMPOSITION OF SULPHIDES

Sulphide	Sample Preparation	Acid Type	Acid Effect	Temperature	Activation Energy (Kcal/mole)	Reference
FeS	precipitate	HCl (0.003~0.1M)	$[HCl]^{1}$	25°C	-	(22)
	natural	HCl (0.05~2M)	$[HCl]^{0.9}$	30~80°C	7.0	(25)
	natural	H_2SO_4 (0.25~1M)	$[H_2SO_4]^{1.3}$	30~80°C	13.2	(26)

of chloride ions may occur on the surface and alter both the surface charge and the distribution of active sites.

On the other hand, according to T.R. Ingraham, et al. the dissolution of pyrrhotite in relatively strong HCl solution may be controlled by a diffusion process, thus accounting for the small activation energy (7 Kcal/mole) and the fact that the leaching rate depends on the square root of the stirring rate in the range of 150 ~ 900 rpm. (25) In addition, in their experiment a change in the interfacial area of the mineral did not affect the dissolution rate.

A. Yazawa, et al. suggested that the formation of a $[FeS - 2H^+]$ activated complex is a rate-determining step for the decomposition of pyrrhotite in sulphuric acid. (26) With this mechanism, they accounted for the facts:

(a) that the activation energy is 12.3 Kcal/mole, which is larger than that for the diffusion controlled reaction,

(b) the dissolution rate is approximately proportional to the surface area of mineral and the molarity of sulphuric acid, and

(c) the dissolution rate does not increase by faster stirring of the solution.

2.4 Induction period in the decomposition of pyrrhotite

The induction period, which is characterized as an initial period of reaction in which the reaction rate is insignificantly small, has been observed in numerous studies of heterogeneous reactions, and many

theories have been proposed to account for it.

In acid decomposition of pyrrhotite, this induction period was regularly observed by several workers. (15), (25), (26) As a general tendency, the induction period is shorter when the temperature and acid concentration of the leaching solution increase. In very strong $HC\ell$ solutions, the induction period seems to disappear. In addition, it was observed that the potential of the leaching solution sharply decreases when the induction period ends.

A. Yazawa, et al. suggested that the induction period is caused by the oxidation of the mineral surface which forms a relatively insoluble oxide film. (26) They found the correlation between the length of the induction period and the amount of oxygen consumed on the pyrrhotite surface during oxidation, this being carefully measured by weighing the amount of H_2O formed during hydrogen reduction of the partially oxidized pyrrhotite.

On the other hand, G. Van Weert, et al. proposed that the preferential dissolution of magnetite, which commonly exists with pyrrhotite, causes the induction period. (15) The magnetite dissolves in hydrochloric acid according to the following reaction;

$$Fe_3O_4 + 8HC\ell \longrightarrow FeC\ell_2 + 2\,FeC\ell_3 + 4H_2O \qquad (1.16)$$

The presence of ferric ion in solution might be correlated with a sudden increase in potential after acid was added into the pyrrhotite slurry. The ferric ion from magnetite would be reduced at the pyrrhotite surface, i.e.,

$$Fe_7S_8 + 14\,FeCl_3 \longrightarrow 21\,FeCl_2 + 8S^o \qquad (1.17)$$

where pyrrhotite is represented by Fe_7S_8 as in the quoted paper (15). This elemental sulphur formed on the pyrrhotite surface would inhibit the attack of acid for a time, the length of which depends on the acid concentration and temperature.

3. Phase Relations of the Fe-Ni-S System

3.1 Fe-S system

The Fe-S phase diagram has been investigated extensively during the last fifteen years, however the details of the diagram below 300°C remain controversial among investigators. This controversy might be accounted for by the sluggish nature of the reactions and some rather complicated phase relations at lower temperature. Nevertheless, a tentative phase diagram for the Fe-S system at low temperature is reproduced in Figure 1-2, as represented by G. Kullerud. (27)

(a) Troilite-hexagonal pyrrhotite region

The troilite-hexagonal pyrrhotite boundary according to Fig. 1-2 shows an approximate agreement with R.A. Yund and H.T. Hall (28) and with R.G. Arnold. (29) At room temperature, the hexagonal pyrrhotite equilibrated with troilite contains about 48 at % Fe. These synthetic studies were supported by studies of natural two-phase mixtures, which showed that the iron-rich troilite is essentially stoichiometric FeS and the co-existing hexagonal pyrrhotite contains 47.9 ±

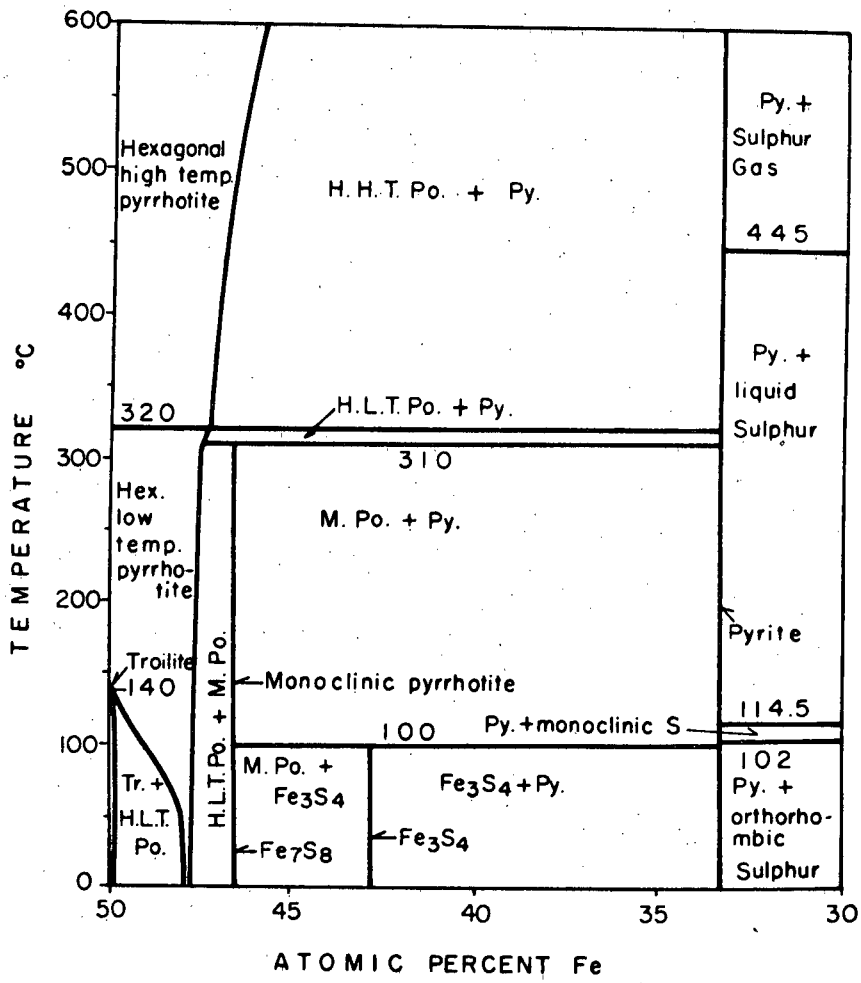

Figure 1-2. Tentative condensed phase diagram of the Fe-S system in the region from 30 to 50 at % Fe. (27)

0.2 at % Fe. (30)

(b) Hexagonal pyrrhotite

After solidification pyrrhotite occupies a large area of solid solution having a hexagonal NiAs structure, with a minimum iron content of about 45 at % at 740°C, correlating to vacancies in the metal sites of the structure. (31) The formula for pyrrhotite might therefore be written Fe1-xS, where x represents the fraction of vacant cation sites in the structure. Above 740°C, this pyrrhotite co-exists with liquid sulphur of above 1 atmospheric pressure and with increasing minimum iron content corresponding to increasing temperature. Below 740°C, hexagonal pyrrhotite exists with increasing minimum iron content as the temperature decreases. The co-existing phase is pyrite, FeS_2.

At 320 ± 5°C, this high temperature hexagonal pyrrhotite goes through an inversion to a low temperature form. This inversion temperature does not seem to be influenced by the composition of the pyrrhotite. Since this inversion was first found by H.Haraldsen, (32), it has been conformed by many workers. The low temperature hexagonal pyrrhotite with a composition close to FeS passes through another inversion on cooling further, and a co-existing troilite phase separates. This inversion is influenced by the composition of pyrrhotite and for FeS it is 140 ± 5°C. (33)

(c) Low temperature hexagonal pyrrhotite-monoclinic pyrrhotite

According to Arnold's work (30), 73% of 82 natural terres-

trial pyrrhotites consist of two-phase mixtures of hexagonal and monoclinic pyrrhotites. Synthetic studies for this two-phase region had been carried out by several workers, as summarized in Table 1-III. The compositions for low temperature hexagonal and monoclinic pyrrhotite and the upper limiting temperature for the two phase region are summarized according to Arnold's work. (29)

As shown in this table, the compositions of hexagonal and monoclinic pyrrhotite, which are equilibrated with each other, are not influenced by temperature significantly. The uncertainty for the upper temperature of monoclinic pyrrhotite seems to be due to the irreversibility of the phase transformation process. The reaction from monoclinic pyrrhotite to hexagonal pyrrhotite + pyrite occurs reversibly as commonly observed. However, the same reaction in the reverse direction has not been observed until R.A. Yund, et al. succeeded in obtaining it after several regrindings of mixtures of hexagonal pyrrhotite and pyrite after 577 days at 150°C. (38) L.A. Taylor succeeded in obtaining this conversion after 86 days at 280°C. (33)

(d) Monoclinic pyrrhotite

A.H. Clark studied the composition limit of monoclinic pyrrhotite using a synthetic technique. (35) He found that monoclinic pyrrhotite tolerates variations in iron deficiency from 46.4 to 46.8 at % Fe, compared with the stoichiometric composition of 46.67 at % Fe for the generally applied formula Fe_7S_8.

TABLE 1-III

SUMMARY OF DATA FOR PHASE COMPOSITIONS AND TRANSFORMATION TEMPERATURES FOR HEXAGONAL AND MONOCLINIC PYRRHOTITE. (29) (Hpo; hexagonal pyrrhotite (Mpo; monoclinic pyrrhotite

Composition of phase (at % Fe)			Maximum Temperature of Formation of Mpo (^{o} C)	Reference
Hpo	Mpo	Temp. (^{o} C)		
47.20 $\pm$ 0.10	46.75 $\pm$ 0.05	$\leq$304 $\pm$ 6	304 $\pm$ 6	(29)
47.2	46.8	290	$\approx$300	(34)
	46.35	70		
	$\approx$46.8	308		
	46.80~46.45	200	308 $\pm$ 5	(35)
	46.75~46.40	75		
47.40	46.75	290	290~325	(36)
	46.73	190		
	46.67	300	$\approx$ 300	(37)

Furthermore, R.G. Arnold states that the compositions of monoclinic pyrrhotite studied by many workers range between 46.7 and 46.5 at % Fe, and the compositions richer in metal than 46.7 at % Fe were probably due to faulty analyses or chemical analyses of impure materials. (30) In a further study, Arnold concluded that this phase may have essentially a fixed composition. (29)

In the works by Arnold (29) and Yund and Hall (38), the stability of monoclinic pyrrhotite was questioned. Yund and Hall observed that a natural monoclinic pyrrhotite was found to be converted to the hexagonal form after one year at 260°C in the work by Kullerud, et al. (39) The slow rate of its breakdown may explain the reported differences in Fe to S ratio of the monoclinic phase. Arnold's reasons are that the assemblage of hexagonal pyrrhotite, + monoclinic pyrrhotite, pyrite, and vapour developed in charges of 45.5 to 47.2 at % Fe (bulk composition) at temperatures of 297 $\sim$ 116°C is not in equilibrium. Furthermore, the sharp and anomalous decrease in the concentration of monoclinic pyrrhotite with the first appearance of pyrite in the charges suggests that monoclinic pyrrhotite is meta-stable.

(e) Smythite, greigite; Fe_3S_4

Smythite, one form of Fe_3S_4, was first reported by Erd, et al. being found in the form of very thin flakes in cavities in a limestone formation. (40) The synthetic smythite was formed by the reaction of ferrous carbonate crystals with sodium sulphide solution. (41)

Skinner, et al. reported another form of Fe_3S_4, greigite, which has the spinel structure as distinct from the rhombohedral structure for smythite. (42) Greigite has been synthesized by the reaction of hydrogen sulphide in ferrous sulphate solutions in the presence of air or by autoclaving fresh ferrous sulphide precipitate at 190°C in an evacuated tube with water. Though it is generally understood that smythite is the high temperature form of Fe_3S_4, while greigite is the low temperature form, the thermal stability region for the phases is not fully known. Therefore, in the diagram (Fig. 1-2) a breakdown of the Fe_3S_4 compound is approximated at 100°C, on the assumption that the phase is barely stable at low temperatures.

(f) Pyrite; FeS_2

Both pyrite and marcasite are commonly found as natural iron disulphide phases. Synthetic experiments indicate that the stability of marcasite is unfavourable without the presence of hydrogen in the system. Therefore, marcasite was excluded as a phase in the pure Fe-S system.

3.2 Fe-Ni-S system

Extensive studies of this system have been made in the last ten years and the phase relationships above 300°C are fairly well understood, though there are discrepancies in the compositions of the phases reported by different authors.

In Figure 1-3, the phase diagram at 650°C is shown accord-

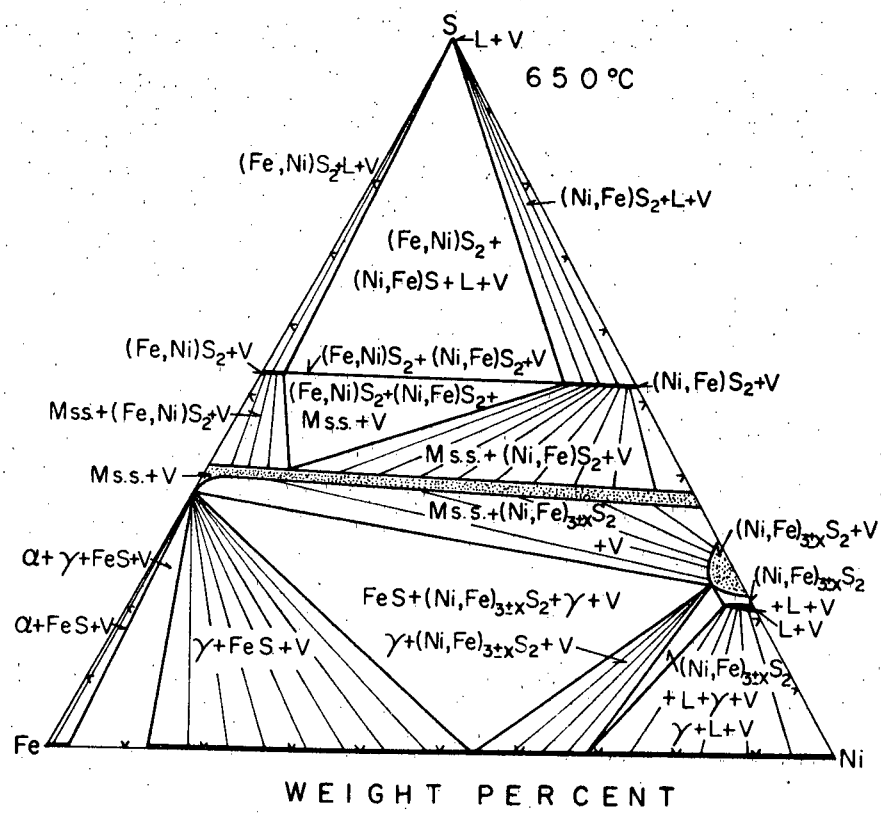

Figure 1-3. Phase relations in the Fe-Ni-S system at 650°C. (27)

ing to G. Kullerud. (27) The extensive hexagonal monosulphide solid solution (M.s.s.), $(FeNi)_{1-x}S$, appears between $Fe_{1-x}S$ and $Ni_{1-x}S$. A wide divariant field extends between the M.s.s. and high temperature heazlewoodite, $Ni_{3\pm x}S_2$, with several percent of iron. The liquid phase, which dominates the central region at higher temperatures, retreats into the corner of the nickel-rich region at 650°C. Pentlandite, $(FeNi)_{9\pm x}S_8$, which is an important mineral in nickel sulphide ore, does not form directly from a liquid in the system nor appears at this temperature. However, at 610°C the M.s.s. and high temperature heazlewoodite react rapidly to form pentlandite.

When the system cools to 300°C, its phase relations are presented in Figure 1-4, which is taken from the work by A. J. Naldrett, et al. (43) The M.s.s. phase is still present between $Fe_{1-x}S$ and $Ni_{1-x}S$ in a narrower band than that at 650°C. Further cooling finally breaks down the continuous band between $Fe_{1-x}S$ and $Ni_{1-x}S$. The temperature of this breakdown was reported as 400~300°C by K.C. Misra, et al. (44); 275 ± 10°C by R.W. Shewman, et al. (45) and 275 ± 5°C by G. Kullerud, et al. (46)

The solubility of iron in the NiS_2 phase at 300°C decreases from that at 650°C. It is noted that on the Ni-S line several new phases appear. They are polydymite, Ni_3S_4 and godlevskite, β-Ni_7S_6. The variation in iron and excess sulphur in Ni_3S_2 decreases to a negligible value at the temperature of the inversion from the high temperature form to the low temperature form (550°C); this is evident in Fig. 1-4 as com-

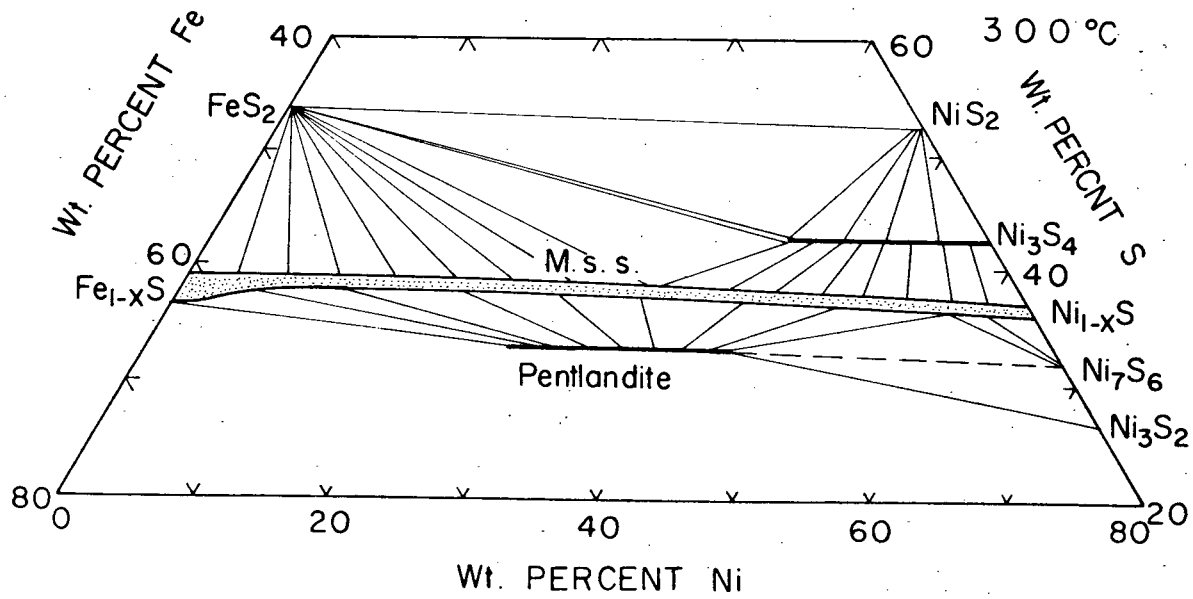

Figure 1-4. Phase relations in the condensed Fe-Ni-S system at 300°C. (43)

pared with Fig. 1-3.

Pentlandite at this temperature co-exists with hexagonal pyrrhotite, the M.s.s. and low temperature heazlewoodite. The tie line between pentlandite and Ni_7S_6 was made with uncertainty because the authors did not find co-existence in their samples, contrary to the results of other workers. Also, the tie line between pentlandite and the (Fe + Ni) alloy phase is not drawn by the authors because of its negligible significance. It is also noted that the Fe to Ni ratio in pentlandite may vary over a wide range. The composition limits of pentlandite have been studied between 600~200°C by several workers. In Table 1-IV, the data for the solubility limits of pentlandite are reproduced from the works by Shewman, et al. and Misra, et al.

According to this table, the agreement in the composition limit is unsatisfactory. This may be due to the difficulty in analysis of the composition of the pentlandite phase. Nevertheless, it can be concluded that the pentlandite phase tolerates a wide compositional change with respect to the Fe to Ni ratio. In contrast, the sulphur solubility does not vary much from the stoichiometric composition of 47.06 at % S for $(Fe4.5Ni4.5)S_8$, especially at lower temperatures.

To obtain an understanding of the phase relations of the Fe-Ni-S system below 200°C, where slow equilibration rates between minerals make experimental work tedious and uncertain, it is helpful to study the phase relations in an ore body. In fact, several attempts have been made to utilize natural sulphide assemblages to study the phase

TABLE 1-IV

COMPOSITION DATA FOR THE PENTLANDITE PHASE
(44) (45)

Temp.(°C)	Fe limit (at % Fe)	Ni limit (at % Ni)	S limit at Fe/Ni=1/1 (at % S)	Reference
600	33.3 29.8~21.1	41.3 24.4~31.9 (at 46.9 at % S)	46.4 46.3~48.0	(44) (45)
500	35.5 34.0~14.7	38.0 19.4~38.0 (at 46.7~47.4 at % S)	46.2~47.3 46.8~47.9	(44) (45)
400	36.8 35.4~20.9	39.3 17.9~32.1 (at 46.6~47.0 at % S)	46.0~46.9 46.8~47.4	(44) (45)
300	39.8	33.8	46.2~46.6	(44)
230	38.8	34.0	45.2~46.9	(44)

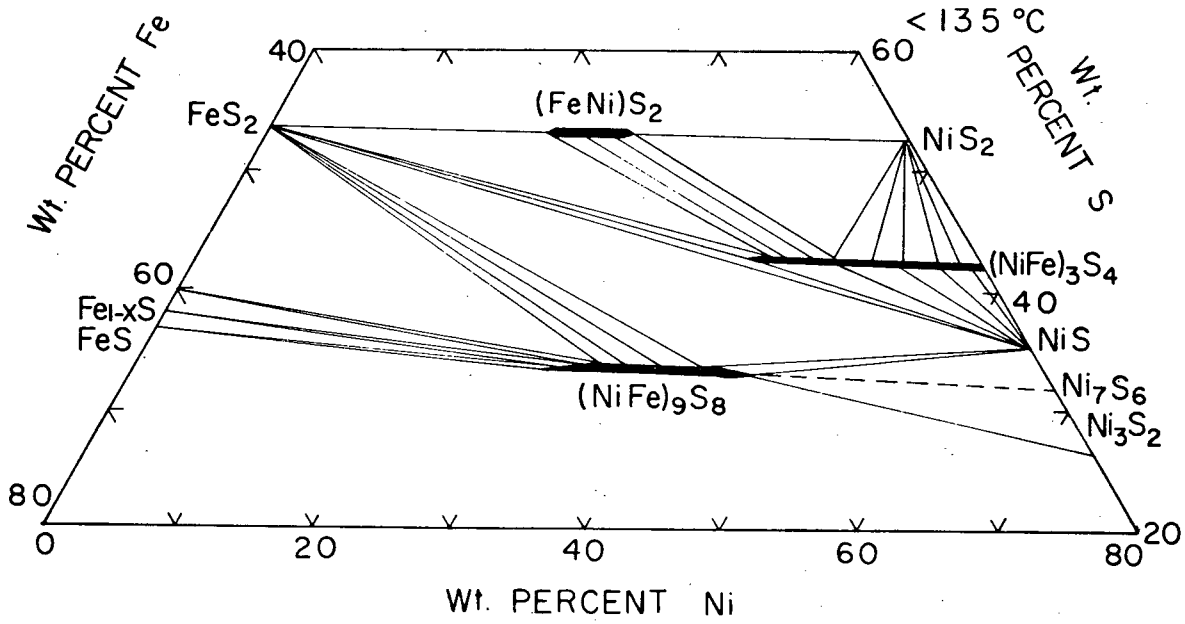

Figure 1-5. Tentative phase diagram in the Fe-Ni-S system at low temperature. (43)

relations at ambient temperatures. For the purpose of these studies a great number of natural minerals were collected from different ore bodies and countries to cover a wide region of the system. In Figure 1-5, a tentative phase diagram below 135°C is shown, as interpreted by Naldret, et al. (43) It is noted that the M. s. s., which was a dominant phase in the central portion of the diagram above 300°C, disappears at this temperature, and as a result, pyrite co-exists with pentlandite. The authors did not observe the pentlandite - Ni_7S_6 relation in the natural assemblages, therefore, the tie line was drawn with uncertainty. Misra, et al. (44), suggested that Ni_7S_6 is an unstable phase at low temperatures and thus excluded from their diagram.

In general, most of the phases in the Fe-Ni-S system tolerate Fe or Ni in their solid solutions because of the similar nature of Fe and Ni atoms. According to Misra, et al. natural pentlandites vary in nickel content from about 18 at % Ni to 34 at % Ni. As envisaged from Fig. 1-5, the pentlandite co-existing with troilite contains the least nickel (18.2 ~ 22.5 at % Ni), on the other hand, the pentlandite co-existing with millerite (NiS) and heazlewoodite (Ni_3S_2) holds the most nickel (32 ~ 34.2 at % Ni). The pentlandite co-existing with hexagonal pyrrhotite and/or monoclinic pyrrhotite, which is the most common pentlandite in the ore bodies of the Sudbury district, contains 24 ~ 29 at % Ni.

The nickel contents in the natural pyrrhotite phases co-existing with pentlandite were examined by Misra, et al. (44), using electron probe analyses. According to their results, the nickel content

of the hexagonal pyrrhotite was 0.14 ~ 0.21 at % Ni, similar to that for the co-existing troilite (0.10 ~ 0.12 at % Ni). Furthermore, those of the co-existing hexagonal pyrrhotite (0.21 ~ 0.72 at % Ni) and monoclinic pyrrhotite (0.19 ~ 0.72 at % Ni) are also very similar, but significantly higher than the data for the troilite-hexagonal pyrrhotite pairs.

4. Scope of the Present Work

In spite of the interest in the acid decomposition reaction of sulphides, few kinetic studies on this reaction are available. As a result, the general mechanisms for the reaction are very uncertain at the present stage.

A kinetic study on the dissolution of pyrrhotite is necessary to clarify the characteristics of the reaction. The following variables are considered in the study:

(1) Acid type,

(2) Acid concentration,

(3) Sulphur activity in sulphide phase,

(4) Cations and anions in solution,

(5) Partial pressure of hydrogen sulphide,

(6) Oxidizing potential of solution,

(7) Temperature.

When the acid decomposition reaction is applied on a pyrrhotite ore, it is necessary to understand the behaviour of other co-existing sulphides with the pyrrhotite in the Fe-Ni-S system in acid solution. On

this basis, the syntheses of the sulphides of the Fe-S, Ni-S and Fe-Ni-S systems were carried out under a stream of H_2S and H_2 mixed gas to control the sulphur activity in the sulphide phase. These synthesized sulphides were used as samples for the acid decomposition reaction. The reaction rates for sulphides were compared to ascertain the selectivity of the acid decomposition reaction on sulphides in the Fe-Ni-S system.

Finally, a nickel sulphide concentrate of natural origin was examined to correlate the fundamental studies of these reactions to applications of potential industrial interest.

Furthermore, a method of integrating such an application into the general scheme of nickel metallurgy is discussed.

CHAPTER II

ACID DISSOLUTION OF PYRRHOTITE

1. Experimental

1.1 Materials

(a) Synthetic sulphides

(i) Iron sulphides

Armco iron spherical powder (under 100 mesh) was sulphidized in a porcelain boat at 700°C for 2 days under H_2S flow. This sulphide was crushed, milled and sieved. The fraction between 200 and 325 mesh (10 grms) was annealed at appropriate temperatures for 24 hrs under an atmosphere of controlled sulphur activity, achieved by changing the partial pressure of H_2S in a H_2S/H_2 gas stream. After annealing, the furnace was cooled and the resulting synthesized sulphides were stored in a vacuum desiccator.

(ii) Nickel sulphides

The synthesizing technique was the same as that for the iron sulphides. Nickel metal of chemical purity was supplied by Fisher Scientific Co.

(iii) Iron-nickel sulphides

Armco iron and nickel metal powder mixtures of equal molar ratio were used to synthesize the iron-nickel sulphides using the same synthetic method as described above.

(b) Natural minerals; pyrrhotite, pyrite

Pyrrhotite rock from the Chichibu Mine, Japan, was used for the powdered sample and the massive electrode. The ground pyrrhotite was prepared under nitrogen atmosphere.

Nickeliferrous pyrrhotite from the Falconbridge Mine Ontario, Canada, was also used in this study.

Pyrite of lost identity, probably from Noranda Mines, Quebec, Canada, was used for the electrochemical experiment. This material was a fine-grained polycrystalline lump sample.

(c) Nickel sulphide concentrate

Nickel sulphide concentrate was kindly supplied by the International Nickel Company of Canada Ltd. Its chemical constituents are listed in Chapter IV

1.2 Reagents

All reagents used in this study were of chemical purity. He, O_2, compressed air and nitrogen gases were used from gas cylinders as received without further purification. Hydrogen gas from the cylinder was passed through a palladium catalysis column and then a phosphorus pentoxide water trap to remove contained oxygen. Hydrogen sulphide as supplied from the cylinder was dried by means of a phosphorus pentoxide trap.

Singly-distilled water was used for the preparation of the solutions.

1.3 Apparatus

Figure 2-1 shows a sketch of the apparatus for the experiment in which the dissolution rate was measured by determining the increase in metal ion concentration of consecutive samples. A 500-ml Erlenmeyer flask immersed in a temperature-controlled water bath was used as a reaction vessel. The rubber bung was fitted with a gas disperser, a solution sampling tube and a gas outlet tube connected to a condenser.

For experiments where the reaction rate was determined by measuring the increase in H_2S pressure of the system, a solution sampling tube was replaced by a powder sample holder which could be dumped to begin the experiment in a closed system, which was connected to a mercury manometer.

Agitation of the solution was performed by a 3.5 cm long teflon-coated magnetic stirrer bar rotated by a variable speed magnetic stirrer located under the water bath.

1.4 Experimental procedure

The reaction vessel with 500 ml of solution was first immersed in the water bath and kept at the required temperature for at least 30 minutes with bubbling gases at 300 ml/min to provide the desired atmosphere. Then the rubber bung was lifted briefly to permit addition of the powdered sample into the solution to start the reaction.

A 3~4 ml aliquot was sampled at appropriate intervals by sucking the solution with the syringe. The aliquots were analyzed for the

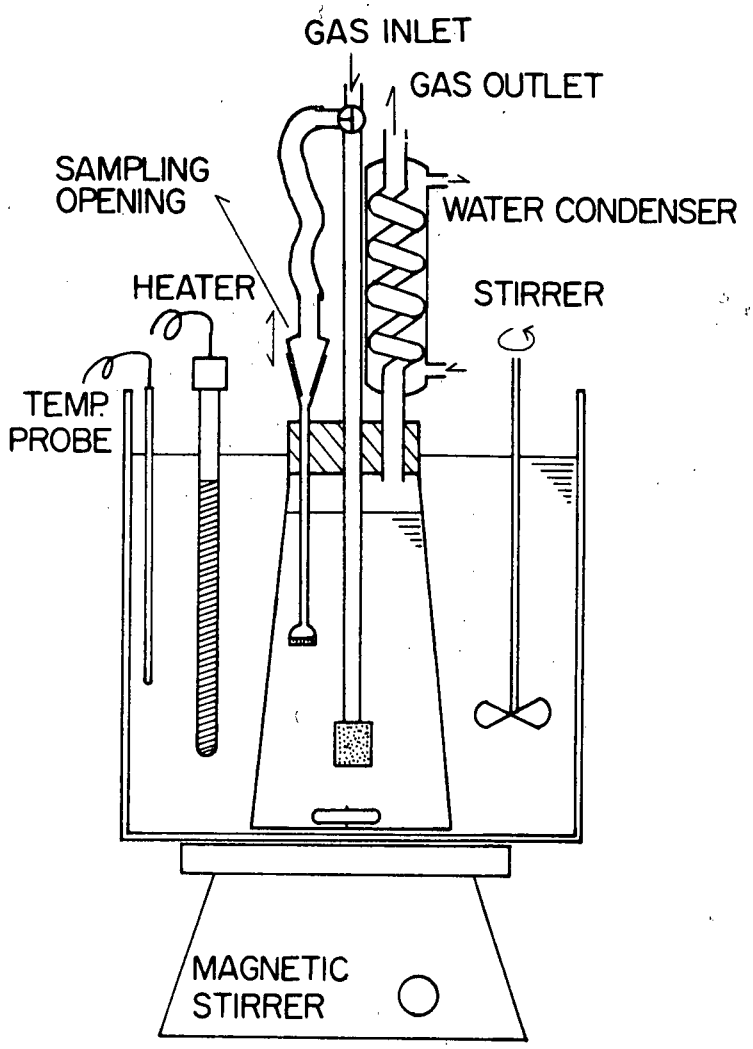

Figure 2-1. The experimental apparatus.

metal ion dissolved.

For experiments incorporating measuring the increase in the H_2S pressure in the system, the powdered sample was placed into the sample holder attached to the inside bottom of the rubber bung. The rubber bung was mounted onto the mouth of the vessel and the solution was purged for 30 minutes with nitrogen gas. After the N_2 flow was stopped and the system was equilibrated with the atmospheric pressure, the sample holder was tilted by the aid of a plunger to drop the sample into the solution. The increase in the pressure of the system due to H_2S evolution was read by the mercury monometer at appropriate intervals.

Agitation of the solution was normally at 1400 rpm, which was the maximum rate obtained from the magnetic stirrer.

1.5 Analytical technique

The analyses for Fe, Ni and Cu in solution were carried out using a Unicam SP 90 atomic absorption spectrophotometer. Prior to every measurement made, a calibration curve was produced with standard solutions. In addition, ferrous ions at higher concentration were estimated using a standard ceric titration. (47)

2. Results and Discussion

2.1 Leaching curves

Synthetic pyrrhotites with sulphur activities fixed at several levels by the conditions of synthesis were leached in 0.1 MHCl solution at 30°C. Helium gas was passed through the solution at 300 ml/min. The

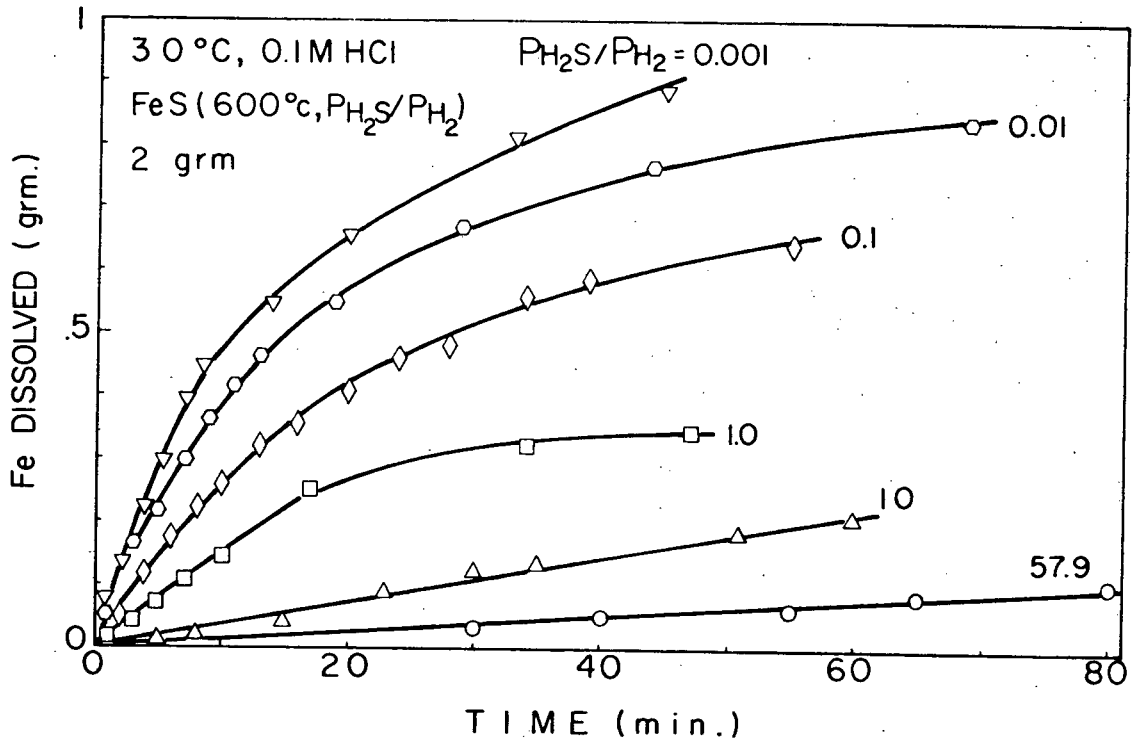

Figure 2-2. Leaching curves for pyrrhotites of different sulphur activities.

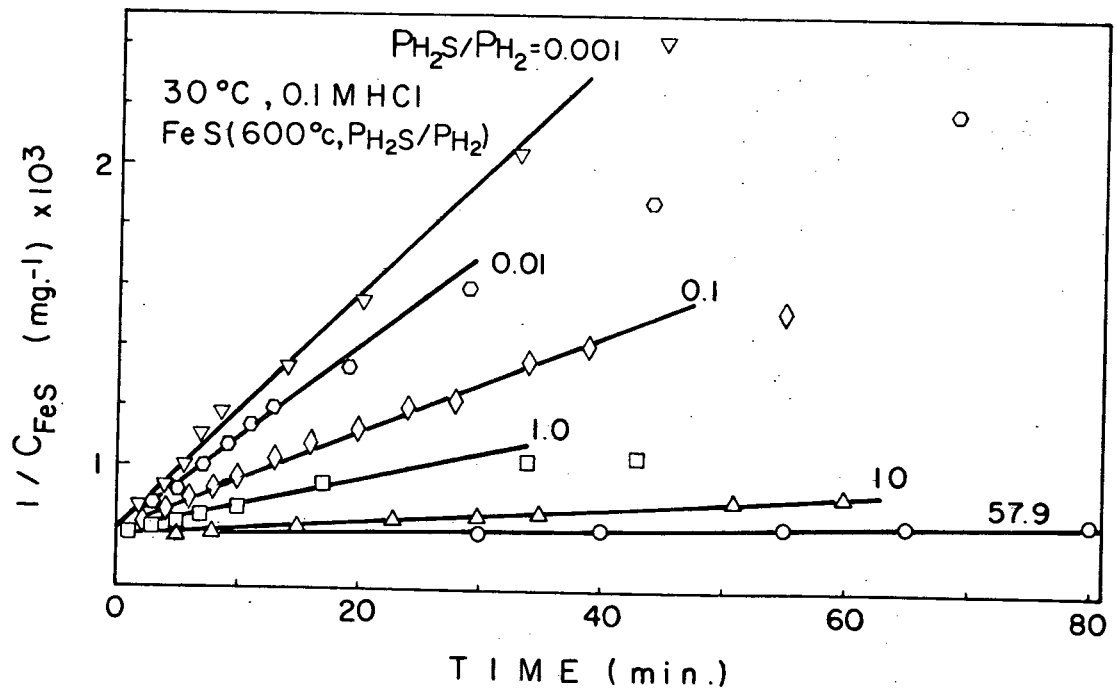

Figure 2-3. 1/(pyrrhotite concentration) versus time during leaching. 30°C, 0.1MHCl, Pyrrhotite of different activities.

increase in the ferrous ion concentration is plotted against leaching time in Figure 2-2. According to these curves, the reaction proceeds without an induction period and at constant rate during an initial period, then slows down in the later stages of the leaching. A. Yazawa, et al. (26) observed that the dissolution rate of pyrrhotite is second order in the concentration (i.e., pulp density) of pyrrhotite up to about 50% of the dissolution, i.e.,

$$-\frac{d[FeS]}{dt} = k_2 \quad [FeS]^2 \quad \left(\frac{\text{mole}}{\ell \text{ min}}\right) \qquad (2.1)$$

where $[FeS]$ means the concentration of pyrrhotite and k_2 is a constant. When this equation is valid, the reciprocal concentration of pyrrhotite and time must have a linear relationship. In Figure 2-3, $1 / (1300 - [Fe^{++}]_t)$ vs time is plotted, where 1300 is approximately the total iron content in 2 grms of pyrrhotite (mg) and $[Fe^{++}]_t$ is the amount of iron dissolved at time t, (mg). According to this figure, an approximately linear relationship is evident up to 50% of the dissolution.

The ratio of the amount of acid in normality to the amount of pyrrhotite in molarity was 4.3 in this work and $4.95 \sim 1.78$ in Yazawa's work. Because of the relatively small ratios, acid depletion during leaching may affect the reaction rate in the later stages. Therefore, an attempt was made to dissolve pyrrhotite in a high ratio of acid to the pyrrhotite, i.e., at values of 86, 172 and 258. Acid concentrations of 1, 2 and 3 M were chosen, while 1 gm of pyrrhotite was weighed for the solid sample. In these runs, a first order dependence, i.e.,

$$- \frac{d[FeS]}{dt} = k_1 [FeS] \qquad (2.2)$$

was found to give a much better fit of the data than a second order dependence, as seen from the log $[FeS]$ vs time linear relationship shown in Figure 2-4.

Equation (2.2) suggests that the dissolution of pyrrhotite proceeds proportionally to the concentration of pyrrhotite without correction for a geometrical effect of the surface area during the dissolution. The decrease in the surface area due to the reduction of the particle size during leaching may be compensated by increases in the surface area by development of pits and roughness.

Since the leaching curves in Fig. 2-2 present a linear initial stage of leaching, the dissolution rate was determined from the slope of this linear region and described in terms of milligrams of metal ion per minute and gram of solid sample (mg/min. grm)

2.2 Effect of the initial surface area

The initial surface area of pyrrhotite present was controlled by the weight of the pyrrhotite charge from 0.3 to 8 grms. Experiments were carried out in 0.1 M HCl solution at 30°C using pyrrhotite synthesized under H_2S/H_2 = 57.9 at 600°C. The results are shown in Figure 2-5, plotting the total dissolution rate vs the sample weight. It is seen that the total dissolution rate of iron is proportional to the sample

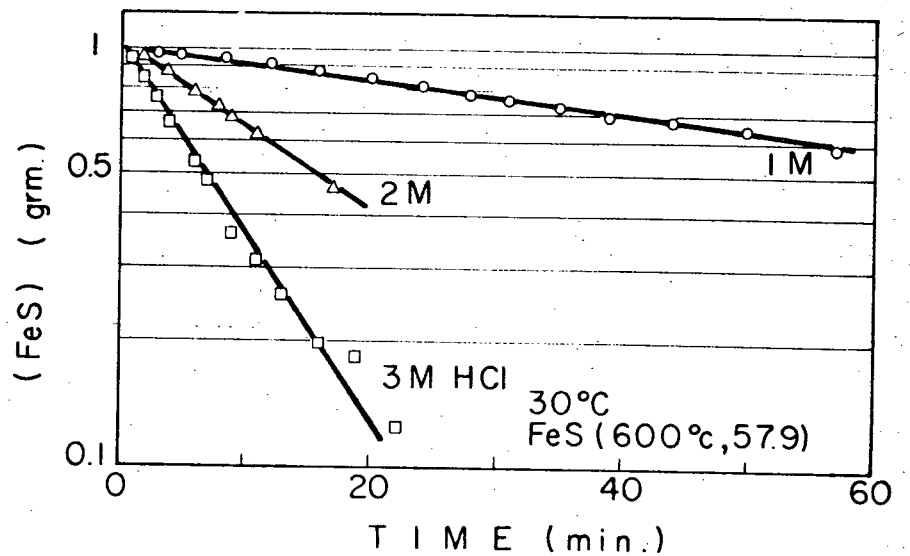

Figure 2-4. Log. (Pyrrhotite Concentration) versus time.

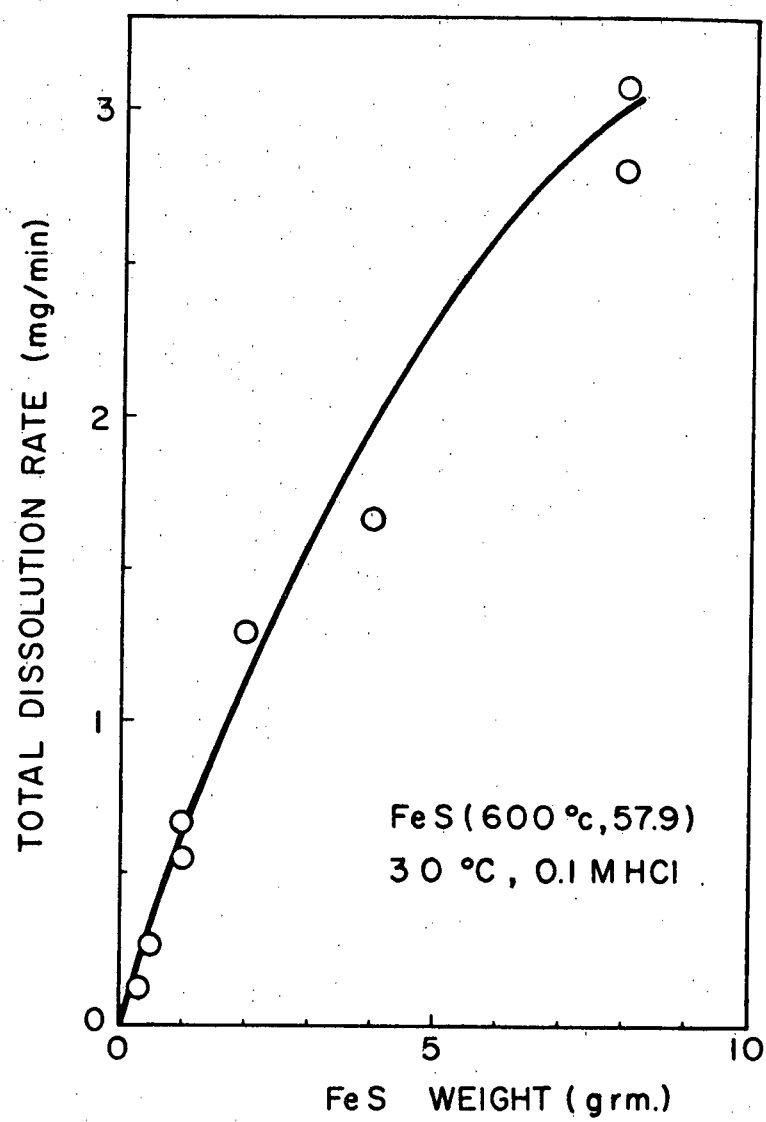

Figure 2-5. Variation in total dissolution rate of pyrrhotite with initial sample weight.

weight up to about 2 grms, but further increases in the surface area do not yield proportional linear dissolution rates.

A non-linearity between the total dissolution rate and the initial surface area may be due to the effect of hydrogen sulphide which is a reaction product. The initial increase in the surface area results in an increase in the total reaction rate without H_2S effect. However, if further increases in the surface area increase the total rate enough to cause build-up of the hydrogen sulphide in solution to levels which suppress the reaction, the total dissolution rate will not follow a linear relationship with the initial surface area at such larger initial area.

2.3 Effect of hydrogen ion concentration

To investigate the effect of acid concentration on the dissolution rate, the concentration of hydrochloric acid was varied from 0.01M to 3M at 30°C. Two kinds of synthetic pyrrhotite were used, one synthesized at 650°C under $PH_2S/PH_2 = 0.001$ and the other at 600°C under $PH_2S/PH_2 = 57.9$*.

Because of its large reaction rate, the low sulphur pyrrhotite was dissolved with the rate being followed by the pressure increase of a closed system, as measured by a mercury manometer connected to the reaction vessel. The conversion of this rate measured by the manometer to the normal rate (mg/min, grm) was made by comparing the

---

* From here on, the synthetic conditions for pyrrhotite are described as FeS (Temperature, the ratio of PH_2S to PH_2). For example, pyrrhotite synthesized at 650°C under $PH_2S/PH_2 = 0.001$ is described as FeS(650°C, $PH_2S/PH_2 = 0.001$.)

rates in 0.1 MHCℓ solution, which were measured both by manometer and by chemical analysis. The rates of this pyrrhotite of low sulphur in HCℓ solution of 0.01 ~ 1.0M are summarized in Table 2-I.

In Figure 2-6, the calculated rates in Table 2-I are plotted against HCℓ concentration. In the same figure, the data of a high sulphur pyrrhotite are also shown. According to these results, within the HCℓ concentration range of 0.01 to 1M the slopes of the straight line in the log (Rate) - log (Concentration) relation are 0.63 for the low sulphur pyrrhotite, FeS (650°C, PH_2S/PH_2 = 0.001), and 0.75 for the high sulphur pyrrhotite, FeS (600°C, PH_2S/PH_2 = 57.9). The dissolution rate for the latter changes its reaction order with respect to the HCℓ concentration above 1M. When the activity of hydrogen ion is considered for the HCℓ concentration using a mean activity value (48), the orders of the reaction rate with respect to the hydrogen ion activity are observed to be 0.64 and 0.77 for the low sulphur and high sulphur pyrrhotite, respectively.

In Figure 2-7, the dissolution rates of pyrrhotite in different acids, i.e., hydrochloric, sulphuric and perchloric acid, are compared using a natural Chichibu pyrrhotite of the same mesh size, 200 ~ 325 mesh, at 30°C. Below 1M acid concentration, the dissolution rate is not influenced by the kind of acid; however, above 1M the difference appears in the order of HCℓ > H_2SO_4 > $HCℓO_4$. Sulphuric acid is a dibasic acid, therefore, the concentration of hydrogen ion is different from the molality. According to the analysis of thermodynamic data in aqueous sulphuric

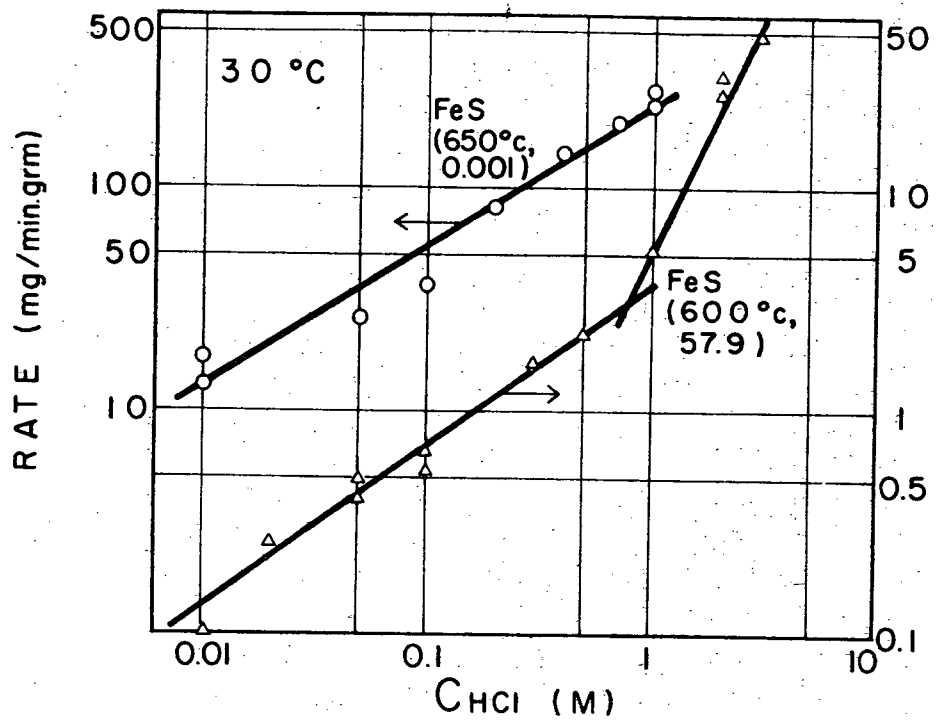

Figure 2-6. Variation in dissolution rates of pyrrhotites with different HCl concentrations.

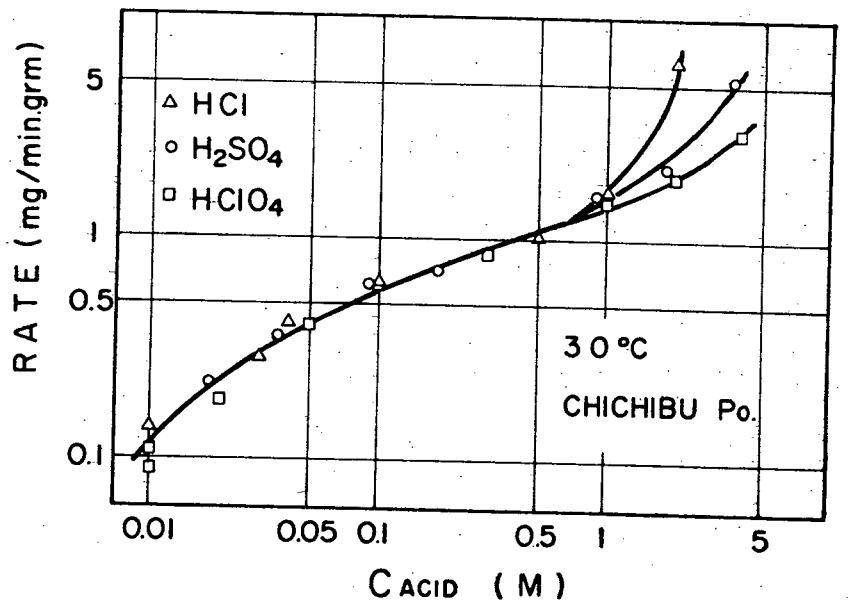

Figure 2-7. Comparison of dissolution rates of natural Chichibu pyrrhotite in H_2SO_4, $HClO_4$ and HCl solutions.

TABLE 2-I

VARIATION IN THE DISSOLUTION RATE OF LOW-SULPHUR PYRRHOTITE (FeS, 650°C, $PH_2S/PH_2 = 0.001$) WITH DIFFERENT CONCENTRATIONS OF HCl

HCl Conc. (M)	Measured Rate (atm/min. grm)	Calculated Rate (mg/min. grm)
0.01	1.31×10^{-3}	17.5
	0.99	13.3
0.05	1.95	26.2
0.1	2.76	37.0*
0.2	6.18	82.9
0.4	10.5	141
0.7	14.5	194
1.0	17.7	237
	20.4	274

* the rate measured

acid by L. T. Romankiw (49), in the concentration range of 0.01 to 4M the concentration of hydrogen ion is related to the concentration of sulphuric acid by the following equation;

$$[H^+] = 1.25\ [H_2SO_4] \qquad (2.3)$$

When we consider the concentration of hydrogen ion instead of the acid concentration, the difference in the rate between sulphuric and perchloric acid above 1M concentration becomes negligibly small, although in both cases they are below the rates for HCℓ.

As mentioned in the previous chapter, although the first order dependence of the acid decomposition rates of sulphides with respect to the hydrogen ion activity was observed by several workers, inconsistencies were found in observations by other workers (See Table 1-II). In addition, the dissolution of iron metal in acidic solutions when accompanied by hydrogen evolution, this reaction apparently having a similar mechanism to that of the acid decomposition of sulphides, does not always obey a first order dependence with respect to the hydrogen ion activity. (50) Furthermore, in hydrochloric acid the effect of chloride ion on the dissolution rate of sulphides must be taken into account when the hydrogen ion activity is changed by increasing the acid strength. The chloride ion effect on the pyrrhotite dissolution may be negligible below an HCℓ concentration of 1M accounting for the data shown in Fig. 2-7.

2.4 Effect of chloride ion

The influence of chloride ion on the dissolution was investigated at 30°C using natural Chichibu pyrrhotite, 0.1 and 1.0 MHCℓ solutions, to which lithium chloride was added as a hydrogen ion independent chloride addition. The addition of lithium chloride in HCℓ solution does not affect the thermodynamic properties of hydrogen ion significantly. (48)

The results are shown in Figure 2-8. According to these data, the dissolution rate at the higher HCℓ concentration is accelerated by the addition of chloride ion to solution; however, at low HCℓ concentration the rate is suppressed by additional chloride ions in solution from LiCℓ.

Acceleration of the dissolution in the presence of the excess chloride ion in 1 MHCℓ may explain the sharp increase in the dissolution rate as the HCℓ concentration exceeds 1M, as shown in Fig. 2-6 and 2-7.

It is commonly understood that the presence of chloride in solution promotes the corrosion process of metallic iron under oxidizing conditions due to the destructive nature of chloride on the protective oxide film.

Under non-oxidizing conditions the effect of chloride ion seems to be rather complex. According to M.H. Jones, et al. in strong HCℓ solution (10%) the NaCℓ and LiCℓ salts accelerate the corrosion of iron. (51) On the other hand, the studies of W.J. Lorenz (52) and

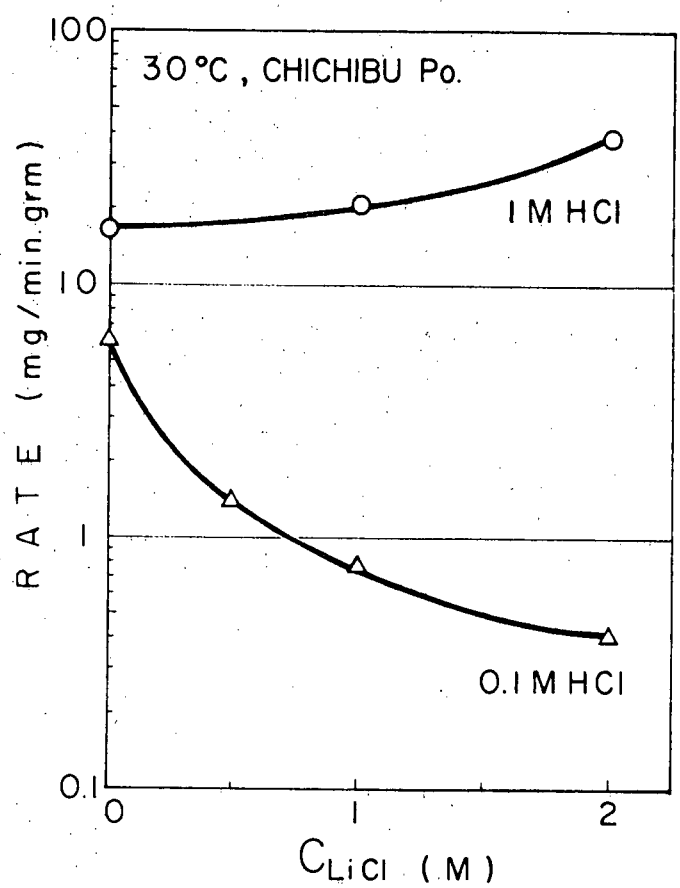

Figure 2-8. Effect of LiCl addition on dissolution rates of natural Chichibu pyrrhotite.

K. Schwabe, et al (53) showed that additions of KCℓ and KBr in weak acids (HCℓ , H_2SO_4) substantially retarded the anodic dissolution of iron. In contrast, K. Nobe, et al. observed that the addition of NaCℓ in 0.1 $NHC\ell O_4$ solution accelerated the anodic dissolution of iron and the dissolution of iron under open circuit conditions. (54)

If it is assumed that a similar reaction mechanism is working on the dissolution of metallic iron as on pyrrhotite in acid solution, i.e., the hydrogen and hydrogen sulphide evolution are both cathodic reactions, and the metal dissolution as a anodic reaction, respectively, the chloride ion effect at the higher HCℓ concentration on pyrrhotite dissolution is consistent with the result of Jones, et al. for the metallic iron corrosion. On the other hand, the chloride ion effect at the lower HCℓ concentration on pyrrhotite decomposition agrees with the results by Lorenz and Schwabe, et al. According to their interpretation, the excess chloride ion in solution adsorbs on the surface to block the reaction sites, thereby suppressing the dissolution of iron.

2.5 Effect of cations

The effect of cupric and nickel ion on the HCℓ dissolution of synthetic low sulphur pyrrhotite was investigated by means of independent cupric and nickel chloride additions. In Figure 2-9, the dissolution rates are plotted against the concentration of cupric and nickel ion. At low concentrations of cupric ion the depletion of copper occurred; therefore, both the initial rate and the rate after the depletion are presented.

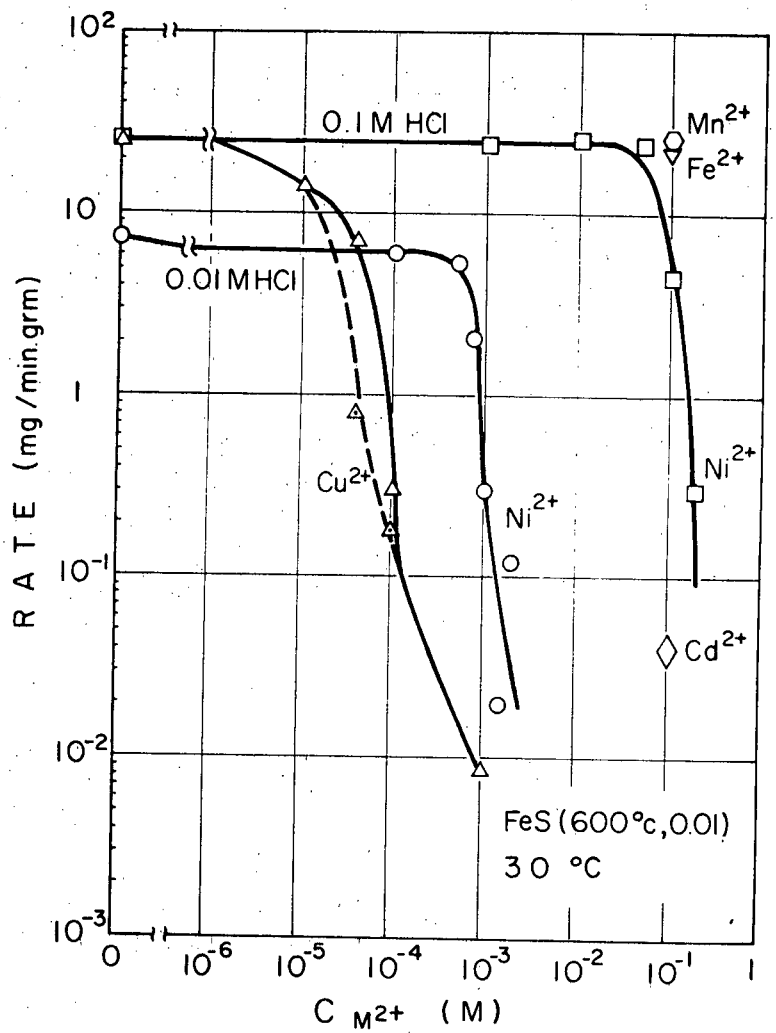

Figure 2-9. Effect of metal cation additions on dissolution rates of pyrrhotite.

According to these results, the dissolution of pyrrhotite is inhibited above a critical concentration of the cations. As little as 10^{-5} M Cu^{++} retards the pyrrhotite dissolution. For nickel ion, the critical concentration is higher and depends on the concentration of HCl.

Furthermore, the effect of $MnCl_2$, $FeCl_2$ and $CdCl_2$ at 0.1 M concentration was studied on the pyrrhotite dissolution. The results are plotted in Figure 2-9. It is evident that Mn^{++} and Fe^{++} ions do not inhibit the dissolution of pyrrhotite under these conditions, but Cd^{++} ion has a pronounced inhibition effect. The inhibition by such cations must be attributed to the formation of surface layers of sulphides less soluble than pyrrhotite. The order of this effect of cations appears to be $Cu^{++} > Cd^{++}$, $Ni^{++} > Fe^{++}$, Mn^{++} and this order seems to correspond to the reverse order for the solubility constant, shown in Table 1-I, i.e.,

$$CuS < CdS < NiS < FeS < MnS$$

Figure 2-10 shows the comparison of the dissolution rates in the absence and presence of ferrous ion at 0.01 M at 30°C in 0.1 MHCl solution using the pyrrhotites with various sulphur activities. From this figure, it is evident that ferrous ion at this concentration does not influence the dissolution rate of pyrrhotite.

In Figure 2-11, the changes in the concentration of metal ions during leaching are shown. Pyrrhotite dissolution in the presence of cupric ion (10^{-4} M) is compared with that without Cu^{++} (shown by a

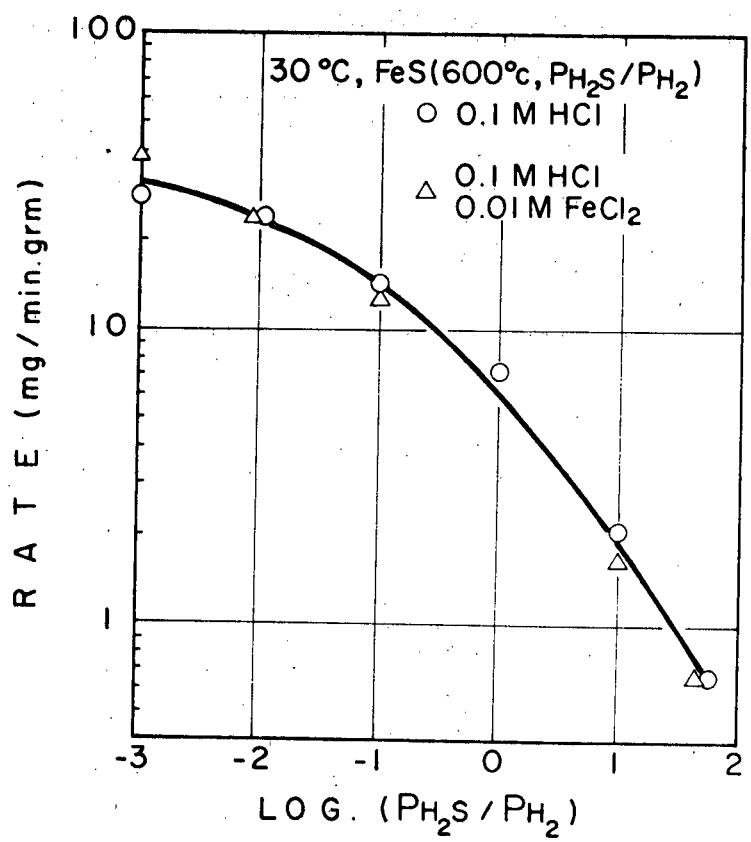

Figure 2-10. Effect of ferrous ion addition (10^{-2} M) on dissolution rates of pyrrhotites of different sulphur activities.

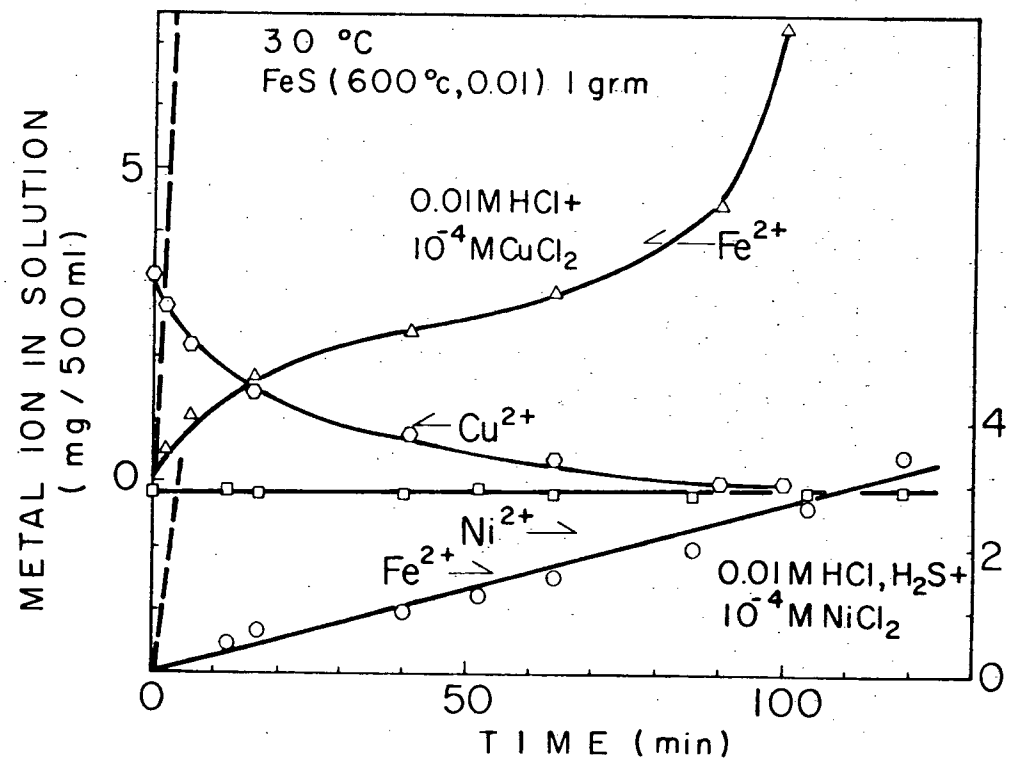

Figure 2-11. Concentration changes of Cu^{++}, Ni^{++}, and Fe^{++} during leaching of pyrrhotite. Broken lines show the Fe^{++} increase in the absence of Cu^{++} and Ni^{++}, respectively.

broken line). The cupric concentration decreases as iron goes into solution, and when all the copper in solution is depleted, the dissolution of pyrrhotite accelerates, although not to the rate of the uninhibited reaction. On the other hand, although the pyrrhotite dissolution in 0.01 MHCℓ solution saturated with H_2S of 1 atm. is retarded by the presence of nickel ion, the nickel ion concentration does not change during leaching. It is possible that the depletion of cupric ions is mainly a displacement with iron on the pyrrhotite surface, while nickel precipitation takes place only in the surface layer and this represents too small a quantity of non-ferrous metal to be detected by solution depletion.

2.6 Effect of hydrogen sulphide in solution

The effect of hydrogen sulphide in solution on the pyrrhotite dissolution was studied by bubbling a mixture of helium and H_2S gases at 300 ml/min. through the solution. Prior to addition of pyrrhotite the gas mixture was passed through the clear leaching solution for at least 30 minutes. The partial pressure of H_2S was varied from 0.01 to 1 atm.

Figures 2-12, 13 represent the results on high sulphur pyrrhotite, FeS (600°C, PH_2S/PH_2 = 57.9) in 0.1 and 1MHCℓ solution and on low sulphur pyrrhotite, FeS (600°C, PH_2S/PH_2 = 0.01) in 0.01 and 0.1 MHCℓ solution, respectively, at 30°C. Figure 2-14 shows the H_2S effect on the low sulphur pyrrhotite at different temperatures. Figure 2-15 shows the comparison of the dissolution rates of different pyrrhotites under atmospheres of only helium and only H_2S, in the HCℓ concentration

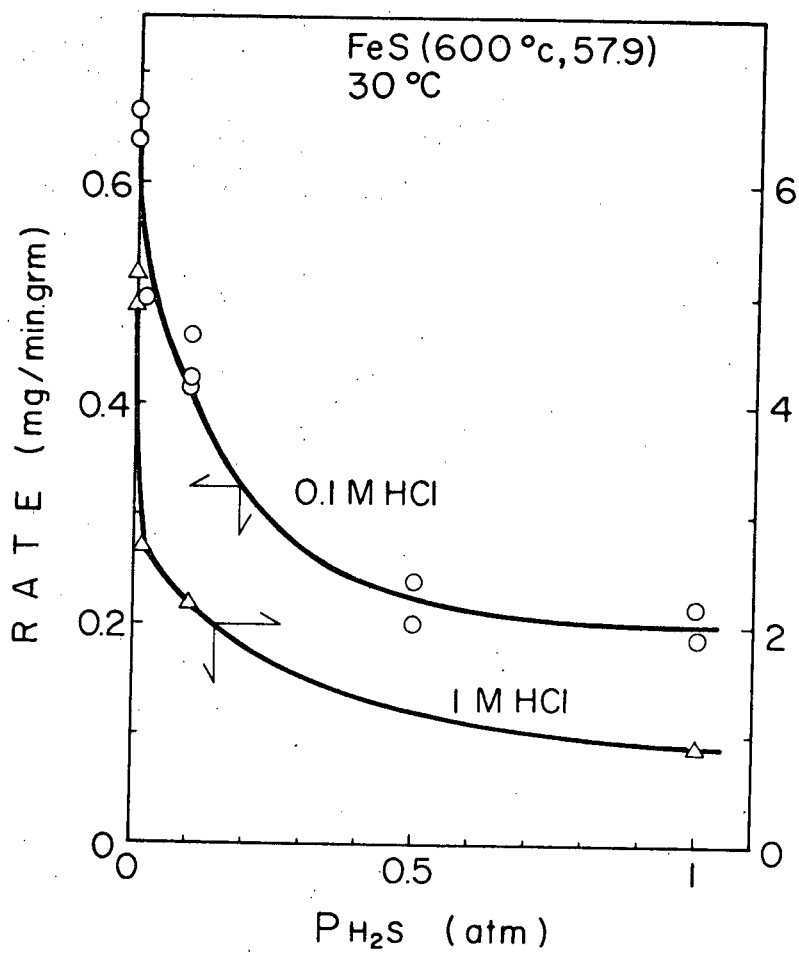

Figure 2-12. Effect of H_2S partial pressure on dissolution rates of high sulphur pyrrhotite.

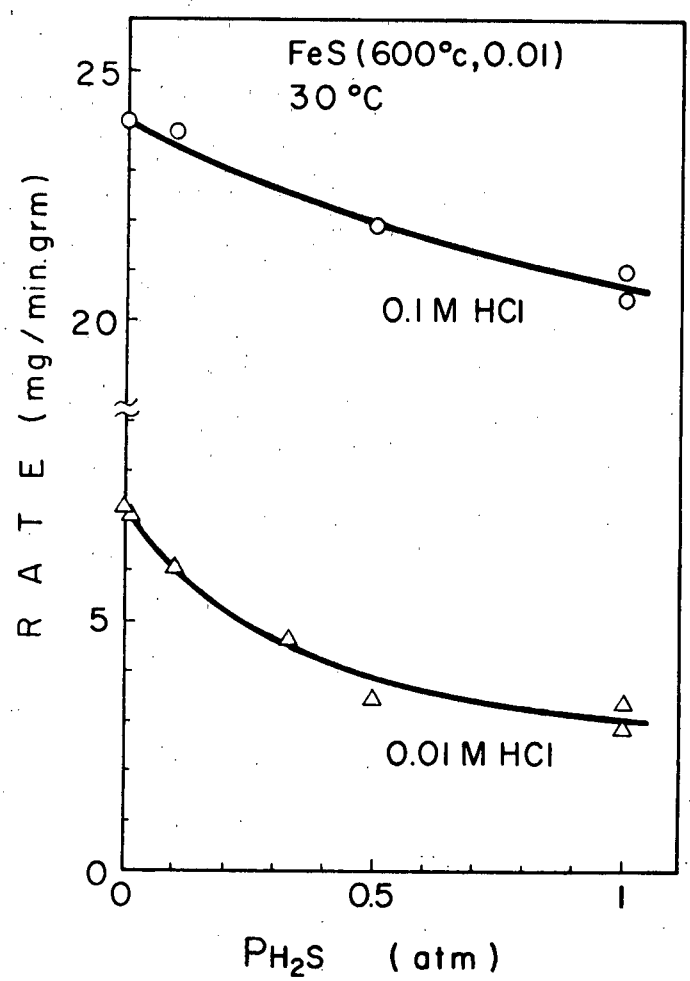

Figure 2-13. Effect of H_2S partial pressure on dissolution rates of low sulphur pyrrhotite.

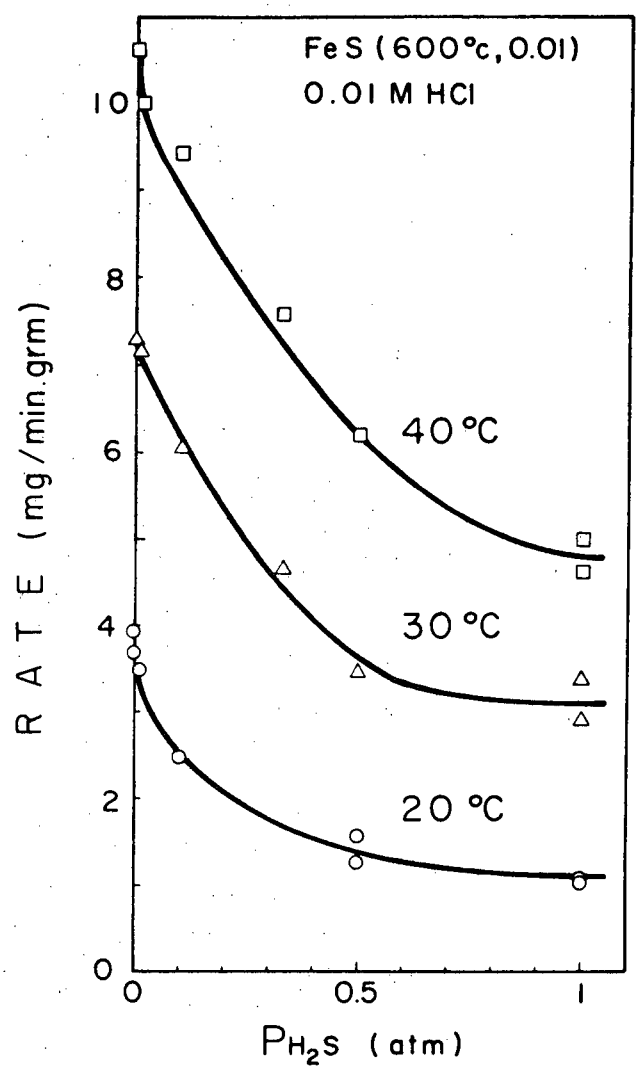

Figure 2-14. Effect of H_2S partial pressure on dissolution rates of low sulphur pyrrhotite at different temperatures.

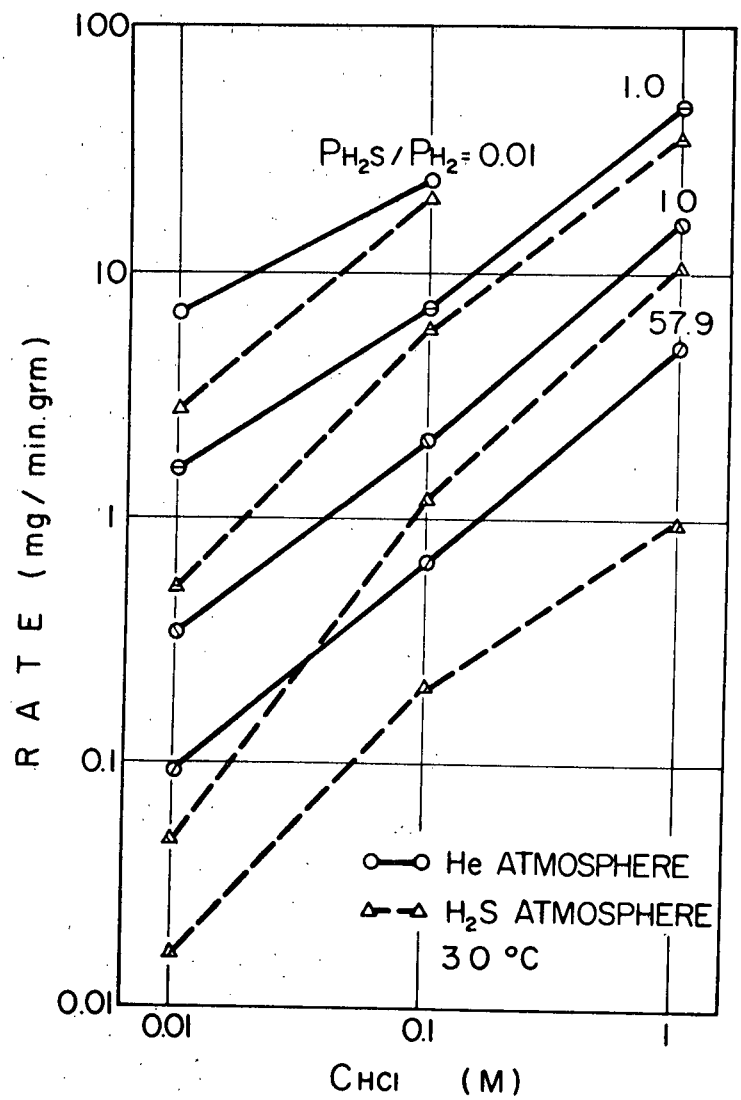

Figure 2-15. Comparison of dissolution rates of pyrrhotites of different sulphur activities in different HCl concentrations under H_2S or He atmosphere.

range of 0.01 ~ 1M at 30°C.

As a summary for the effect of H_2S on pyrrhotite dissolution, the following statements can be made:

(1) An H_2S pressure as small as 0.01 atm reduces the dissolution rate of some pyrrhotites,

(2) The inhibiting effect of H_2S is more pronounced in solutions of lower HCℓ concentration,

(3) At the same HCℓ concentration, the pyrrhotite with high sulphur activity is more susceptible to the H_2S inhibition than that with low sulphur activities.

The inhibition by H_2S of the dissolution of pyrrhotite may be interpreted by the following possible mechanisms:

(1) If the reaction rate is controlled by the diffusion of H_2S from the surface to the bulk of the solution, H_2S in solution reduces the driving force for the H_2S diffusion, which is estimated as the difference in the concentration of H_2S at the pyrrhotite surface and the bulk of the solution.

(2) If the reaction rate is controlled by the reaction at the pyrrhotite surface, the H_2S in solution promotes the reverse ($Fe^{++} + H_2S \longrightarrow FeS + 2H^+$). As a result, the net reaction rate of dissolution, which is a difference between the forward and reverse reaction rates, decreases as the concentration of H_2S increases.

(3) If the reaction rate is controlled by the chemical reaction at the surface as in the previous case, the H_2S in solution may adsorb on the pyrrhotite surface to block the reaction sites and reduce the reaction rate of pyrrhotite.

It is known that the concentration of H_2S in solution is directly proportional to the vapour pressure of H_2S above the solution in the range of the H_2S pressure and of the HCl concentration, in which the experiments were carried out. (55), (56) This linear relationship between the solubility and the partial pressure of H_2S was also found in this work, shown in Appendix I. Therefore, if the inhibition mechanism (1) is valid, the pyrrhotite dissolution rate can be expressed in terms of the partial pressure of H_2S by the following equation;

$$\text{Rate} = Ko\,(C^{S}_{H_2S} - k\,PH_2S) \qquad (2.4)$$

where Ko, k are constants, $C^{S}_{H_2S}$ is the concentration of H_2S at the pyrrhotite surface and PH_2S is the partial pressure of H_2S. Equation (2.4) suggests that the pressure of H_2S decreases the dissolution rate linearly provided that the change in the H_2S pressure does not affect the values of Ko and k. However, this relationship was not found in the experiments shown in Figures 2-12~14. It is concluded that the H_2S inhibition on the dissolution cannot be due to the mechanism (1).

According to Romankiw, et al. (23), the rate equation for the dissolution of zinc sulphide is described by the following equation;

$$\frac{d[Zn^{++}]}{dt} = Ao\,(kF\,[H^{+}] - kB\,[Zn^{++}]^{1/2}\,PH_2S^{1/2}) \qquad (2.5)$$

where Ao; surface area of zinc sulphide, kF, kB; the rate constants of forward and backward reaction, respectively, [ ]; concentrations of components and PH_2S; the H_2S partial pressure. Therefore, an increase in the partial pressure of H_2S results in the decrease in the dissolution rate of zinc sulphide due to the increase in the rate of the backward reaction (the precipitation of zinc sulphide). Although the dissolution rate of pyrrhotite was suppressed by the partial pressure of H_2S, which may suggest a possibility of the mechanism (2), it was found that ferrous ions up to 0.1 M did not influence the dissolution rate of pyrrhotite, as shown in Figure 2-9, 10. From this fact, it can be concluded that the inhibition mechanism (2) does not explain the dissolution as observed in these experiments.

According to O. L. Riggs, et al. (57), the corrosion rate of iron in the presence of inhibitor can be expressed in the following equation;

$$\frac{d[Fe^{++}]}{dt} = k_1\,(1 - \Theta) + k_2\,\Theta \qquad (2.6)$$

where Θ is the fraction of the surface covered by the adsorbed inhibitor, k_1 is the rate constant for the uninhibited reaction and k_2 is the rate constant for corrosion of the completely covered surface. On the other hand, E.B. Maxed, et al. have carried out a systematic quantitative treatment of poisoning of heterogeneous catalysts. (58), (59) They ob-

served that if the activity of a metallic catalyst is plotted against the amount of poison present, a graph is obtained in which the activity of the catalyst usually first falls linearly or approximately linearly with increasing poison content. Then it is followed by an inflexion in the graph, after which the activity of the catalyst falls far less steeply with further increase in the poison content. This observation is quantitatively expressed by the following equation in terms of the poison coverage, Θ,

$$A_{cat.} = kc\,(1 - \alpha\Theta) \tag{2.7}$$

where $A_{cat.}$ is an activity of catalyst, and kc and α are constants. Equation (2.7) is similar in form to the modified equation (2.6), i.e.,

$$\frac{d\,[Fe^{++}]}{dt} = k_1 - (k_1 - k_2)\,\Theta \tag{2.8}$$

The coverage of adsorbant, Θ, is in general not linearly proportional to its content in the media, but in the form of a complex isotherm. Therefore, if the inhibition of H_2S on the pyrrhotite dissolution is due to the mechanism (3), the inhibited rate can be expressed quantitatively by the equation;

$$\text{Rate} = Ro\,(1 - \beta\,\Theta) \tag{2.9}$$

Where Ro is the rate uninhibited by H_2S, β is a constant and Θ is a surface coverage of H_2S on the pyrrhotite surface, which is a function of the H_2S partial pressure. W.H. Cone, et al. carried out an experiment to

measure the amount of H_2S adsorbed on NiS, PbS, CdS and FeS in solution at 1 atm of H_2S pressure and 25°C. According to their results, the amount of H_2S adsorbed was dependent on the sulphide. For the pyrrhotite, 2.3×10^{-4} moles H_2S was adsorbed on 4.5×10^{-4} moles of pyrrhotite in neutral solution, although no indication was given of the particle size of the pyrrhotite.

2.7 Estimation of the H_2S activity at the pyrrhotite surface

When the effect of nickel ion on the dissolution of pyrrhotite was investigated, inhibition was observed above certain critical nickel ion concentrations, which vary with the $HC\ell$ concentration (shown in Fig. 2-9). From the results in Fig. 2-9, these critical concentrations are approximately 7×10^{-4} and 8×10^{-2} M Ni^{++} for 0.01 and 0.1 M $HC\ell$ solution, respectively.

At least two alternate mechanisms for the inhibition of pyrrhotite dissolution by nickel ion can be suggested;

(1) an exchange reaction between nickel ion and iron in solid phase to form an insoluble (Fe + Ni) compound at the surface.

(2) the precipitation of nickel sulphide at the surface by the reaction, $Ni^{++} + H_2S \longrightarrow NiS + 2H^+$, the precipitated NiS material nucleating on and reacting with the pyrrhotite phase to form a surface layer that is considerably less soluble than pyrrhotite.

Although W.E. Ewers (61) found that nickel-uptake on pyrrhotite occurred above 200°C in $3MNiC\ell_2$ solution, it is uncertain

whether this happens near room temperature. Furthermore, mechanism (1) cannot account directly for the observation that the critical concentration of nickel ion for inhibition is dependent on the acid concentration.

According to mechanism (2), the critical nickel concentration for inhibition is expected to be approximately second order with respect to the HCℓ concentration, provided that the H_2S activity is approximately constant. In this case, it is evident that the H_2S activity at the pyrrhotite surface may be rather larger than that in solution, due to the generation of H_2S at the surface during active dissolution of pyrrhotite. Also, the nucleation of NiS on the surface requires less supersaturation than nucleation and precipitation in the solution, where there may be no nucleation sites. This may account for the fact that the precipitation of NiS does not occur in the bulk of solution at the critical concentration, but only on the pyrrhotite surface.

On the assumption of equilibrium for nickel sulphide precipitation, i.e.,

$$H_2S \text{ (at surface)} + Ni^{++} = NiS(\alpha) + 2H^+$$

based on α-NiS as the precipitate (62), the equilibrium constant is defined as;

$$K = \frac{aH_2S \cdot aNi^{++}}{aH^{+2} \cdot a\alpha\text{-NiS}} \qquad (2.10)$$

where (a) means the activity of each component at the pyrrhotite surface.

Equation (2.10) is transformed to (2.11) in terms of aH_2S:

$$aH_2S = \frac{a^2_{H^+} \cdot a_{\alpha\text{-NiS}}}{a_{Ni^{++}}} K \qquad (2.11)$$

With equation (2.11), the activity of H_2S at the pyrrhotite surface* can be calculated from K obtained from thermodynamic properties of α-NiS, H_2S and Ni^{++}, (a_{H^+}), which is assumed to be the bulk activity of H^+ ion, and ($a_{Ni^{++}}$) assumed to be the bulk activity of Ni^{++} ion. Furthermore, according to equation (2.11), the critical activity of Ni^{++} changes as a_{H^+}, a_{H_2S} change at constant $a_{\alpha NiS}$. The change in aH_2S may be affected by changes in the bulk concentration of H_2S and H^+ as well as by the precise properties of the pyrrhotite surface, under conditions where H_2S is being generated.

Figure 2-16 represents the dissolution rate of low sulphur pyrrhotite in 0.01 MHCℓ at 30°C vs the nickel concentration in solution under different H_2S partial pressures. From this figure, it is evident that the critical concentration of nickel ion varies with H_2S partial pressure, i.e., the larger the H_2S partial pressure, the smaller the critical concentration. Its value was estimated by graphical extrapolation, as shown in Fig. 2-16.

In Table 2-II, the critical concentration of nickel for various conditions obtained by the above method are summarized and

---

* The activity at the surface and in the bulk of the solution are the same when there is no flux of H_2S from the surface. Since there must be such a flux, the equilibrium condition can be assumed only at the surface.

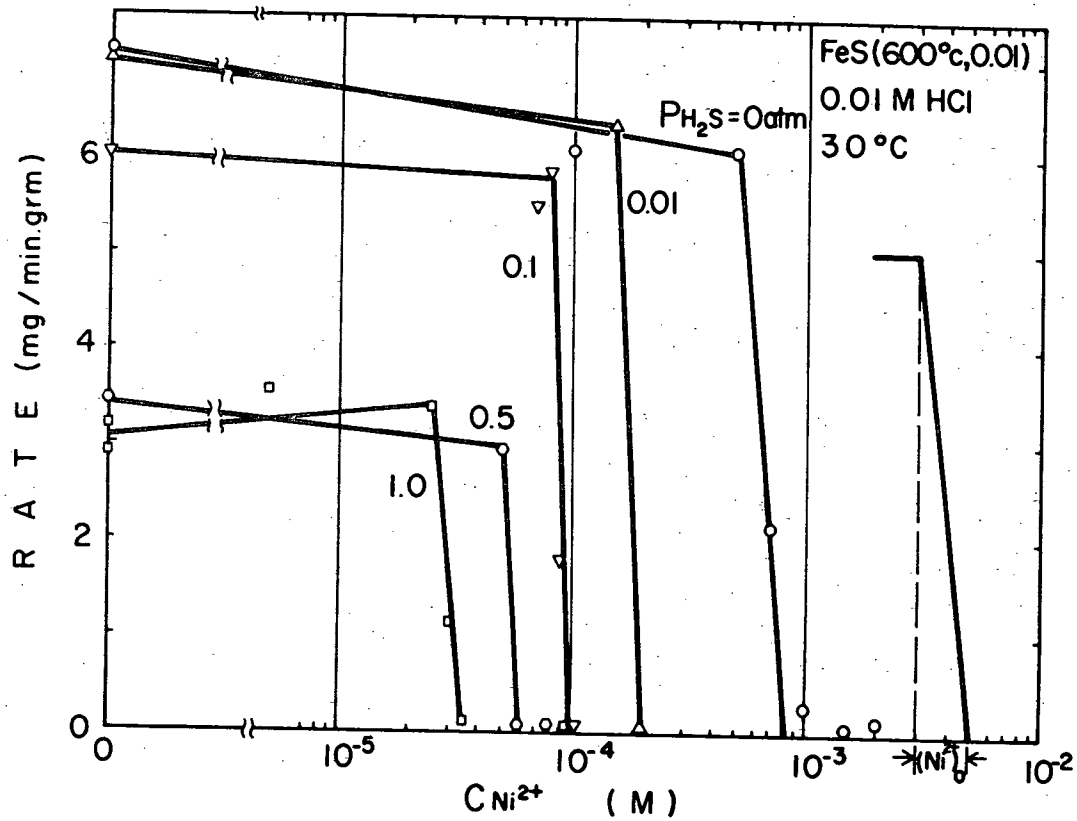

Figure 2-16. Effect of Ni^{++} ion on dissolution rates of low sulphur pyrrhotite under various H_2S partial pressures. Graphic estimation for the critical concentration of Ni^{++}.

TABLE 2-II

SUMMARY OF DATA FOR $[Ni^{++}]_o$ AND aH_2S

Leach Condition	PH_2S*	$[Ni^{++}]_o$	K**	aH_2S***
		FeS (600°C, PH_2S/PH_2 = 0.01)		
20°C	1.0	$2.0 \sim 2.5 \times 10^{-5}$	2.09	8.4 ~ 10
0.01 MHCl	0.103	5.0 ~ 6.0	2.09	3.5 ~ 4.2
	0.014	10 ~ 20	2.09	1.0 ~ 2.1
30°C	1.0	$2.5 \sim 3.5 \times 10^{-5}$	1.47	4.2 ~ 5.9
0.01 MHCl	0.5	5.0 ~ 6.0	1.47	2.5 ~ 2.9
	0.107	8.0 ~ 10	1.47	1.5 ~ 1.8
	0.019	15 ~ 20	1.47	0.74 ~ 0.98
	0.009	50 ~ 80	1.47	0.18 ~ 0.29
30°C	1.0	$1.5 \sim 2.0 \times 10^{-2}$	1.47	0.74 ~ 0.98
0.1 MHCl	0.13	3.7 ~ 5.5	1.47	0.27 ~ 0.40
	0.03	4.8 ~ 11	1.47	0.13 ~ 0.31
40°C	1.0	$4.0 \sim 5.0 \times 10^{-5}$	1.03	2.1 ~ 2.6
0.01 MHCl	0.33	4.7 ~ 6.5	1.03	1.6 ~ 2.2
	0.113	12 ~ 14	1.03	0.74 ~ 0.86
	0.024	20 ~ 30	1.03	0.34 ~ 0.52
		FeS (600°C, PH_2S/PH_2 = 57.9)		
30°C	1.0	$0.70 \sim 2.0 \times 10^{-4}$	1.47	74 ~ 210
0.1 MHCl	0.1	1.0 ~ 3.0	1.47	49 ~ 150
	0.01	5.0 ~ 10	1.47	15 ~ 29
	0.0009	8.0 ~ 15	1.47	9.8 ~ 18
30°C	1.0	$1.0 \sim 3.0 \times 10^{-2}$	1.47	49 ~ 147
1.0 MHCl	0.1	2.0 ~ 5.0	1.47	29 ~ 73
	0.013	4.0 ~ 10	1.47	15 ~ 37
	0.006	15 ~ 20	1.47	7.4 ~ 9.8

* PH_2S was calculated in consideration of the H_2S evolved from the pyrrhotite.

** K for each temperature was estimated from ΔH^o and ΔF^o using the van't Hoff isochore.

*** The standard state for aH_2S is the same as that used by Latimer (10) for aqueous H_2S.

the activities of H_2S assuming equilibrium with α-NiS are calculated using equation (2.11). Since there are no thermodynamic data available for the calculation of activities of hydrogen and nickel ions in the aqueous $NiCl_2 + HCl$ system, the concentrations of these ions were considered to be equivalent to activities.

In Figure 2-17, these calculated activities of H_2S at the pyrrhotite surface are plotted against the partial pressure of H_2S above the solution on a double logarithmic scale. Based on these results and the above interpretation, the H_2S activity at the surface would appear to vary over a wide range depending on the temperature, the acid concentration and the type of pyrrhotite subjected to the experiments and fit an empirical relation of the form;

$$aH_2S = A\,PH_2S^{n} \qquad (2.12)$$

where A and n are constants, PH_2S is H_2S partial pressure. A and n are calculated from the data in Fig. 2-17 and summarized in Table 2-III. As seen in Fig. 2-17, the estimated activity of H_2S at the pyrrhotite surface is in general much higher than that in the bulk of the solution, i.e., when the partial pressure of H_2S is unity, the H_2S activity in solution is approximately 0.1 around room temperature. In addition, the estimated H_2S activity at the surface of the high sulphur pyrrhotite is apparently much higher than that at the surface of the low sulphur pyrrhotite. The very high estimated H_2S activity at the pyrrhotite surface is partly due to the choice of α-NiS and the use of its thermodynamic data in the

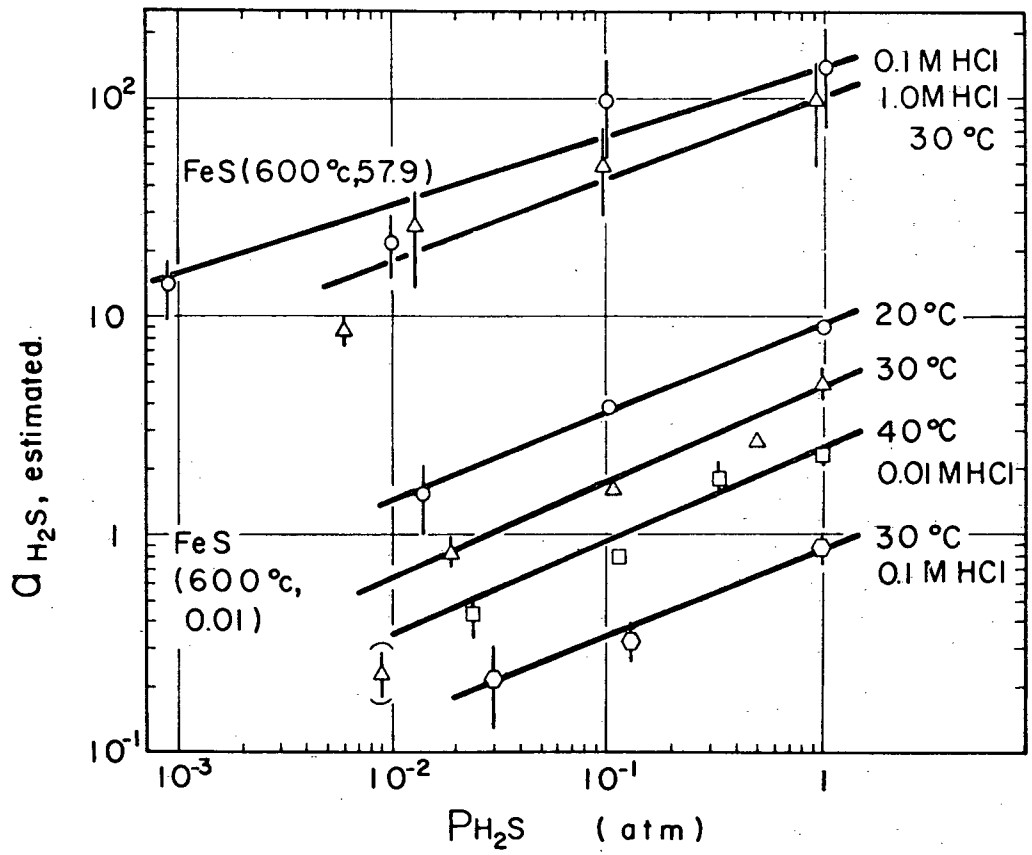

Figure 2-17. Variations in estimated H_2S activity at the pyrrhotite surface with H_2S partial pressure.

TABLE 2-III

VALUES FOR A AND n IN EQUATION (2-12)

FeS(600°C, PH_2S/PH_2 = 0.01)

	A	n
0.01 MHCl		
20°C	9.4	0.41
30°C	4.9	0.55
40°C	2.6	0.49
0.1 MHCl		
30°C	0.83	0.39

FeS(600°C, PH_2S/PH_2 = 57.9)

0.1 MHCl		
30°C	160	0.36
1 MHCl		
30°C	110	0.43

calculations, and would be much lower if the actual surface NiS were equivalent to a low ($<<1$) · α-NiS activity. However, a quantitative estimation for the thermodynamic properties at the surface is not possible.

The temperature dependence of the surface activity of H_2S on the low sulphur pyrrhotite can also be interpreted in terms of changes in the form of the NiS surface film, i.e., changes in the activity of α-NiS.

The variation in the surface H_2S activity with the HCl concentration cannot be explained for the time being.

In view of the above discussion, it is clear that, while mechanism (2) is qualitatively better than mechanism (1) for inhibition, it does not agree quantitatively with all of the experimental facts, and ultimately another mechanism, perhaps a more sophisticated variation of one of the above, is still required for complete understanding of this inhibiting effect of nickel ions on the dissolution of pyrrhotite.

2.8 The relation between surface activity of H_2S and inhibition by H_2S

According to equation (2.9), the inhibition of pyrrhotite dissolution by H_2S can be correlated to the H_2S coverage at the pyrrhotite surface, which is a function of the activity of H_2S in solution. Meanwhile, the relationship of the activity (partial pressure) of H_2S and the estimated surface activity of H_2S was obtained in the previous section. Therefore, when we assume that the linear relation between the surface coverage of

H_2S and the estimated H_2S surface activity is held, equation (2.9) can be transformed in terms of aH_2S;

$$\text{Rate} = Ro\,(1 - \gamma\, aH_2S) \qquad (2.13)$$

where γ is a constant. The above assumption seems to be justified according to the data summarized in Appendix II.

In Figures 2-18~20, the data of the dissolution rate of pyrrhotite under different H_2S partial pressures in Fig. 2 - 12~14 are replotted against estimated aH_2S, obtained from data presented in Table 2-I. From these figures, the correlation between the dissolution rate and aH_2S in equation (2.13) can be found.

In Figures 2-19, it is evident that the difference in inhibition of the dissolution of pyrrhotite by H_2S 0.1 MHCl solution as compared to 0.01 MHCl solution results from the smaller estimated surface H_2S activity. From the data in Fig. 2-20, the Ro and γ values are calculated for each temperature and summarized in Table 2-IV.

TABLE 2-IV

Ro AND γ VALUES FOR 20, 30 AND 40°C
in 0.01 MHCl, FeS (600oC, $PH_2S/PH_2 = 0.01$)

	20°C	30°C	40°C
Ro	3.8	7.5	11.3 mg/min. grm
γ	0.079	0.120	0.216

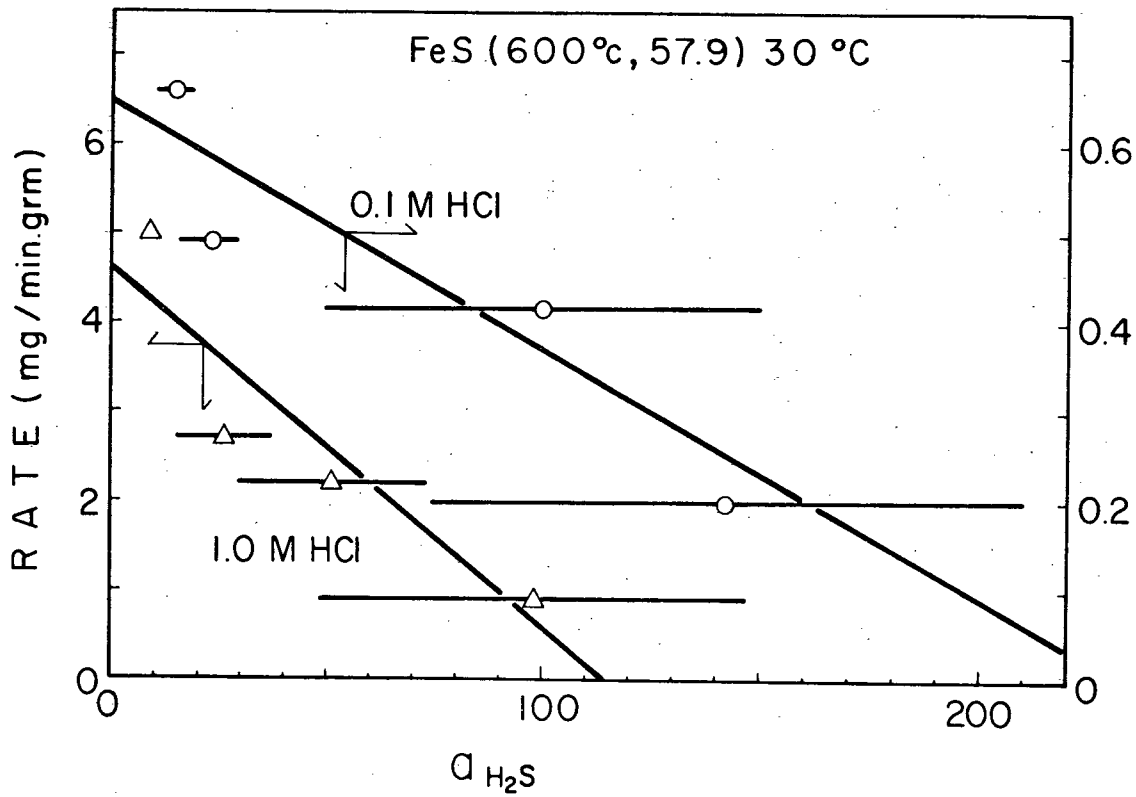

Figure 2-18. Relationship between H_2S activity and dissolution rates of high sulphur pyrrhotite.

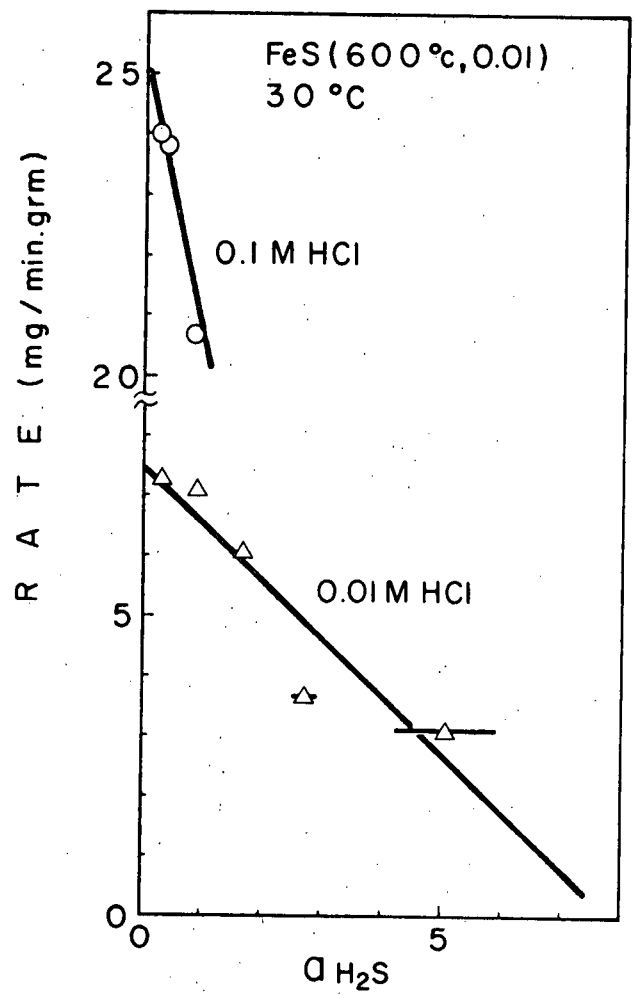

Figure 2-19. Relationship between H_2S activity and dissolution rates of low sulphur pyrrhotite.

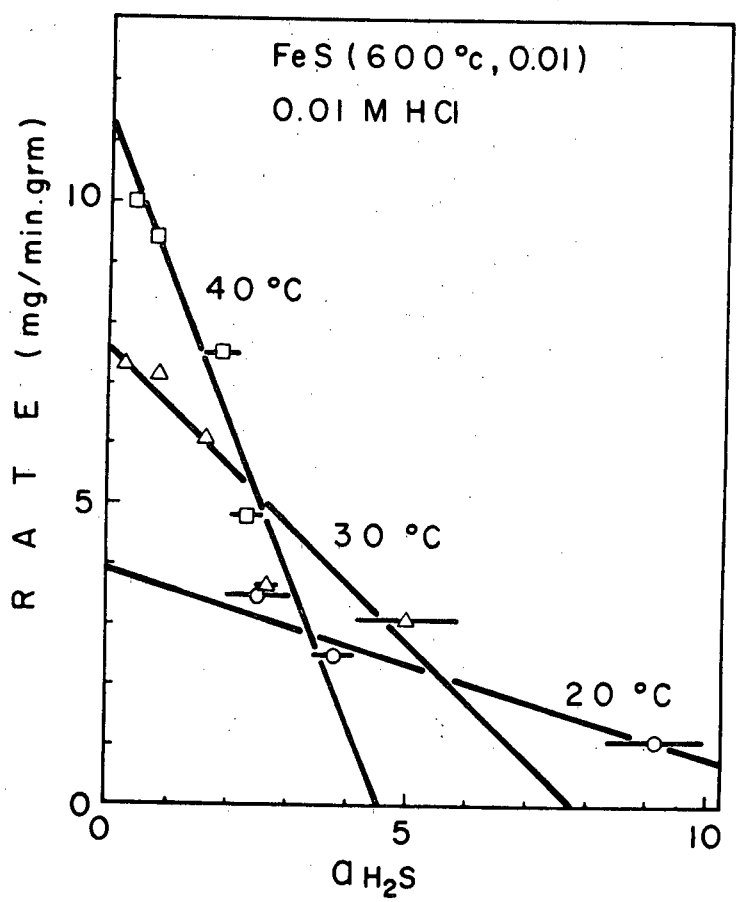

Figure 2-20. Relationship between H_2S activity and dissolution rates of low sulphur pyrrhotite at 20, 30, and 40°C.

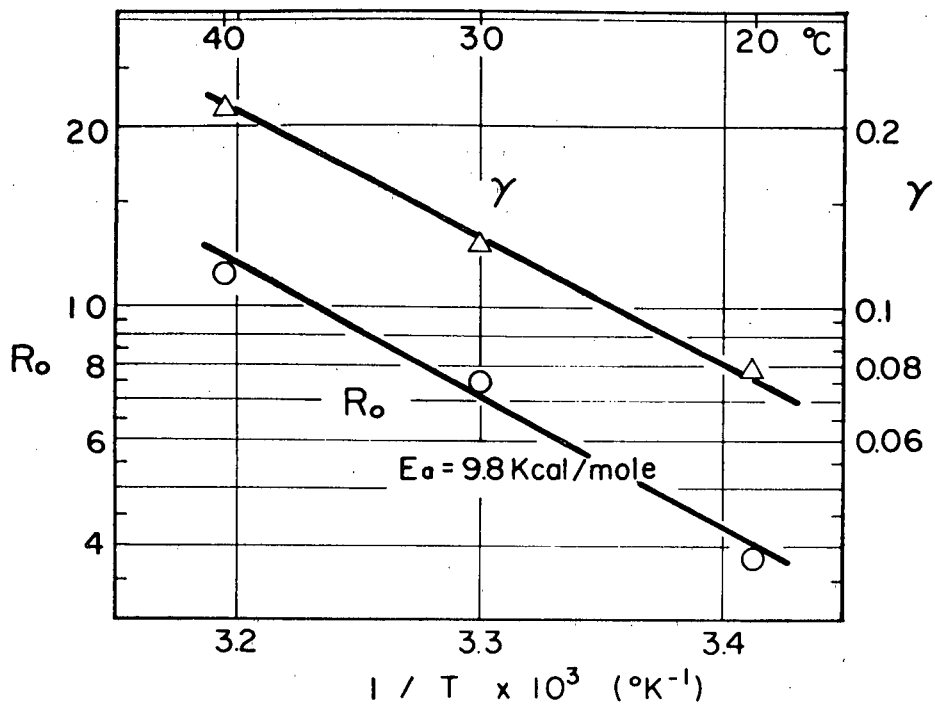

Figure 2-21. Arrhenius plot of Ro and γ for low sulphur pyrrhotite.

In Figure 2-21, the Ro values, which are the dissolution rates of pyrrhotite in the absence of H_2S on the surface, for each temperature are plotted against the reciprocal absolute temperature to estimate the activation energy for Ro.

The activation energy calculated from the slope of the line is 9.8 Kcal/mole. On the other hand, the γ values, whose physical meaning is the effectiveness of inhibition of H_2S molecule at the pyrrhotite surface, are also plotted in Fig. 2-21 for each temperature. As temperature increases, the γ value increases with a similar temperature dependence to that of Ro. The increase in γ value with temperature may be attributed to the activation of H_2S molecules at the surface to increase the effectiveness of poisoning. Though the activation energy for γ value seems to be equivalent to that for Ro, no explanation for this can be made.

2.9 Effect of oxidant in solution

The effect of oxidants present in solution on the acid decomposition of pyrrhotite was investigated using oxygen gas, potassium dichromate, ceric sulphate, potassium permanganate and hydrogen peroxide. All of these oxidants slowed the dissolution of pyrrhotite to an almost negligible rate, though the critical concentration of each oxidant, above which the effect of oxidant first appears, depends on the identity of the oxidant, the acid concentration and the kind of pyrrhotite.

In Figure 2-22, the effect of partial pressure of oxygen on

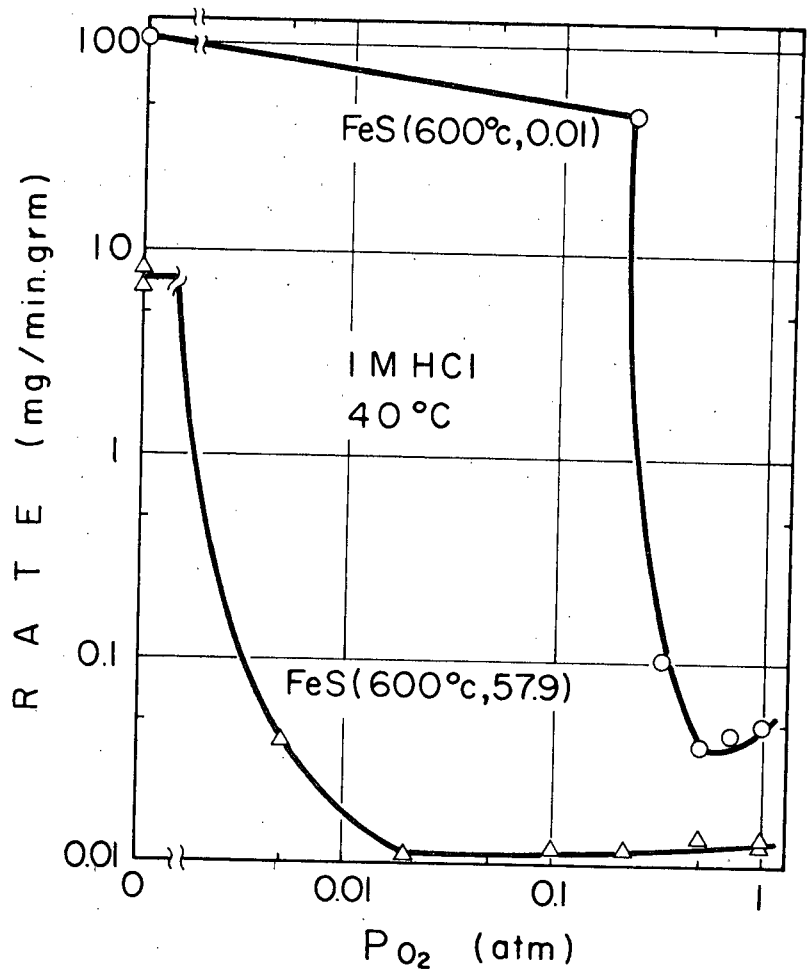

Figure 2-22. Effect of partial pressure of oxygen on dissolution rates of pyrrhotites.

pyrrhotite dissolution in 0.1 MHCl solution at 40°C is shown using two kinds of pyrrhotite. From this figure, it is noted that the critical partial pressure of oxygen for the low sulphur pyrrhotite is much higher (about 2 orders of magnitude) than that for the high sulphur pyrrhotite.

In Figure 2-23, the oxidant effect using potassium dichromate is shown. The critical concentration of $K_2Cr_2O_7$ is highest for the low sulphur pyrrhotite, and increases as the acid concentration increases. The minimum inhibited rate of dissolution is generally about 1/100 of the uninhibited rate, as compared to a factor of 1/1000 for inhibition of this reaction by oxygen (Fig. 2-22). A further increase in the concentration of $K_2Cr_2O_7$ beyond the point, where the minimum rate is reached, increases the dissolution rate again, but the mechanism of dissolution is now the oxidative decomposition of pyrrhotite with elemental sulphur formation.

(1) Nature of the inhibition

High sulphur pyrrhotite, FeS (600°C, PH_2S/PH_2 = 57.9), was first leached in 1 or 1.8 M H_2SO_4 solution in the presence of 10^{-3} M ceric sulphate at 40°C for about 150 minutes. Then the leaching was stopped and the powder sample was filtered and washed with distilled water. This partially leached powder was then leached again in acids in the absence of oxidant. Figure 2-24 represents the amount of Fe dissolved during these experiments. In the presence of ceric ions, inhibition develops in 10~20 minutes, and dissolution rates after about 100

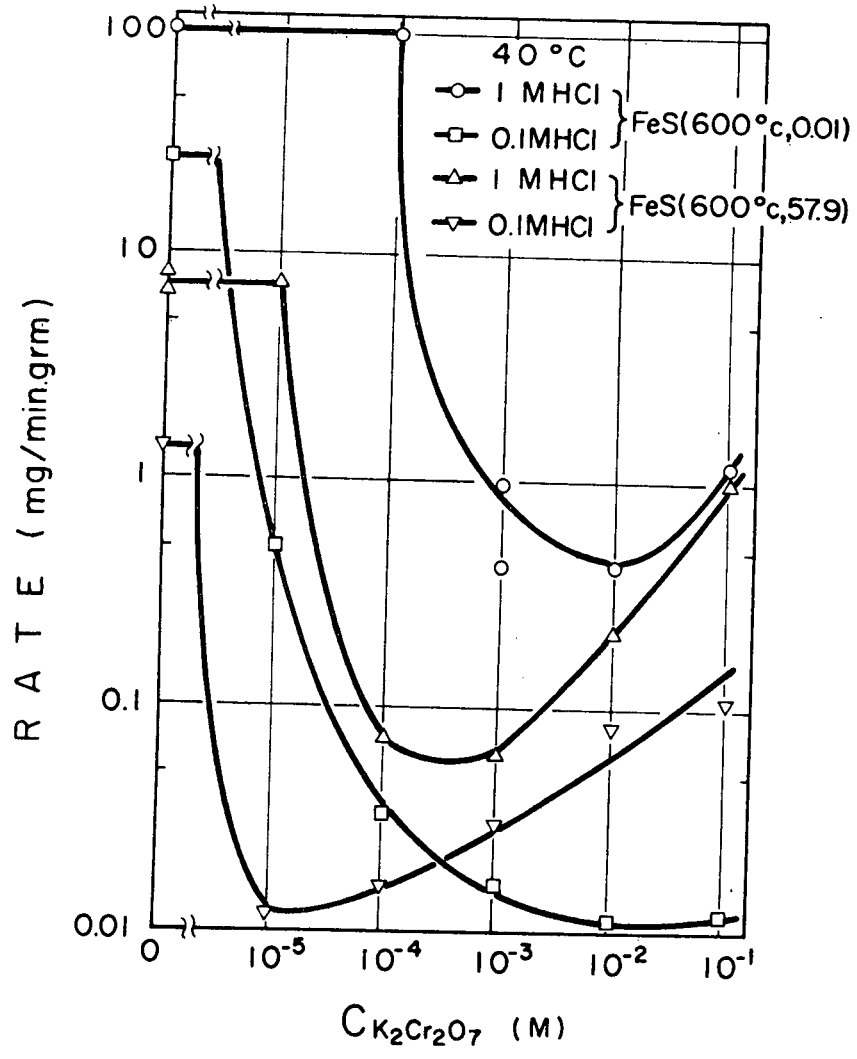

Figure 2-23. Effect of concentration of potassium dichromate on dissolution rates of pyrrhotites.

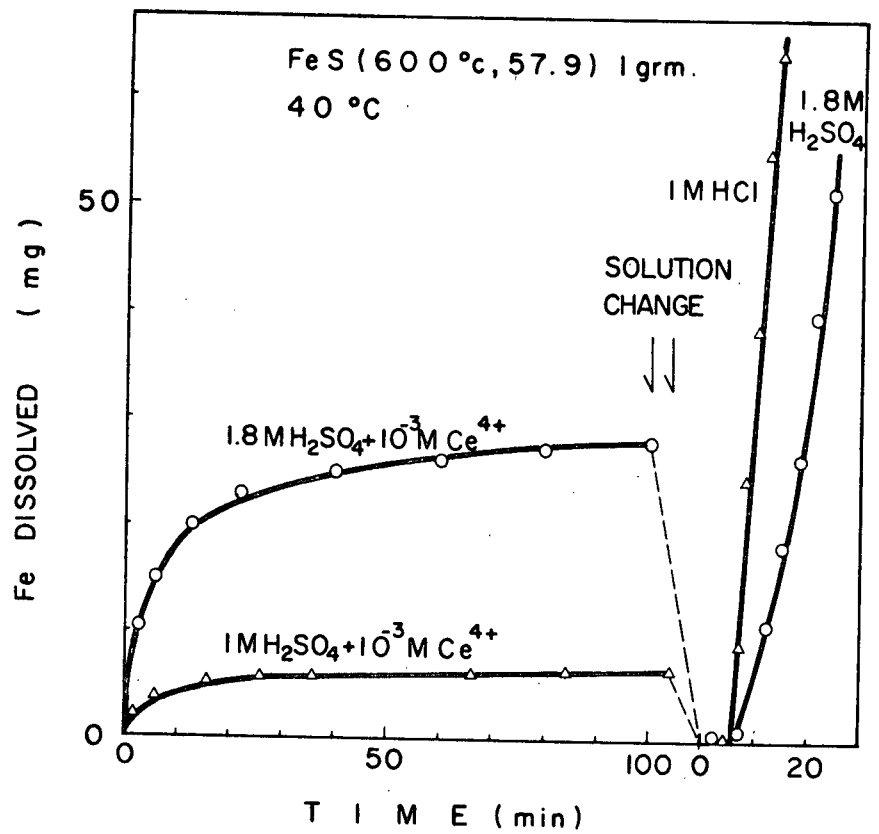

Figure 2-24. Effect of Ce^{4+} ion (10^{-3} M) on the dissolution of iron from high sulphur pyrrhotite.

minutes are very slow. With a solution change removing the oxidant (Ce^{4+} ions), the dissolution resumes again after several minutes of an induction period.

A further study of the reactivation of inhibited pyrrhotite was carried out using oxygen as an oxidant. The dissolution of pyrrhotite was first undertaken in 1M HCl solution at 40°C under oxygen bubbling. Then after selected periods the oxygen stream was switched to helium and leaching was continued under the helium atmosphere. The amount of iron dissolved during leaching was plotted for typical runs in Figure 2-25. The leaching curves show a slow dissolution under oxygen followed by rapid dissolution under helium after an induction period, of duration related to the length of the leaching period with oxygen. The induction time, τ, was graphically estimated from the leaching curve as shown in Fig. 2-25.

Figure 2-26 represents the dependence of the induction period, τ, on the time of leaching under oxygen in 1M HCl for two kinds of pyrrhotite. According to these results, the induction period is longer for high sulphur pyrrhotite than that for low sulphur pyrrhotite under equivalent conditions. From the data shown in Fig. 2-25, 26, it can be concluded that the inhibited pyrrhotite is reactivated in acid solution by removal of the oxidant from the solution after an induction period. The meaning of the induction period is not fully understood; however, from the results in Fig. 2-26 it can be supposed that during the induction period the dissolution of an oxidized surface, of thickness increasing with duration of oxidation, is taking place. The growth of the film during

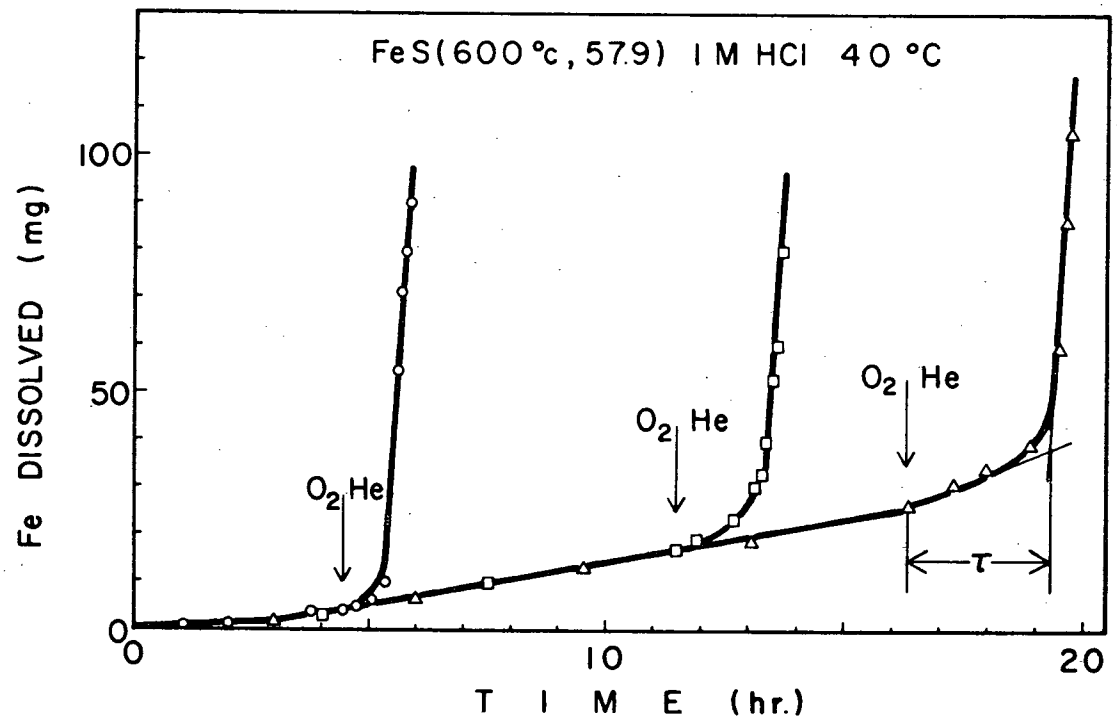

Figure 2-25. Inhibition and reactivation of dissolution of high sulphur pyrrhotite under O_2 and He atmospheres. Graphic estimation for the induction period (τ).

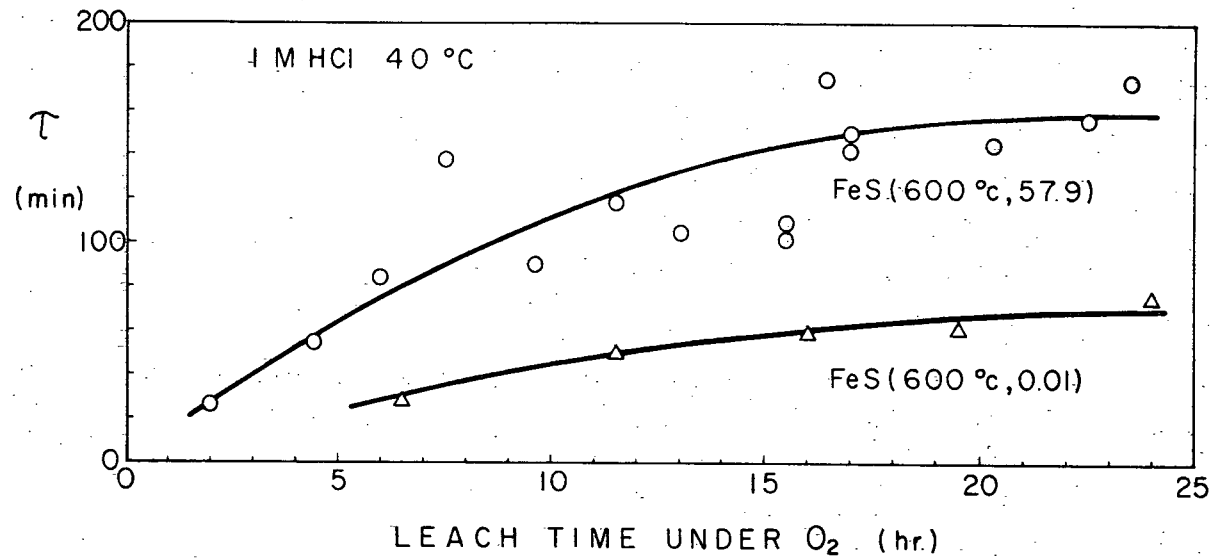

Figure 2-26. Dependence of the induction period (τ) on leach time in the presence of oxygen.

exposure to oxidation according to the parabolic law, followed by linear dissolution of the film after the oxidant is removed, will account for the shape of the curve in Fig. 2-26. (62)

An extensive effort to identify compounds on the oxidized pyrrhotite surface was not made in this work. X-ray diffraction indicated only pyrrhotite on a specimen oxidized with oxygen in 1M HCl at 40°C for 24 hrs. The dissolution of high sulphur pyrrhotite, FeS (600°C, $PH_2S/PH_2 = 57.9$), was carried out in 1M HCl and H_2SO_4 solution under oxygen, while the temperature of the water bath was gradually raised from 30 to 97°C. In Figure 2-27, both the amounts of iron dissolved and the temperature were plotted against time. In sulphuric acid, the dissolution of iron is almost negligible even at the maximum temperature reached. On the other hand, in hydrochloric acid the dissolution of iron is rapidly promoted with increasing temperature, though inhibition by oxygen still takes place at any temperature. This suggests that the surface film is a kind of oxide, since it is commonly known that chloride ions promote the dissolution of oxides and passive films on metallic surfaces. Furthermore, when the pyrrhotite immersed in the oxygenated 1M HCl solution at 40°C for 23 hrs was filtered and washed with carbon disulphide, then leached in fresh 1M HCl solution, the dissolution of pyrrhotite did not resume in 2 hrs. If inhibition by oxygen resulted from sulphur formation at the surface, the washing by carbon disulphide should remove this sulphur and thereby expedite dissolution in fresh acid.

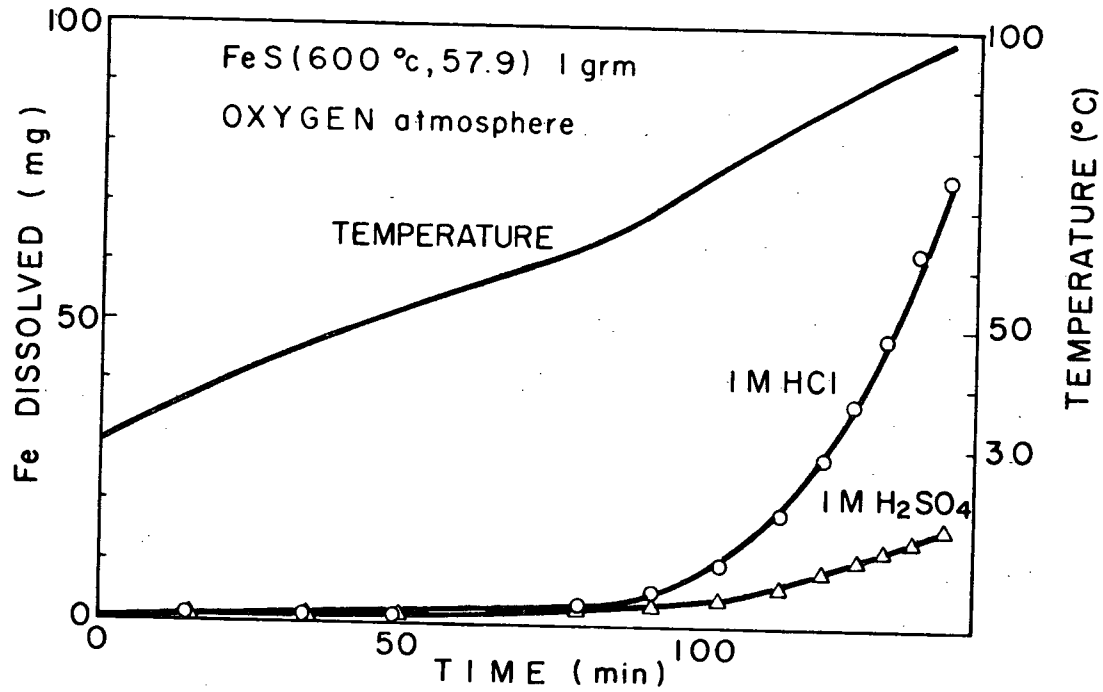

Figure 2-27. Iron dissolution from high sulphur pyrrhotite under oxygen atmosphere with increasing temperature.

2.10 Effect of imposed electrochemical potential

The electrochemical aspect of the dissolution of ionic crystals has been discussed by several workers. (63, 64, 65) It is noted that the transport of ions from the crystal ion to the solution is influenced by the potential at the crystal surface, i.e., the transport of anions is promoted by more negative potentials and that of cations by more positive potentials, accompanied by changes in the surface activities of cations and anions.

It is generally understood that the sulphide crystal possesses both ionic and covalent bonding. Therefore, the effect of imposed potential on the chemical dissolution of sulphides may be more complicated.

In this study, an H-shaped cell, which consists of two 250 ml beakers connected with a sintered glass disc, was used for the electrolytic cell. One side of the cell contained a Pt-gauze counter electrode, a gas bubbler and a gas outlet tube. The other side of the cell consisted of a sulphide working electrode, a gas bubbler, a Luggin-capillary, a solution sampling tube and a gas outlet tube.

The electrode potential was measured with the KCl saturated calomel electrode through the Luggin-capillary. All experiments were carried out under a bubbled helium atmosphere. After placing 200 ml electrolyte in two compartments, He gas was bubbled through the electrolyte for at least 30 minutes, then the potentiostatic electrolysis of the sulphide working electrode was started using a Wenking potentiostat. The electrochemical data (such as potential, current and accumulated

coulombs) were collected during electrolysis, and a 2∼3 ml aliquot of solution was sampled at selected intervals.

All experiments were undertaken at room temperature (≈ 20°C). The dissolution of metal during electrolysis was determined from slopes of the plots of metal dissolved vs time. The amount of metal dissolved under cathodic conditions was simply obtained from the analytical data. Since anodic current produces metal ions in solution, the metal dissolved by the chemical reaction was calculated (assuming Faraday's laws) from the analyzed amount of metal in solution and the amount of anodic current passed using equation (2.14);

$$[M_{diss.}] = [M_{analy.}] - \frac{Q \times M}{96500 \times n} \qquad (2.14)$$

where $[M_{diss.}]$ is the amount of metal dissolved due to the chemical reaction in grms, $[M_{analy.}]$ is the amount of metal analyzed in solution in grms, Q is number of coulombs passed anodically, M is molecular weight of metal and n is valence of metal ion.

In Figure 2-28, the results on the natural Chichibu pyrrhotite are shown. The dissolution rate of iron was transformed into current density units based on Faradays laws for equivalent anodic processes, so that comparisons with the electrolytic current density could be made. According to Fig. 2-28, it is noted that the anodic current density and the dissolution rate during anodic electrolysis are negligible in the potential region studied, but that cathodic potential led to large dissolution rates

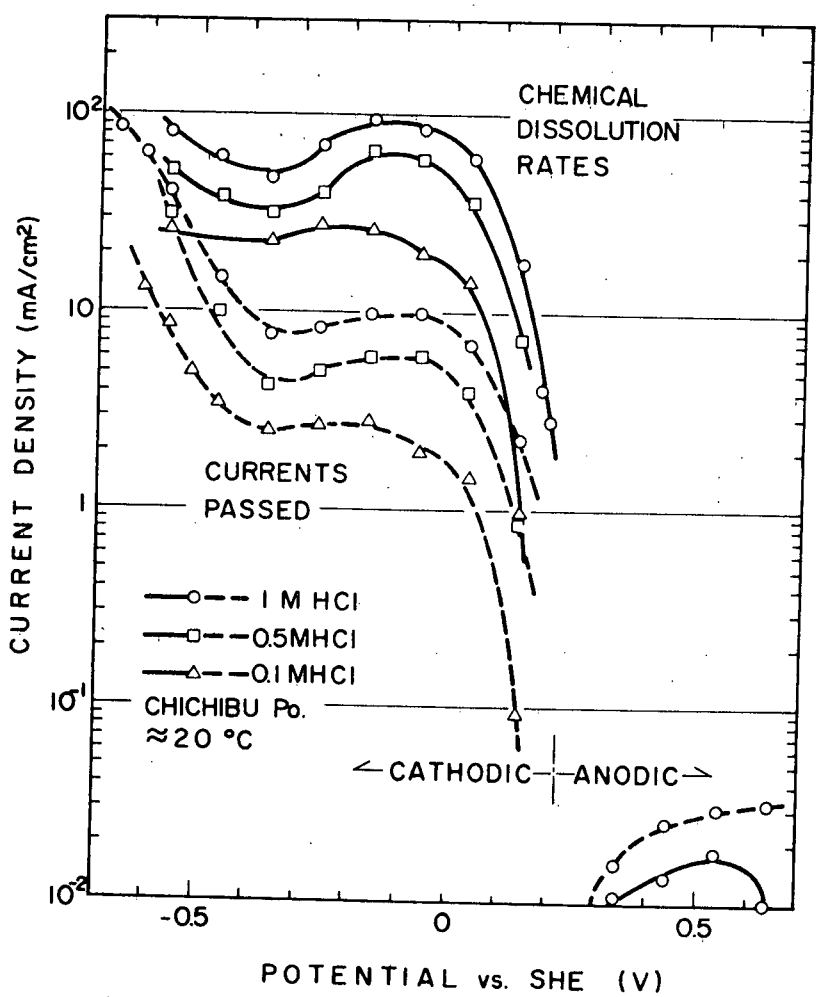

Figure 2-28. Current and dissolution rate versus imposed potential on Chichibu pyrrhotite.

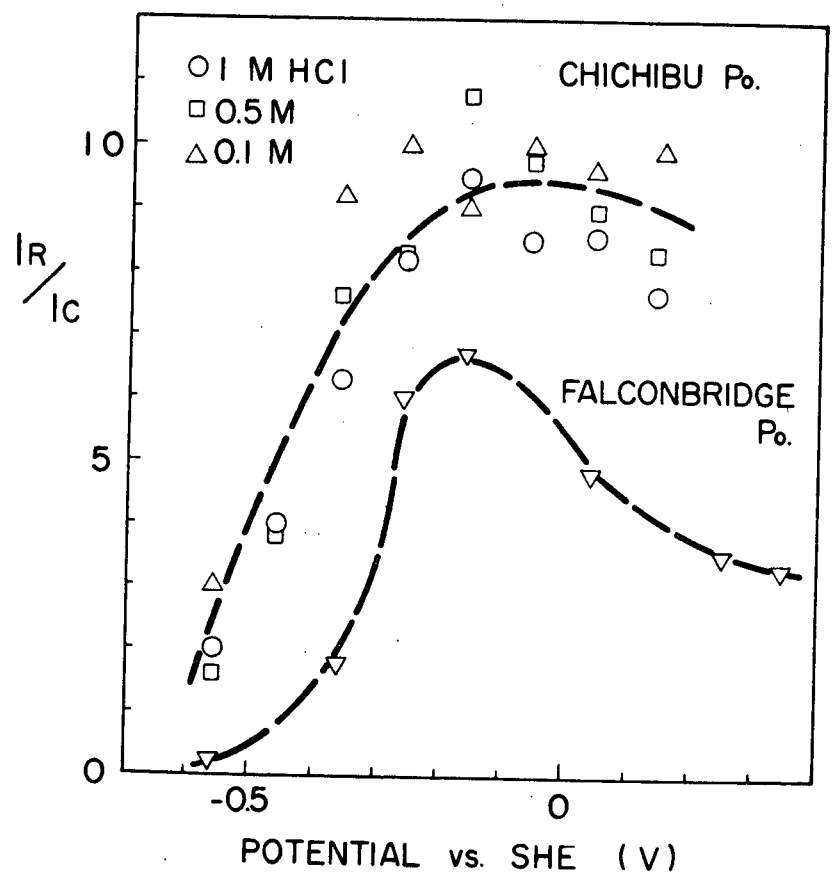

Figure 2-29. Variation in I_R/I_C ratio with imposed potential in cathodic region for Chichibu and Falconbridge pyrrhotites.

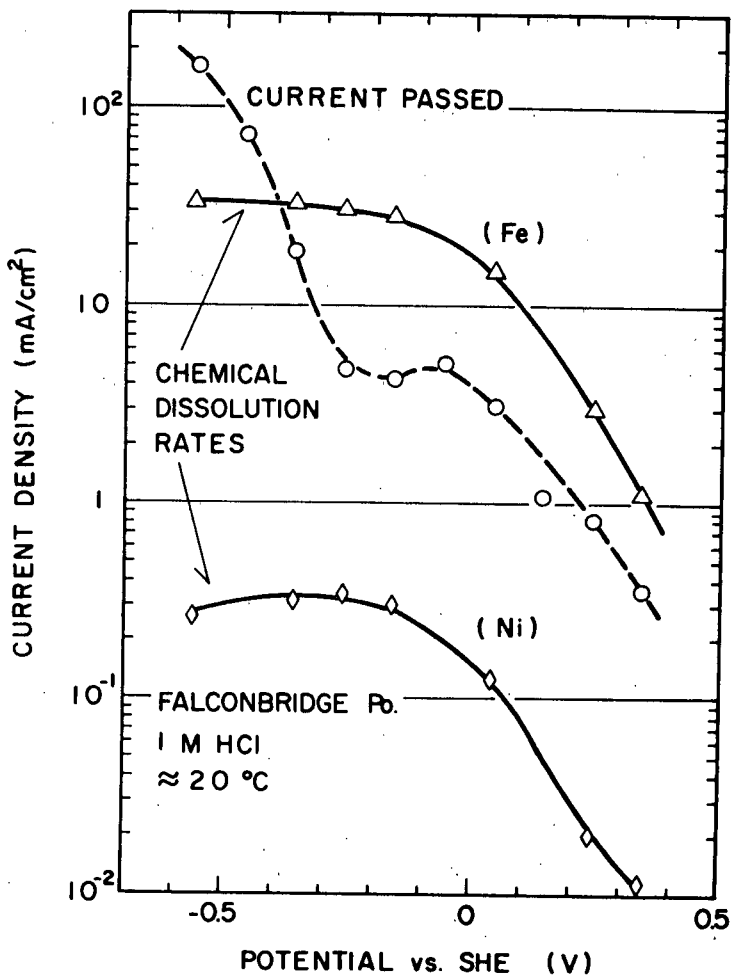

Figure 2-30. Current and dissolution rate versus imposed potential on Falconbridge pyrrhitite.

and current densities. Furthermore, in the cathodic range of +0.2 ~ - 0.6V (vs. S.H.E.), the dissolution rate of iron is in general much larger than that an equivalent anodic current density would yield by Faradays laws. The ratios of the dissolution rate of iron in equivalent anodic current to the observed cathodic current are plotted against potential in Figure 2-29. The ratios sharply decrease below -0.4 V, presumably due to simultaneous hydrogen discharge. The data are too scattered to permit any conclusions regarding the effect of acid concentration, except that it is small.

Figure 2-30 represents the cathodic polarization curve and the dissolution rate of Falconbridge nickeliferrous pyrrhotite in 1M HCl solution. The dissolution rates of both iron and nickel were obtained, and were found to have a ratio of approximately 100, which reflects the nickel content of the pyrrhotite phase. It is noted that the results in this figure are similar to those in Fig. 2-28. The ratios of the dissolution rate of iron to the cathodic current are also plotted in Fig. 2-29 with those for Chichibu pyrrhotite and are found to be somewhat smaller than those obtained for the latter, but the maximum ratio for both minerals appears at the same voltage, about - 0.15 V.

The same experiments were carried out in 1M HCl solution using natural pyrite; FeS_2. The results are shown in Figure 2-31. Though a significant difference in reactivity between two pyrite electrodes is observed, it is noted that above -0.2 V the cathodic currents are smaller than those obtained in the pyrrhotites and below - 0.2 V a rapid

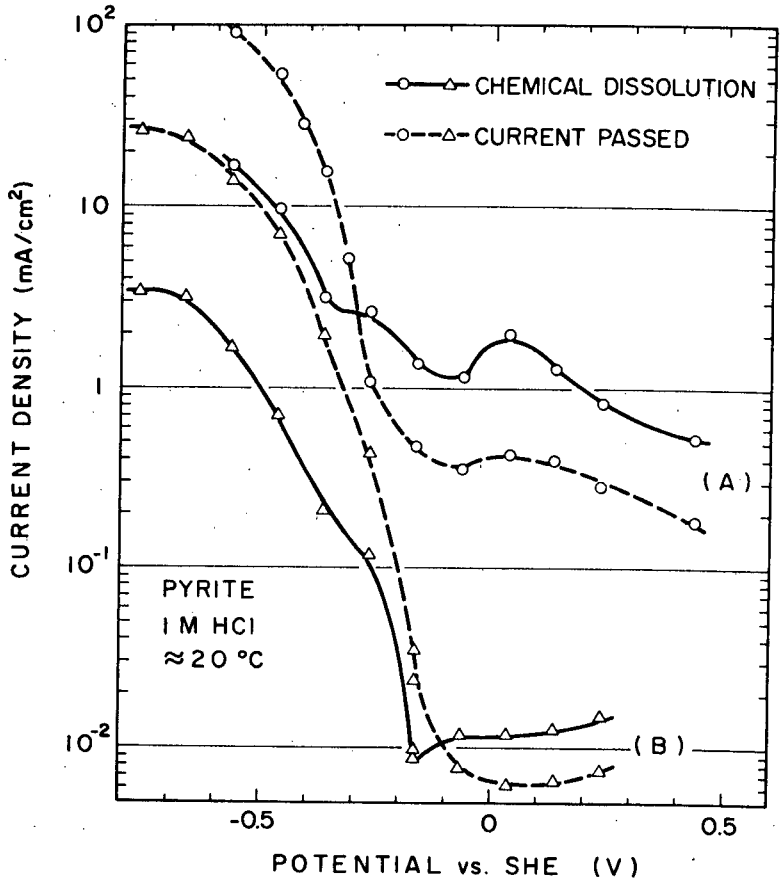

Figure 2-31. Current and dissolution rate versus imposed potential on pyrite.

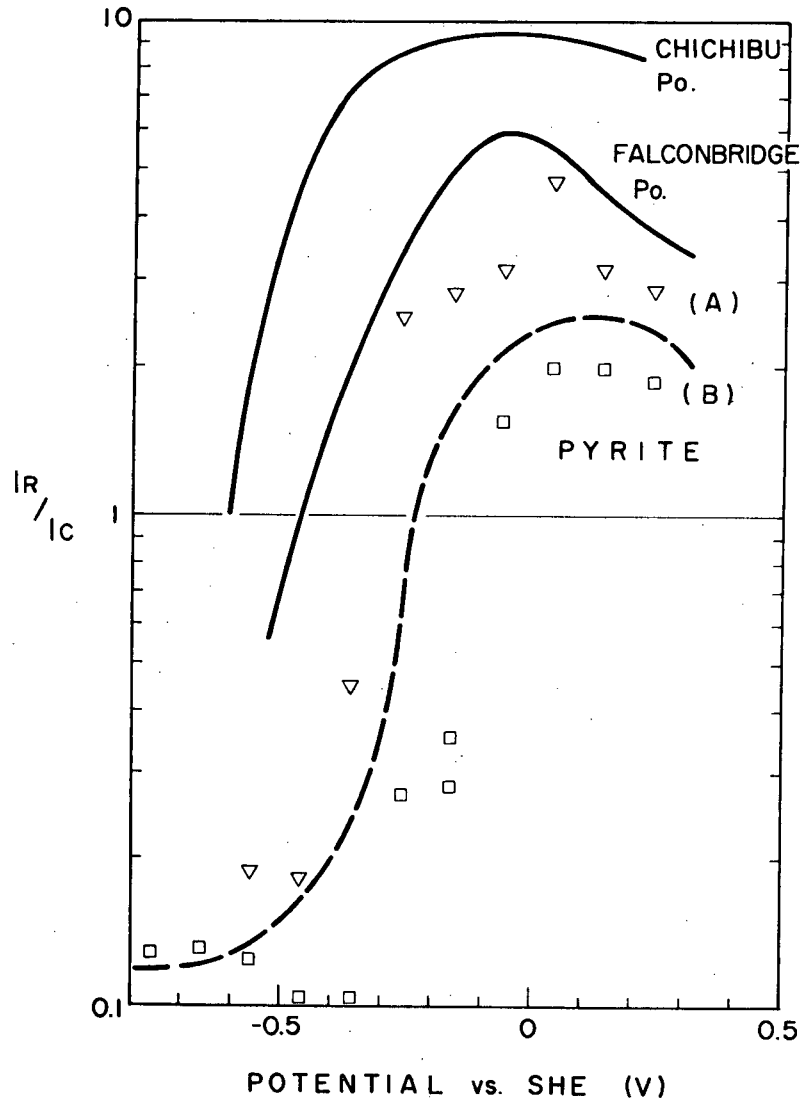

Figure 2-32. Variation in I_R/I_C ration with imposed potential for pyrite and pyrrhotites.

increase in the cathodic current with potential is observed. Meanwhile, the chemical dissolution rate follows the shape of the polarization curve. The sharp increase in dissolution rate below - 0.2 V was not observed in the pyrrhotite case. In addition, chemical analysis of the out-let gas from the cell resulted in the detection of H_2S only when the potential was set below - 0.2 V.

In Figure 2-32, the ratios of the chemical dissolution rate to the cathodic current are plotted and seen to be smaller than those for the pyrrhotites at all potentials. A sharp drop is observed for this ratio around - 0.20 $\sim$ - 0.15 V for both pyrite and pyrrhotites.

According to Engell (65), when an ionic crystal is subjected to an electrochemical potential, the chemical dissolution rate of the crystal depends on the imposed potential, and its dependence is expressed by the equations;

$$\frac{d \ln r}{d E} = (\alpha_A |Z_A| - \alpha_B |Z_B|) \frac{F}{2RT} \qquad (2.15)$$

$$= (|Z_A| - \alpha_B |Z_B|) \frac{F}{RT} \qquad (2.16)$$

$$= (\alpha_A |Z_A| - |Z_B|) \frac{F}{RT} \qquad (2.17)$$

where r is a dissolution rate of an ionic crystal, E is potential, α_A, α_B are transfer coefficients for the cation (A) and the anion (B), respectively, Z_A, Z_B are valences for the cation (A) and the anion (B), respectively, F is Faraday constant, R is the gas constant and T is temperature (^{o}K). Equation (2.15) is applied on the case where the

transports of both anion and cation are combined in the rate determining step, while for rate-control by the anion transport equation (2.16) applies and for the cation transport equation (2.17) is applicable.

From the data in Fig. 2-28 and 30, the values of $d \ln r/dE$ for the pyrrhotites are calculated; yielding values of -30 and -10 for Chichibu and Falconbridge natural pyrrhotites, respectively. For pyrrhotite, $|Z_A| = |Z_B| = 2$ and $0.3 < \alpha_A, \alpha_B < 0.7$ (assumed); therefore, a value of -30 for Chichibu pyrrhotite is consistent with equation (2.17) and a value of -10 for Falconbridge pyrrhotite more consistent with equation (2.15)

Meanwhile, pyrrhotite, when it is cathodized, forms hydrogen sulphide according to the equation;

$$Fe_{1-x}S + 2y\,H^+ + 2y\,e \longrightarrow Fe_{1-x}S_{1-y} + y\,H_2S \qquad (2.18)$$

The new pyrrhotite phase, $Fe_{1-x}S_{1-y}$, may dissolve chemically;

$$Fe_{1-x}S_{1-y} + 2(1-x)H^+ \longrightarrow (1-x)Fe^{++} + (1-x)H_2S + (x-y)S \qquad (2.19)$$

with a larger dissolution rate than that of the $Fe_{1-x}S$ phase. The ratio of the chemical dissolution rate to the cathodic current is then expressed by the following equation;

$$\frac{I_R}{I_C} = \frac{2(1-x)}{2y} = \frac{1-x}{y} \qquad (2.20)$$

In general, for natural pyrrhotite the value (1-x) varies from 1 to 0.875.

The values obtained for I_R/I_C (shown in Fig. 2-29) are about 9 for Chichibu pyrrhotite and 3.5 ~ 7 for Falconbridge pyrrhotite. Values of 7 ~ 9 are reasonable considering the above factors, when $y \approx x$. Furthermore, the close resemblance between the dissolution curve and the cathodic polarization curve as a function of potential is more understandable in terms of this explanation than by means of Engell's equations.

For pyrite, the dependence of the dissolution rate on potential may be interpreted as the cathodic reduction of sulphur in the pyrite phase, because significant dissolution of pyrite was observed only when H_2S evolution by a cathodic current occurred. The potential below - 0.2 V, at which H_2S evolution occurs, is low enough to evolve hydrogen as well. Therefore, the ratio of the chemical dissolution rate to cathodic current is very small compared with ratios of the pyrrhotites. On the other hand, below - 0.2 V the pyrrhotite phase becomes iron saturated and probably discharges hydrogen; therefore, no equivalent further increase in the chemical dissolution rate was observed.

3. General Discussion

The acid decomposition reaction of sulphides proceeds through the following simple steps:

(1) Diffusion of hydrogen ions from the bulk solution to the solid-liquid interface,

(2) Reaction between hydrogen ions and sulphur species at the solid-liquid interface,

(3) Diffusion of reaction products, HS^- or H_2S and metal cations from the reaction sites to the bulk solution.

According to the reaction models by Ingraham (12) and Locker (21), which were mentioned in Chapter I, the reaction occurs at the sulphide-solution interface. However, when a sulphide has a very high decomposition rate, the dissociation of the solid may occur first with subsequent reaction between hydrogen ions and sulphide ions in the vicinity of the solid surface. In this case, the reaction between hydrogen ions and sulphide ions is in general, fast because of a homogeneous reaction. Therefore, the transport of hydrogen ions from the bulk solution to the sulphide ions or the transport of reaction products from the vicinity of the surface of the solid to the bulk solution will be the slowest step for the reaction.

To account for the results in the dissolution of iron sulphides, the transport of hydrogen ions cannot be the slowest step in the process, because firstly the dissolution rate depends on the composition of solid phase, which does not seem to influence the transport process of hydrogen ions, and secondly the estimated rate for the hydrogen ion diffusion controlled reaction is approximately 10^{-5} moles/sec. cm^2 for a hydrogen ion concentration of 1 M (21), and the maximum rate for pyrrhotite under the same conditions is estimated to be about 10^{-9} moles/sec. cm^2.

The transport of reaction products, which are ferrous ions and sulphide species of HS^- or H_2S, also does not seem to control the

reaction rate, since ferrous ions in solution do not affect the dissolution rate up to a concentration of 10^{-1} M, and the hydrogen sulphide in solution does not slow the dissolution rate linearly as would be expected in a reaction controlled by the transport of products from the reaction zone to the bulk solution. Therefore, the dissolution rate of pyrrhotite must be controlled by the chemical reaction on the pyrrhotite surface under the conditions employed in this study. The term "the chemical reaction" refers to general processes involved in the heterogeneous reaction, including adsorption of reactants, surface chemical reactions and desorption of products.

This chemical reaction controlled dissolution of pyrrhotite is consistent with a value of 9.8 Kcal/mole for the activation energy obtained from pyrrhotite dissolution kinetics. Locker, et al. (21) claimed that the dissolution of II-VI compounds (ZnS, ZnSe, CdS and ZnS + CdS) is controlled by the slow adsorption step of hydrogen ions on the solid surface, as mentioned in Chapter I. From the present work on pyrrhotite, the identification of the rate determining step from the three mentioned processes can not be made. However, the parameters, which promote the dissolution of pyrrhotite, are listed as;

(1) a low excess sulphur in pyrrhotite,

(2) a high concentration of hydrogen ion in solution,

(3) a high concentration of chloride ion at high acid concentration,

(4) a low imposed potential by electrochemical means or chemical redox environments.

On the other hand, the parameters to suppress the dissolution of pyrrhotite are;

(1) a high excess sulphur content in pyrrhotite,

(2) a high concentration of chloride ion at low acid concentration,

(3) the presence of cations in solution forming sulphide precipitates less soluble than pyrrhotite,

(4) hydrogen sulphide in solution,

(5) a high imposed potential; that is, an oxidizing environment.

CHAPTER III

ACID DECOMPOSITION OF COMPOUNDS IN THE Fe-Ni-S SYSTEM

This chapter describes the work done to investigate the selectivity of the acid decomposition reaction on the compounds in the Fe-Ni-S system. This work is ultimately applicable to acid decomposition reactions on pyrrhotite ores and nickel concentrates, since they consist mainly of the minerals in the ternary Fe-Ni-S system.

1. Experimental

The experimental method is the same as that used and described in Chapter II. In addition, a Debye-Scherrer camera was used to take powder diffraction patterns for identification of the phases present in the starting materials.

The compounds covered in this study were synthesized from mixtures of iron and nickel powders under atmospheres of H_2S-H_2 mixed gases of different H_2S/H_2 ratios in order to control the sulphur activity in the compounds. In Figure 3-1, the region in the Fe-Ni-S system, which was covered in this work, is schematically described by broken lines. The numbers in the figure represent;

(1) Fe-S system (600°C, $PH_2S/PH_2 = 0.001 \sim 57.9$),

(2) Ni-S system (600°C, $PH_2S/PH_2 = 0.001 \sim 57.9$),

(3) Fe-Ni-S system (Fe = Ni = 1 = 1)(600°C, $PH_2S/PH_2 = 0.001 \sim 57.9$),

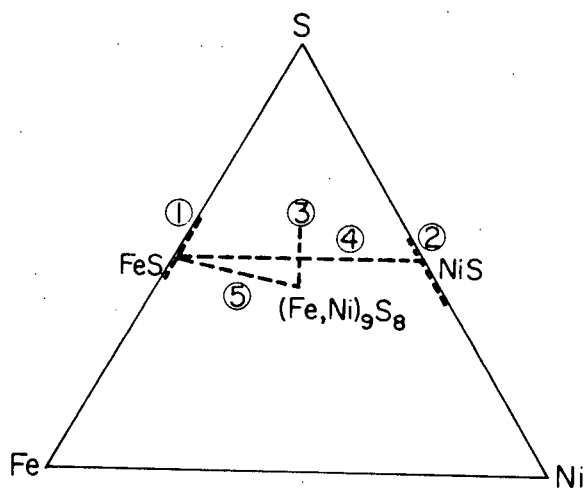

Figure 3-1. Schematic presentation of regions studied in Fe-Ni-S system.

(4) FeS-NiS system (600°C, $PH_2S/PH_2 = 1$),

(5) FeS - $(FeNi)_9 S_8$ system (600°C, $PH_2S/PH_2 = 0.001$).

2. Results and Discussion

2.1 Dissolution of compounds in the Fe-S system

The initial dissolution rate for the compounds in the Fe-S system was calculated from the data presented in Fig. 2-2 in 0.1 M HCl at 30°C. The rate data are plotted against the H_2S/H_2 ratio of the atmosphere under which the compounds were synthesized at 600°C for 24 hrs, in Figure 3-2 (reproduced from Fig. 2-10). According to thermodynamic data presented by T. Rosenqvist (66), in the range from 0.001 to 57.9, H_2S/H_2 ratios at 600°C the phases expected are $Fe_{1-x}S$ close to the stoichiometric composition of FeS at the lower end of this range and $Fe_{1-x}S$ ($x \approx 0.14$), which co-exists with pyrite at a H_2S/H_2 ratio of 57.9 at 600°C. The influence of the excess sulphur content in pyrrhotite on the acid decomposition rate is evident from the figure, the rate change being 50 fold for an H_2S/H_2 ratio decrease from 57.9 to 0.001. The dotted lines in Fig. 3-2 represent the changes in the activities of iron and stoichiometric FeS estimated from the thermodynamic data by P. Toulmin, et al. (67) and K. Niwa (68) plotted in arbitrary units. The curve of the dissolution rate does not correlate with either the a_{Fe} or the a_{FeS} line. This means that the dissolution rate constant of pyrrhotite is not a simple function of the thermodynamic properties of the solid phase at synthesis conditions.

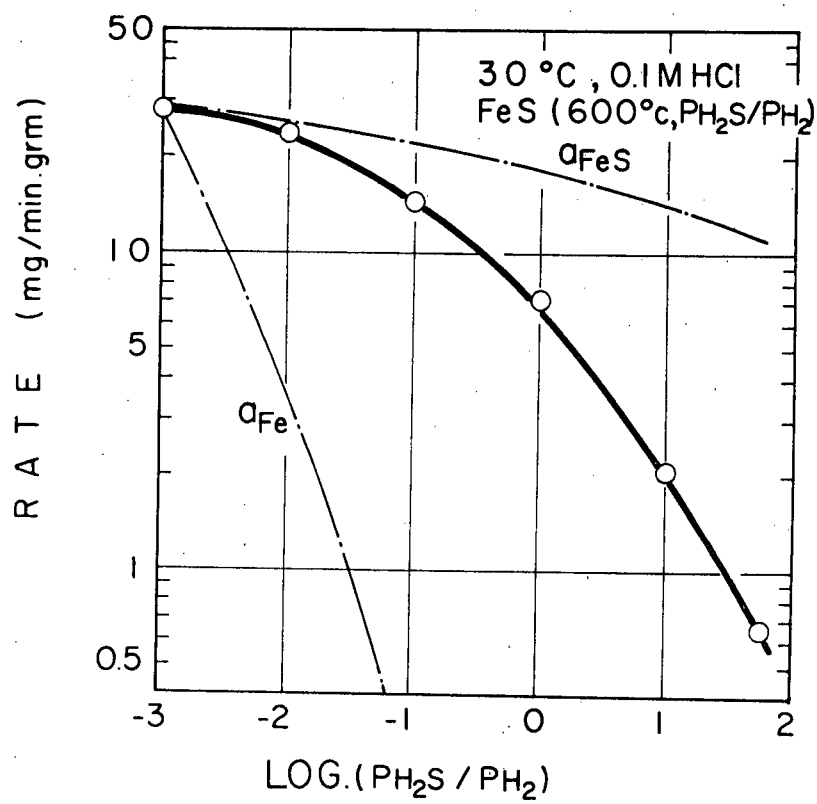

Figure 3-2. Dissolution rates versus sulphur activity of pyrrhotites. The activities of FeS and Fe in the pyrrhotite are shown in arbitrary scale.

2.2 Dissolution of compounds in the Ni-S system

The dissolution rates of the Ni-S compounds in 0.5 M HCl solution at 40°C are compared in Figure 3-3. These are much slower than those of the equivalent Fe-S compounds. According to thermodynamic data by Rosenqvist, in the range of 0.001 to 57.9 of PH_2S/PH_2 ratio at 600°C the stable phases are: $Ni_3S_{2\pm x}$ ($x \approx -0.17$) for the lower end of the range, and $Ni_{1-x}S$ ($x \approx 0.05$) for the high sulphur end, (very close to the $Ni_{1-x}S$ - NiS_2 two phase boundary). The dissolution behaviour of these sulphides is different from that of the Fe-S materials and may reflect the presence of different phases in this system. The dissolution rate in the $Ni_3S_{2\pm x}$ region shows a minimum around the composition of Ni_3S_2 and deviations in both directions from the stoichiometric composition of Ni_3S_2 seem to increase the dissolution rate of nickel from these compounds. On the other hand, in the $Ni_{1-x}S$ region the dissolution rate has a maximum value around the stoichiometric composition of NiS and small deviations from this composition do not decrease the dissolution rate; however, large decreases in the dissolution rate of this phase correlate with substantial deviations from the H_2S/H_2 ratio in equilibrium with the stoichiometric NiS material.

2.3 Dissolution of the compounds in the Fe-Ni-S system

The phases with equimolar ratio of Fe to Ni were synthesized under controlled sulphur activity atmospheres at 600°C by the same method described previously. These compounds were leached in

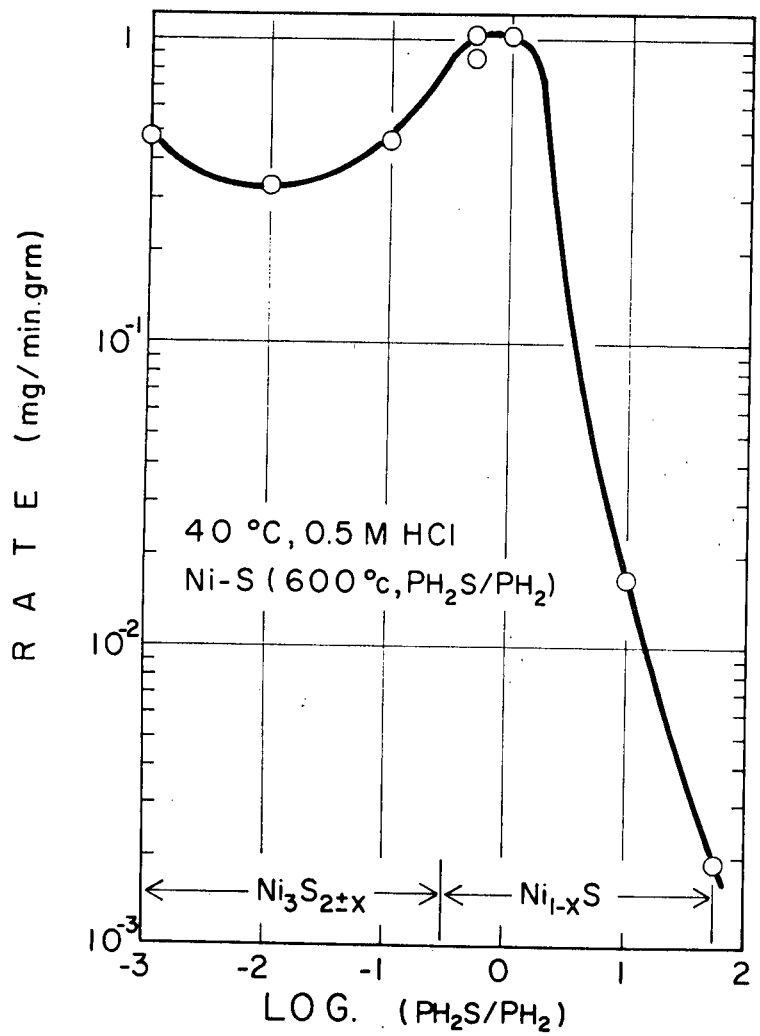

Figure 3-3. Dissolution rates versus sulphur activity of various phases in the Ni-S system.

0.1 M HCl at 30°C. The increase in the concentration of Fe and Ni in solution was found to be linear with time and the molar ratio of Fe to Ni ion was unity for all compounds examined. In Figure 3-4, the analytically determined dissolution rates of these compounds in 0.1 M HCl at 30°C is plotted against the synthesis PH_2S/PH_2 ratio. According to these data, up to a PH_2S/PH_2 ratio of 0.01, pentlandite, $(FeNi)_{9\pm x}S_8$ dissolves faster than other compounds and the dissolution rate of pentlandite decreases as the sulphur activity increases. When the phase, $(NiFe)_{1-x}S$ starts appearing, the dissolution rate drops sharply and further increases in sulphur activity lead to further decreases in the dissolution rate. The material synthesized at $PH_2S/PH_2 = 57.9$ was virtually insoluble under the applied leaching conditions.

2.4 Dissolution of the compounds of $Fe_{1-x}S$ and $Ni_{1-x}S$

The phases $Fe_{1-x}S$ and $Ni_{1-x}S$ form a monosulphide solid solution (M.s.s.), i.e., $(FeNi)_{1-x}S$, for all ratio of Fe to Ni in the temperature range between about 950°C and about 275°C, as mentioned in Chapter I. This solid solution is not stable below the lower limiting temperature; however, low phase transformation rates lead to metastable retention of the higher temperature phase at room temperature for ordinary laboratory experimental time periods.

Powdered $Fe_{1-x}S$ and $Ni_{1-x}S$ ($-$ 325 mesh) were mixed in appropriate ratios and heat-treated at 600°C under a PH_2S/PH_2 ratio of unity for 24 hrs. After synthesis, the powder mixture was air-cooled

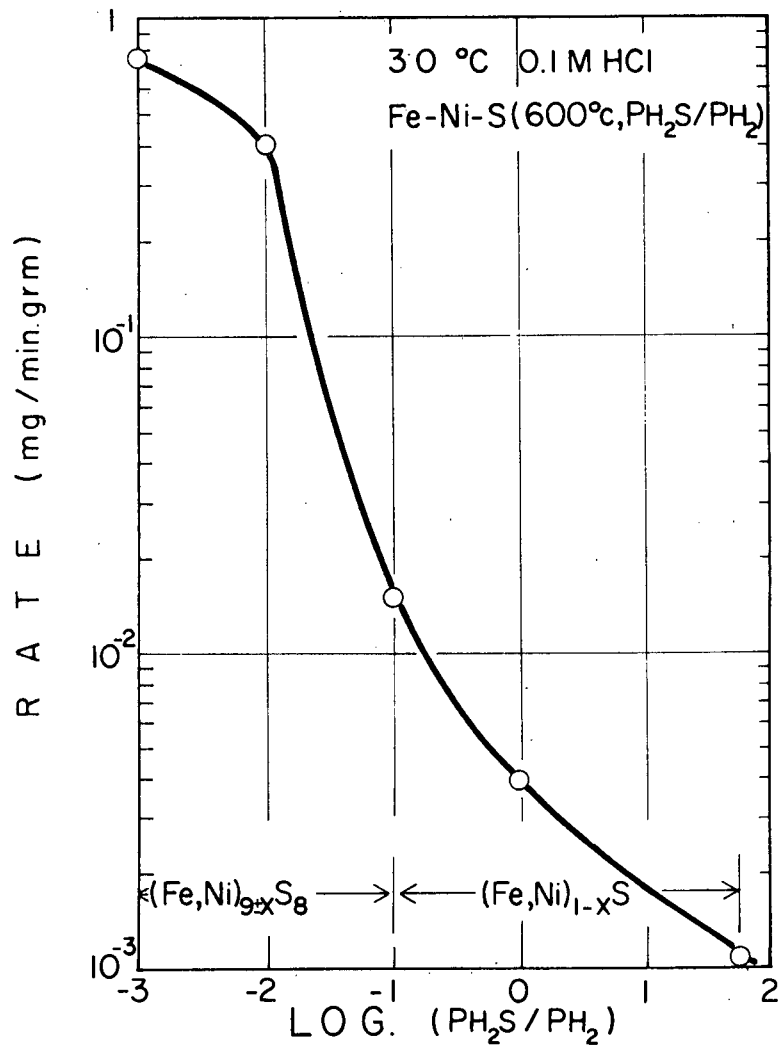

Figure 3-4. Dissolution rates versus sulphur activity of various phases in (Fe:Ni=1:1)-S system.

to the room temperature and used for leaching tests. In each leaching experiment, no preferential dissolution of either iron or nickel occurred and the ratio of iron to nickel dissolved was equal to that in the solid phase.

In Figure 3-5, the dissolution rates for iron and nickel are plotted against mole fraction of $Ni_{1-x}S$ in the mixture. The dissolution rate for $Fe_{1-x}S$ and $Ni_{1-x}S$ was measured using powder sized between 200 and 325 mesh synthesized under the same conditions. The M.s.s. material dissolved much more slowly than either of the limiting phases, and falls to a minimum value at around 0.7 of $Ni_{1-x}S$ mole fraction. The composition of the system at this rate minimum can be correlated with a discontinuity in the spacing of the (102) plane as observed by Shewman, et al. (45)

2.5 Dissolution of pyrrhotite co-existing with pentlandite

Pyrrhotite forms a homogeneous solid solution with nickel up to a maximum somewhere between 0.5 and 1 atomic percent nickel at room temperature, and above this limiting nickel content normally equilibrates with a pentlandite phase, as observed in nature. In this section, the effect of the nickel content of pyrrhotite on the dissolution of pyrrhotite was investigated. The addition of nickel to pyrrhotite was made by mixing the pyrrhotite powder (+ 200 mesh) and the $(FeNi)_{1-x}S$ powder (− 325 mesh) at the desired ratios, and annealing them at 600°C for 24 hrs under an atmosphere of $PH_2S/PH_2 = 0.01$. Under this

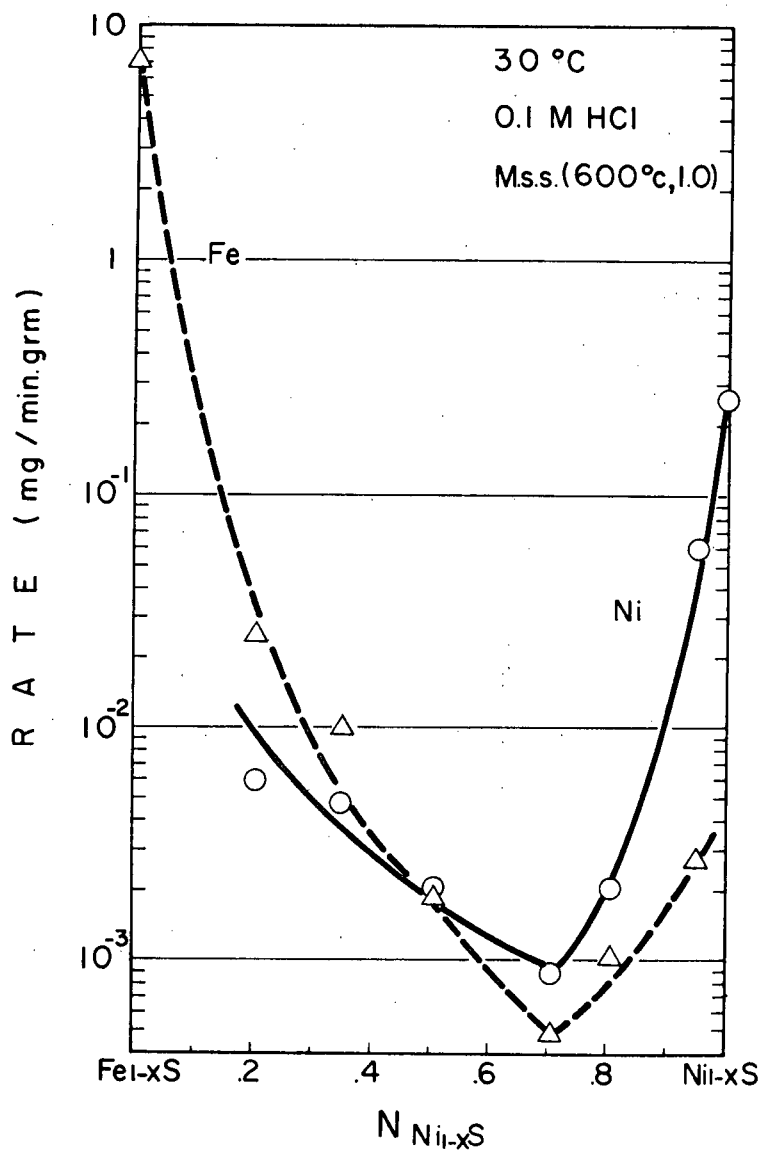

Figure 3-5. Dissolution rates versus mole fraction of $Ni_{1-x}S$ of monosulphide solid solution.

condition of synthesis, the excess nickel, if present, forms the pentlandite phase with pyrrhotite saturated with nickel. After furnace cooling the synthesized sample, the usual dissolution runs were carried out at 30°C in 0.1 MHCl solution. The amounts of iron and nickel dissolved were analyzed at certain intervals and the dissolution rates for each metal were determined.

The results are shown in Figure 3-6. The initial dissolution rate of the pyrrhotite is not changed with up to 0.5 at % nickel, but is distinctly lower at 1.25 at % nickel and higher to about 75% of the initial dissolution rate. The nickel dissolution rate rises with nickel content of the pyrrhotite as expected, but at higher nickel contents than 2.5 at % this rate levels off. Since, according to the data in Fig. 3-2 and 3-4, the pentlandite dissolves 60 times slower than the pyrrhotite under the same sulphur activity, it can be assumed that the measured dissolutions of nickel and iron are overwhelmingly due to the dissolution of the pyrrhotite phase in the mixture. Only when the maximum solubility of nickel in the pyrrhotite is exceeded, would pentlandite exist, and with further increases in nickel in the prepared material an increase in the dissolution rate of nickel cannot be expected without dissolution of pentlandite.

In the upper part of Figure 3-6, the ratio of the molar dissolution rate of iron to that of nickel is compared with the molar ratio of iron to nickel in the mixed powder. According to the results, the discrepancy between these two ratios starts at around 1.25 at % nickel.

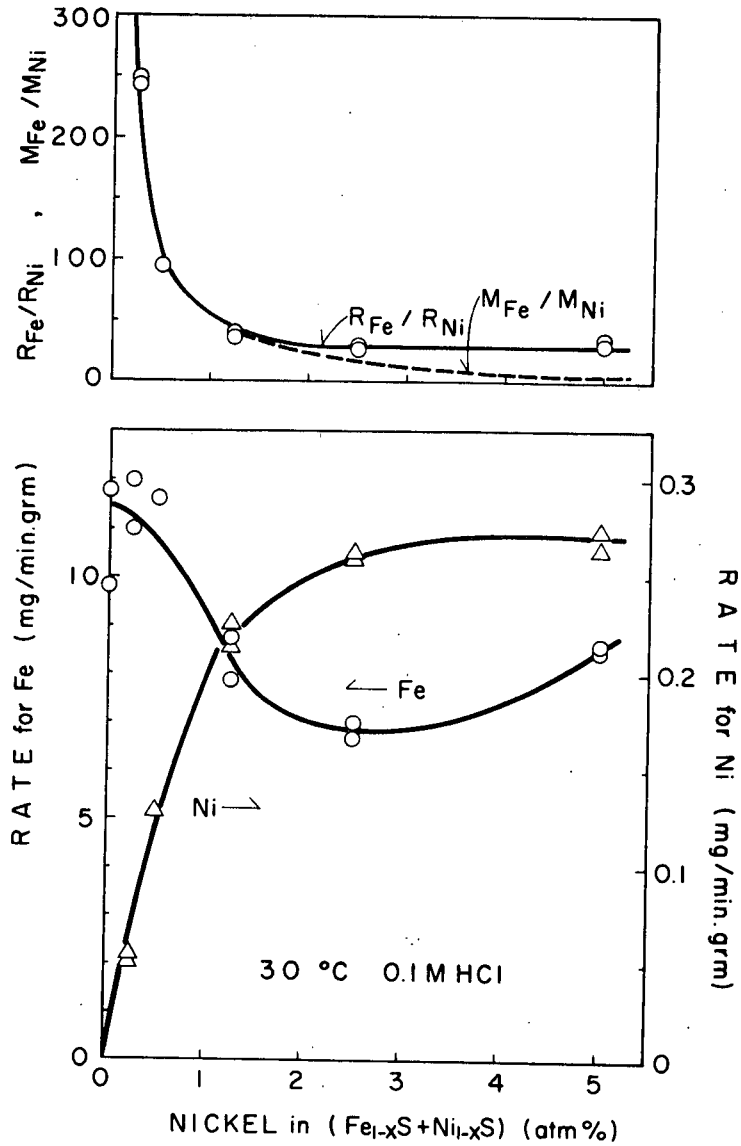

Figure 3-6. Dissolution rates of iron and nickel, the ratios of the rates, and the atomic ratio of iron and nickel versus atomic percent nickel in mixture of pentlandite and pyrrhotite.

Therefore, it can be concluded that 1.25 at % nickel is close to the maximum solubility of nickel retained in pyrrhotite synthesized at 600°C under an atmosphere of $PH_2S/PH_2 = 0.01$.

In general, the maximum solubility of nickel in natural pyrrhotite was found to be less than 1 at % (see Chapter I). However, a general increase in solubility with temperature between phases in alloy systems is observed, and an increase in solubility of nickel in the pyrrhotite at 600°C would be expected on these grounds.

2.6 Inhibition effect of oxidant on the Fe-Ni-S compounds

As mentioned in the previous chapter, the dissolution of pyrrhotite is heavily inhibited in the presence of oxidant in solution. The inhibition effect by oxidant on the compounds in the Ni-S and Fe-Ni-S systems was also investigated using oxygen.

The phase $Ni_3S_{2\pm x}$ synthesized at 600°C under an atmosphere of $PH_2S/PH_2 = 0.01$ was leached in 1 M HCl and H_2SO_4 solutions at 40°C under helium, oxygen and helium atmospheres, sequentially. The results are shown in Figure 3-7. The initial dissolution of nickel is accelerated by the introduction of oxygen into solution, but later it declines and practically stops after 25 minutes in 1 M H_2SO_4 solution and after 145 minutes in 1 M HCl solution. The subsequent introduction of helium displacing the oxygen leads to resumption of dissolution after an induction period (longer in sulphuric acid than in hydrochloric acid).

In Figure 3-8, the results on $Ni_{1-x}S$ synthesized at 600°C

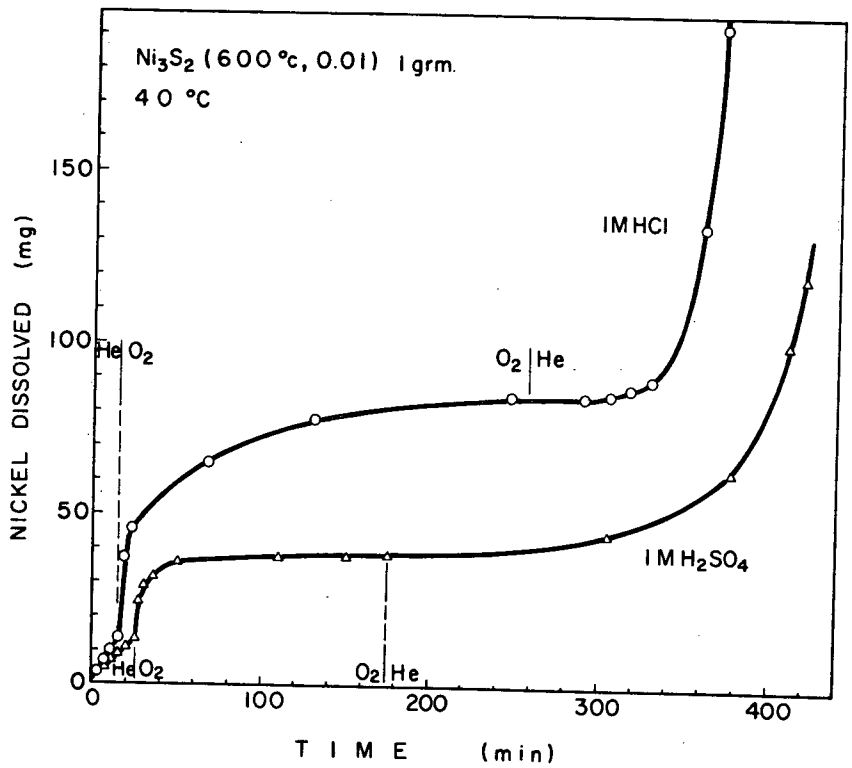

Figure 3-7. Dissolution of nickel from $Ni_3S_{2\pm x}$ under helium and oxygen atmospheres.

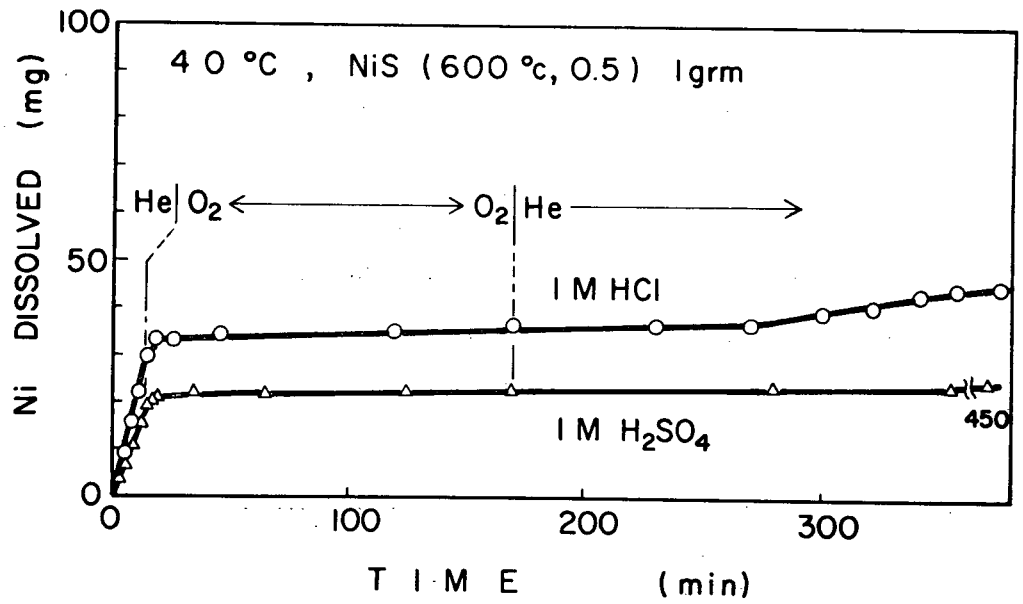

Figure 3-8. Dissolution of nickel from $Ni_{1-x}S$ under helium and oxygen atmospheres.

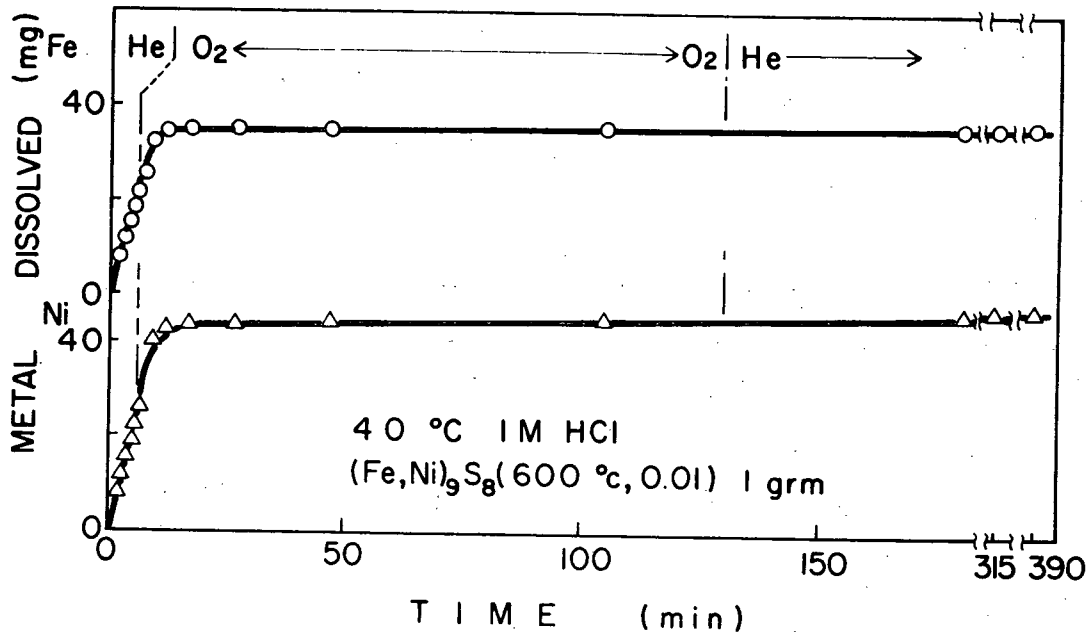

Figure 3-9. Dissolution of iron and nickel from $(FeNi)_9S_8$ under helium and oxygen atmospheres.

under an atmosphere of $PH_2S/PH_2 = 0.5$ are shown. In this case, the initial dissolution of nickel stopped as soon as oxygen was introduced and the reactivation of the sulphide did not occur in the experimental period after helium was re-introduced into the solution.

The results in Figure 3-9, are on pentlandite with equimolar nickel and iron synthesized at 600°C under an atmosphere of $PH_2S/PH_2 = 0.01$, in 1 M HCl solution at 40°C. The initial dissolution of nickel is briefly accelerated and then stopped by the introduction of oxygen. The iron dissolution rate is similar, although the brief acceleration of dissolution appears to be missing. The re-introduction of helium gas in the system does not reactivate the pentlandite surface within an experimental period of 260 minutes.

From these data, it can be concluded that the passivation films formed by oxygen during dissolution are more stable on $Ni_{1-x}S$ and on pentlandite, $(NiFe)_9S_8$, than on $Ni_3S_{2\pm x}$.

3. General Discussion

The acid dissolution rates of phases in the Fe-Ni-S system (synthesized at 600°C) in 0.1 M HCl solution at 30°C are summarized in Figure 3-10. Phases in the Ni-S binary system were not studied at 30°C in 0.1 M HCl solution and so were assigned rates corresponding to one-tenth of the measured rates at 40°C in 0.5 M HCl solution. The approximate iso-dissolution rate lines were then drawn on a portion of the ternary phase diagram in this figure. For the simplifica-

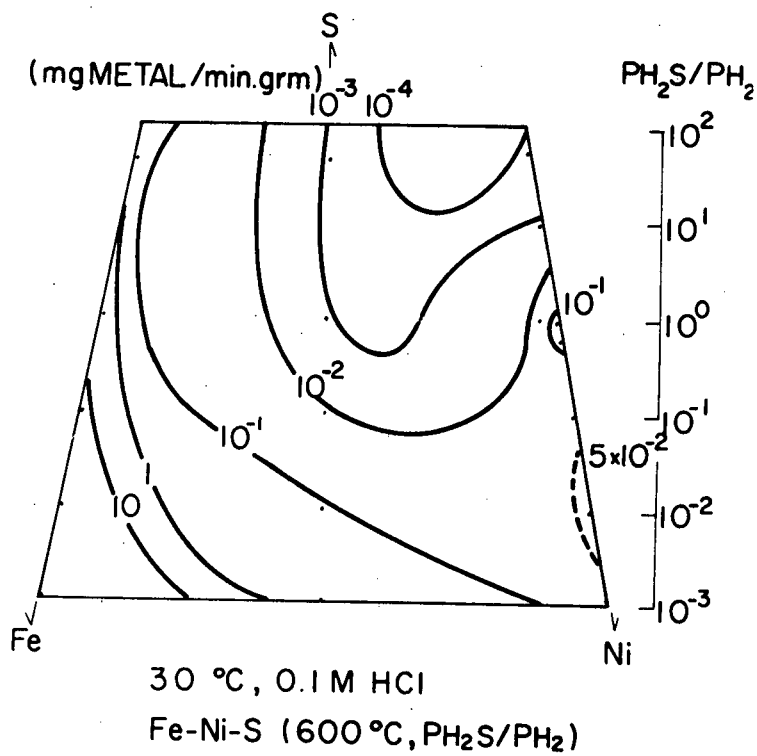

Figure 3-10. Iso-rate contours for the acid decomposition of the phases in the condensed Fe-Ni-S system.

tion, the phase relations were not considered and the sulphur activity (PH_2/PH_2 ratios at synthesis temperature) was employed instead of the sulphur composition. From this schematic diagram, it can be seen that the dissolution rate ranges from 10 to 10^{-4} (mg M^{++}/min. grm), the high rate region lying along the Fe-S system and the low rate region dominating the high sulphur and middle part of the diagram.

The application of the results in Fig. 3-10 to natural mineral assemblages must be carefully done because the results were obtained on compounds synthesized at 600°C and the phase relations at 600°C are different from those of natural assemblages. However, the results can be directly applied to heat treated ores and pyrometallurgically produced sulphides in this system at around this temperature.

The low rate region, which dominates the mid-section of the high sulphur area, can be interpreted qualitatively in terms of FeS activities based on composition. S.D. Scott, et al. (69) found that the activity of FeS in the monosulphide solid solution at 930°C deviates negatively from Raoult's law. Therefore, the dissolution rates of the monosulphide solid solution are lower than those expected from the rates of pure $Fe_{1-x}S$ and $Ni_{1-x}S$ phases. However, this interpretation cannot explain why the minimum rate in the M.s.s. phase range is three orders of magnitude smaller than that of the pure phase while the activity change of FeS in the M.s.s. phase is only one order lower. The activity coefficient, (a_{FeS}/N_{FeS} in M.s.s.), ranges from 0.7 to 0.9 for compositions of the M.s.s. phase between 7 and 40 at % Ni.

The compounds of the Ni-S and Fe-Ni-S systems are also susceptible to inhibition by oxidants. Therefore, the presence of these oxidants must be avoided for the purpose of acid dissolution of these minerals and compounds. The inhibition can be accounted for by mechanisms similar to that of pyrrhotite in view of the similarity in chemical properties of iron sulphides and nickel or (nickel + iron) sulphides.

CHAPTER IV

DISSOLUTION OF NICKEL CONCENTRATE IN ACID SOLUTION

It is evident from the results on the acid decomposition of the synthetic sulphide phases in the Fe-Ni-S system, that differences in rate for different compositions are fairly large so that the upgrading of sulphide concentrates consisting of pyrrhotite and pentlandite might be possible by selecting proper conditions for such acid decomposition reactions. Specifically, acid solutions of the appropriate concentration apparently dissolve pyrrhotite at a significant rate while pentlandite and other sulphides (i.e., chalcopyrite, pyrite, and gangue) should remain essentially undissolved.

The upgraded residues after the dissolution of pyrrhotite are both suitable and desirable for known nickel processes, since no valuable components are eliminated. At the same time the pregnant leach solution from which hydrogen sulphide has been stripped, contains ferrous salts which can be the source of various iron compounds as determined by further treatment of the solution.

1. Experimental

A sample of nickel concentrate was obtained from Sudbury district ores as a donation from the International Nickel Company of Canada Limited. This concentrate analyses 5.92% Ni, 2.4% Cu, 37.9% Fe and 25.9% S according to the company assay supplied.

The experimental set-up and procedure were the same as those used in the previous sections for the normal dissolution experiments, except a 1000 ml Erlenmeyer flask was used instead of 500 ml. The equipment used for the electrolysis experiment is described later in this chapter.

During the leaching run, aliquots of several mls were sampled from the leach pulp to analyse for nickel, iron and copper at selected intervals. Other metals and non-metallic inpurities were not determined.

2. Results and Discussion

2.1 Acid leaching of Ni-concentrate

In preliminary experiments, the Ni-concentrate was found to be very much less soluble in weak acid than the equivalent synthesized compounds. In Figure 4-1, the iron extraction from the Ni-concentrate is shown in hydrochloric and sulphuric acids during stepwise concentration increases every 10 minutes at 60 and 80°C. According to these results, the dissolution, in sulphuric acid is insignificantly small at all concentrations, while dissolution in hydrochloric acid starts at around 3M acid concentration after an induction period, which is shorter at 80°C. To investigate the nature of the induction period and the immunity of the Ni-concentrate to sulphuric acid, the pyrrhotite powder was prepared by crushing lump nickeliferrous pyrrhotite from the Falconbridge Mine in Ontario under a nitrogen atmosphere, thus

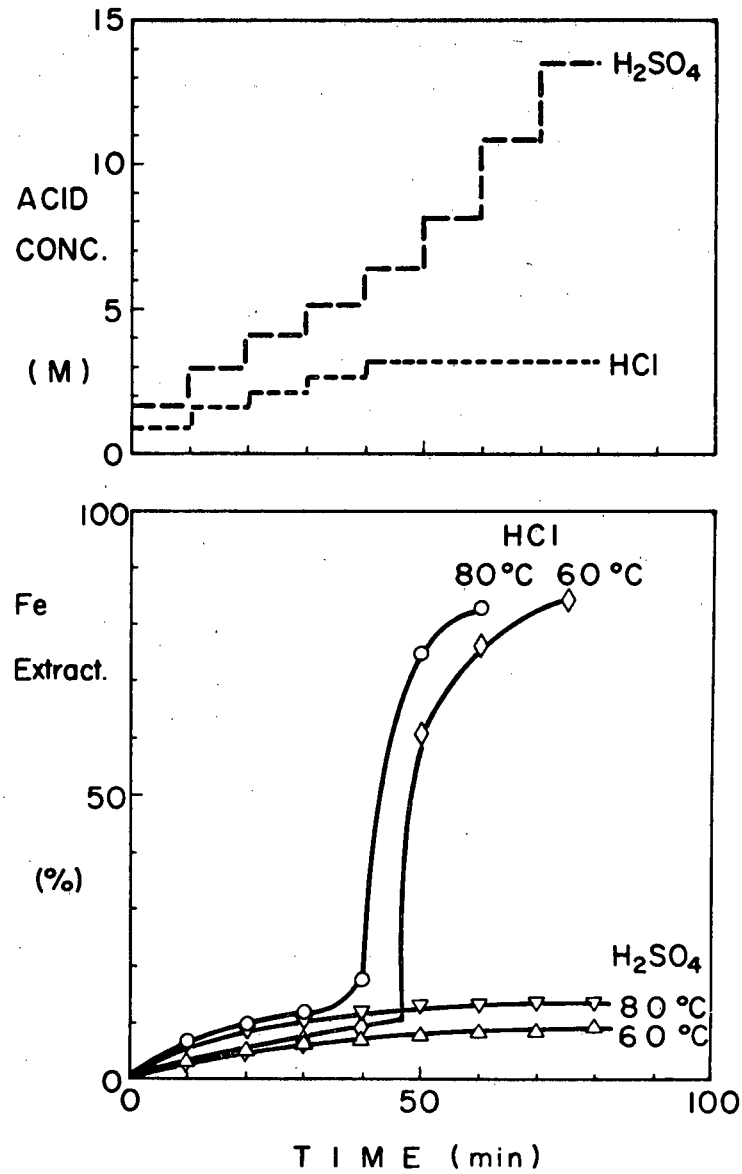

Figure 4-1. Iron extraction from the nickel concentrate (30 grm) with step-wise increase in acid concentrations at 60 and 80°C.

avoiding air oxidation of the powder. This hand crushed pyrrhotite powder (− 50 mesh) was then leached in 1M hydrochloric acid and 1.8M sulphuric acid at 60°C. The results are shown in Figure 4-2. In both cases, the dissolution starts as soon as pyrrhotite contacts the solution. The decrease in the dissolution rate in hydrochloric acid solution at later stages is probably due to decreasing in acid strength.

From these facts, it can be concluded that pyrrhotite is a well-known mineral that is oxidized easily with air even at room temperature; therefore, during milling and flotation the surface of pyrrhotite must be oxidized and this oxidized surface inhibits the mineral decomposition in acids. In addition, strong hydrochloric acid can dissolve this oxidized surface reasonably quickly and soon exposes a fresh pyrrhotite surface that is reactive.

2.2 Effect of chloride addition

It is commonly known that chloride ions destroy the passive surface film on most metals to activate the corrosion process. If the surface of pyrrhotite in the Ni-concentrate is oxidized, an addition of chloride onto the leaching solution should promote the dissolution of the oxidized surface and as a result the dissolution of pyrrhotite.

In Figure 4-3, the result in the NaCl + 1.8 M H_2SO_4 solution is shown at 60°C with a 10% pulp density. The addition of 1 M NaCl did not activate the system, but that of 2.5 and 5 M NaCl results in the dissolution of pyrrhotite after 20 and 9 minutes of the induction

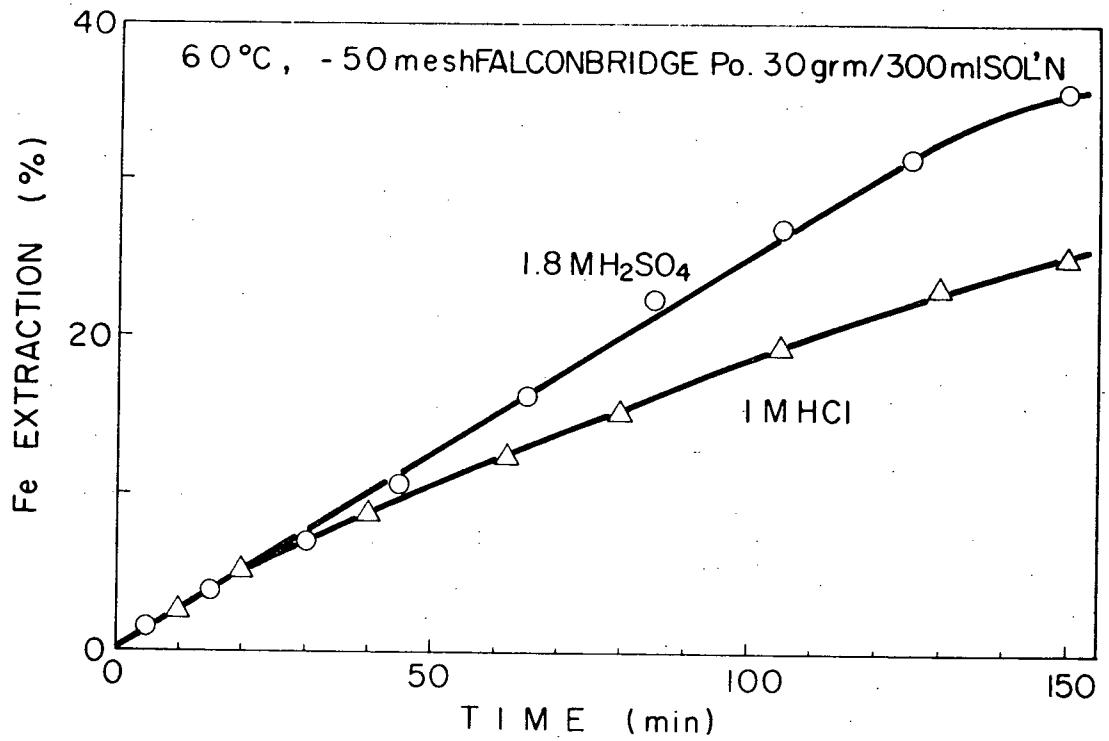

Figure 4-2. Iron extraction of hand-crushed Falconbridge pyrrhotite. Pulp density = 10%.

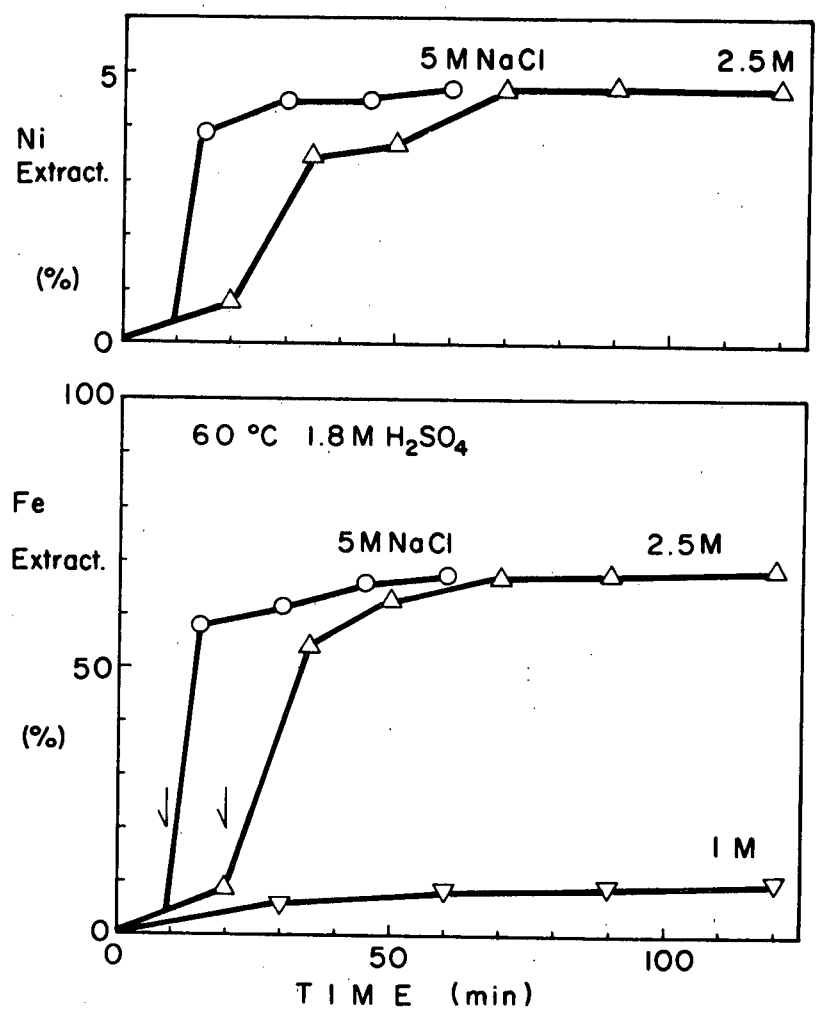

Figure 4-3. Effect of NaCl addition on the H_2SO_4 dissolution of the nickel concentrate. Pulp density = 10%.

period, respectively.

In Figure 4-4, the extractions of Ni and Fe from the Ni-concentrate in the NaCl + HCl or H_2SO_4 system are shown. The maximum iron extraction is about 80%, where pyrrhotite and other iron compounds, i.e., oxide, are leached. On the other hand, the maximum nickel extraction is about 4.5%, which is due to the complete dissolution of nickel in the pyrrhotite phase. Increasing the concentration of H_2SO_4 from 1.8 to 3.6 M yields higher iron extraction, but the same nickel extraction which suggests that increased acid dissolves more of the iron from compounds other than pyrrhotite existing in the Ni concentrate. The induction period in all the systems seems to be shorter as the acid strength and the NaCl addition increase.

As summarized in Fig. 4-4, the acid decomposition of Ni-concentrate showed fair selectivity, for almost all the pyrrhotite and other iron compounds dissolve and leave pentlandite and chalcopyrite behind in the residue, the exact separations depending on the leaching conditions. However, from the industrial point of view, a mixture of chloride and sulphuric acid may not be attractive because of the complexity involved in the separation of chloride and sulphate. Therefore, strong hydrochloric acid is probably the most suitable reagent for the dissolution of the pyrrhotite from the Ni-concentrate.

2.3 Electrolysis of the Ni-concentrate

When pyrrhotite is exposed to reduction potentials more

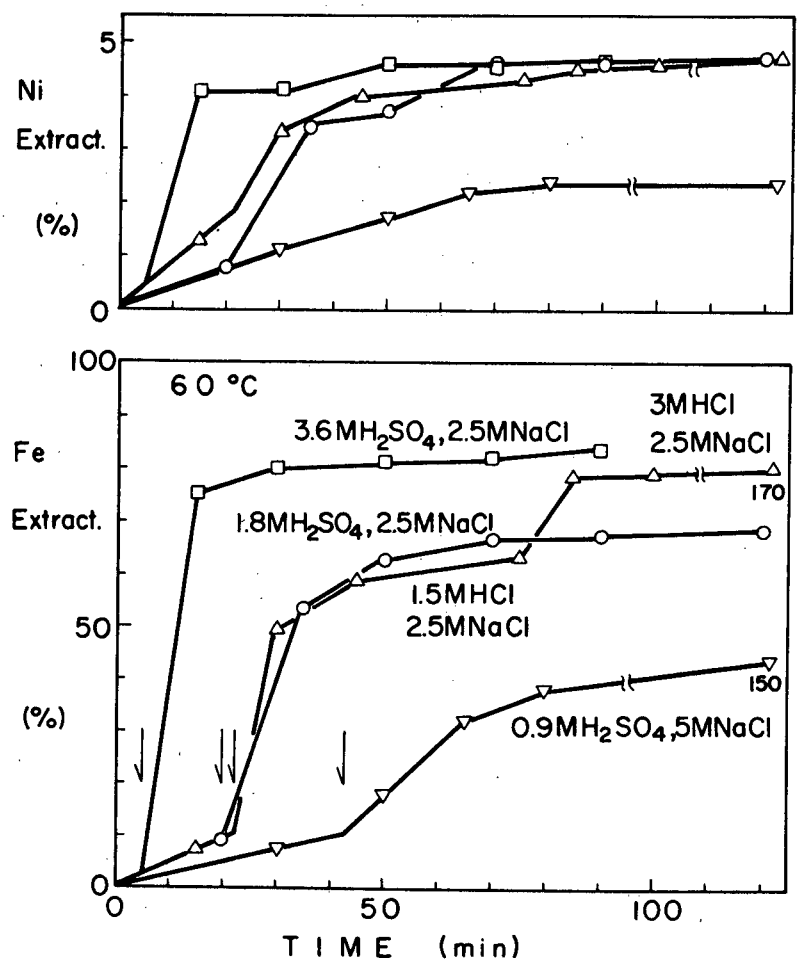

Figure 4-4. Iron and nickel extractions by various combinations of acid and NaCl. Pulp density = 10%.

negative than its rest potential, its dissolution rate increases, as mentioned in Chapter II. In addition, if the surface of pyrrhotite is oxidized and the potential is low enough to reduce the oxidized surface, the cathodically imposed potential on pyrrhotite will promote the dissolution rate.

An experiment was carried out to dissolve the Ni-concentrate using the cathodic compartment of an electrolytic cell. The electrolytic cell design is shown in Figure 4-5. A cylindrical graphite cathode, a propeller stirrer, a thermister probe tube, a gas in-let tube and a porous porcelain cup-shaped diaphragm were placed in a 1500 ml beaker. A graphite anode was located inside the porcelain cup. To avoid air oxidation of the catholyte, the top of the beaker was covered with a plastic sheet. The whole cell structure was put on a hot plate and the cell temperature was controlled by a thermistor temperature controller.

The experiment was carried out in the following way: first 800 ml of the electrolyte was placed in the cell, then helium gas was bubbled through the solution and after approximately 30 minutes the Ni-concentrate was dumped into the catholyte of the cell and the electrolysis was started. At selected intervals an aliquot of the catholyte solution was sampled to analyze for metal content.

The results in Figure 4-6 represent the cathodic polarization curves in the cell at room temperature. A Luggin-capillary was inserted into the electrolytic cell to measure and control the potential

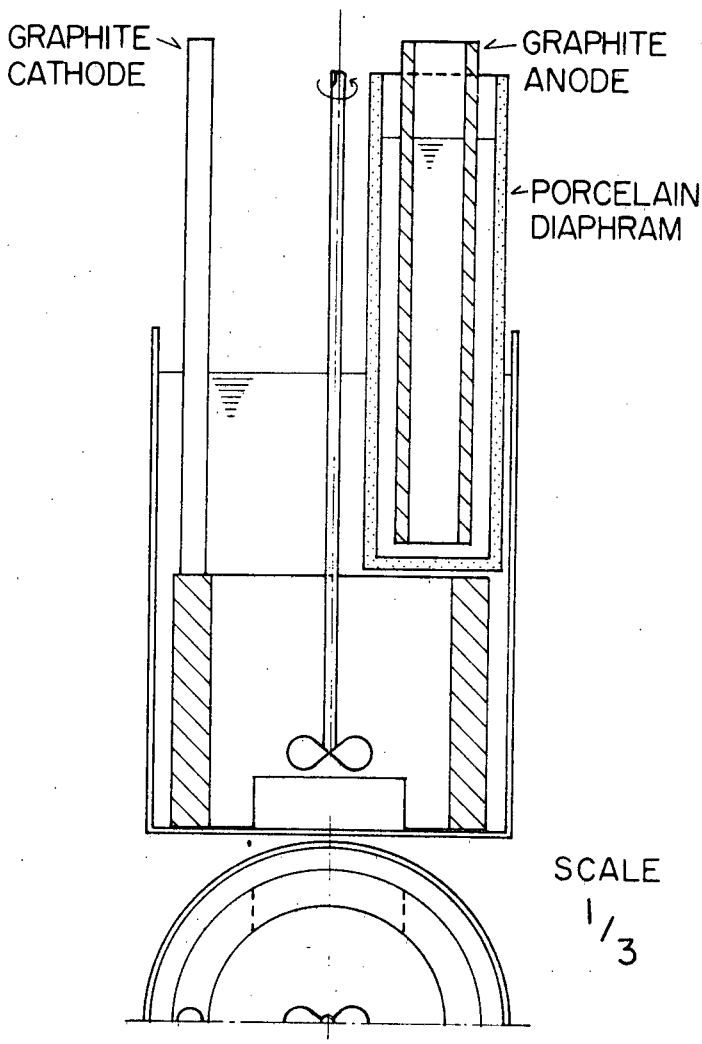

Figure 4-5. The cell used for cathodic electrolysis of nickel concentrate slurry.

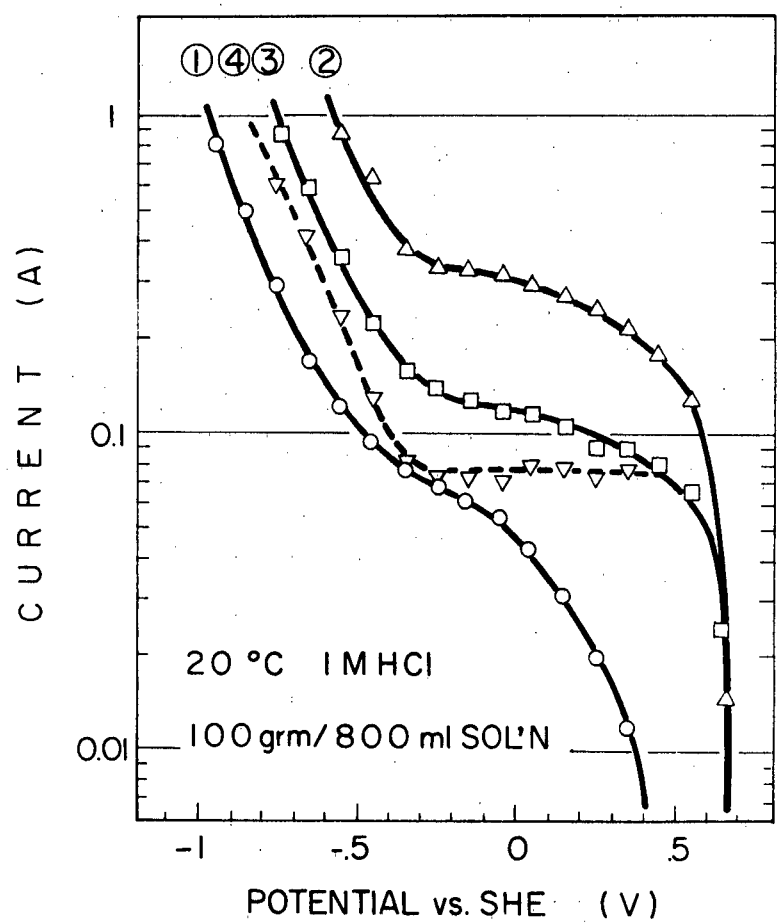

Figure 4-6. Cathodic polarization curves under various conditions.

at the cathode. The curves were obtained potentiostatically using a Wenking potentiostat. The current was measured after one minute at each potential. Curve (1) represents the cathodic polarization of the graphite electrode without any solid present in 1M HCl solution. Curve (2) is the polarization curve for the system of 1M HCl (800 ml) + 100 grms of the Ni-concentrate, which was charged into the cell in the as-received condition. Curve (3) was made under the same conditions as that for (2), but the Ni-concentrate was first washed with 1 M HCl solution and then with distilled water prior to charging into the electrolytic cell. Curve (4) represents the difference in current between curves (3) and (1).

According to these results, the cathodic current without solids is significant in the range of potential swept. When the Ni-concentrate was not washed, the cathodic current was found to be much larger, possibly because of the reduction of oxidized flotation re-agents in this potential range. In any case, the cathodic current is reduced by washing the solid with HCl solution and water, as shown as curve (3). The polarization curve (3) minus the curve (1) obtained in the absence of solids represents the net cathodic current due to solids reduced at the graphite cathode and is shown as curve (4). In this case, a sharp increase in current just below the rest potential of about 650 m V (vs S.H.E.) is obtained, reaching a limiting current of 70 $\sim$ 80 mA between 550 and - 350 mV and then rising again below - 350 mV. In the potential region below - 350 mV the electrochemical reduction of the Ni-

concentrate occurs and accounts for a maximum of about 65% of the total cathodic current, the remainder of the current reacting faradaically on the graphite cathode, presumably by hydrogen discharge.

In Figure 4-7, the dissolution of iron from the Ni-concentrate is plotted against time under various conditions in sulphuric acid at 55°C. Before electrolysis the dissolution of iron is nominal, but starts in 10 to 20 minutes after beginning of electrolysis under these experimental conditions. The dissolution also continues for a time after electrolysis is stopped, as can be seen from the curves in the figure. For the dissolution in 3.6 M H_2SO_4 solution, the amount of iron dissolved decreases after it reaches the maximum, this being due to precipitation of ferrous sulphate. From these data in Figure 4-7, we can conclude that the importance of the cathodic reduction of the Ni-concentrate is in the initiation of the dissolution; since afterwards the reaction proceeds without the cathodic electrolysis. During the initiation period the cathodic current through the pulp may be consumed by the reduction of an oxidized surface layer or oxidative species in the Ni-concentrate or in the electrolyte. This dissolution rate of the Ni-concentrate in the initial stage, where the electrolysis has been just started, will be called "the initial dissolution rate", Rinit., and the dissolution rate in the later stage, where the dissolution can proceed without electrolysis, will be called "the second dissolution rate", R sec.

In Figure 4-8, the initial dissolution rate of the Ni-concentrate is plotted against the amount of solid in 800 ml of electrolyte of

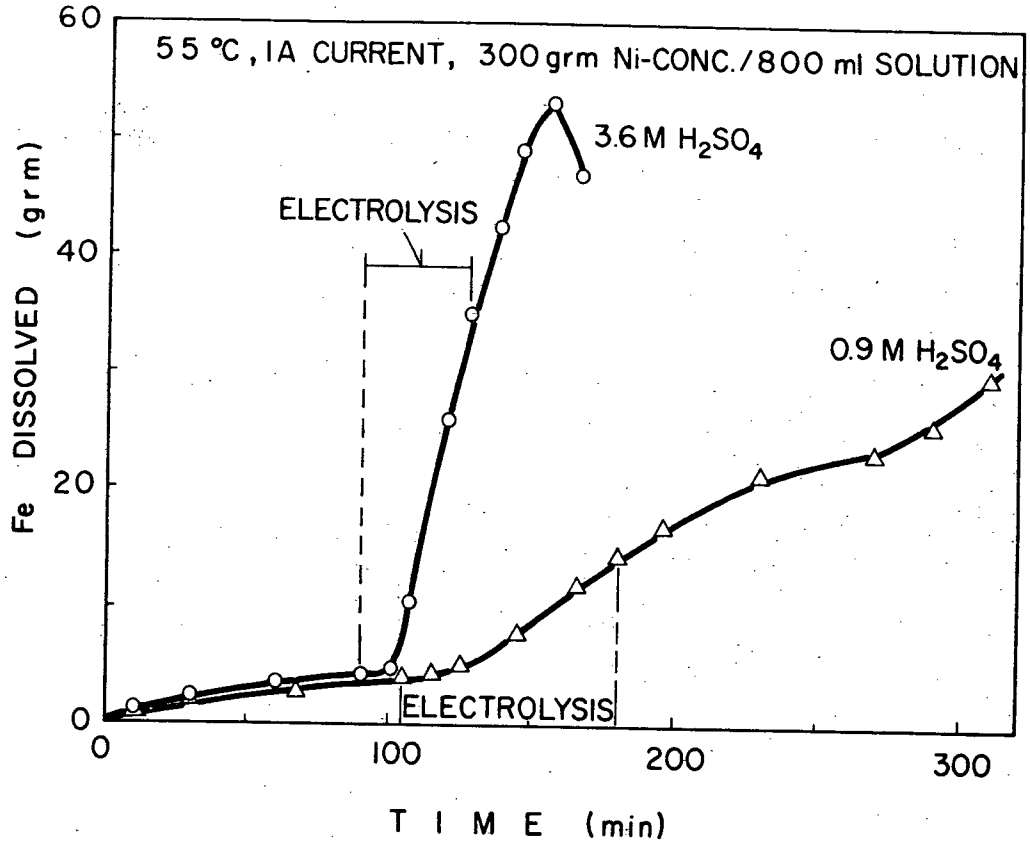

Figure 4-7. Iron dissolution of a nickel concentrate slurry before, during, and after electrolysis.

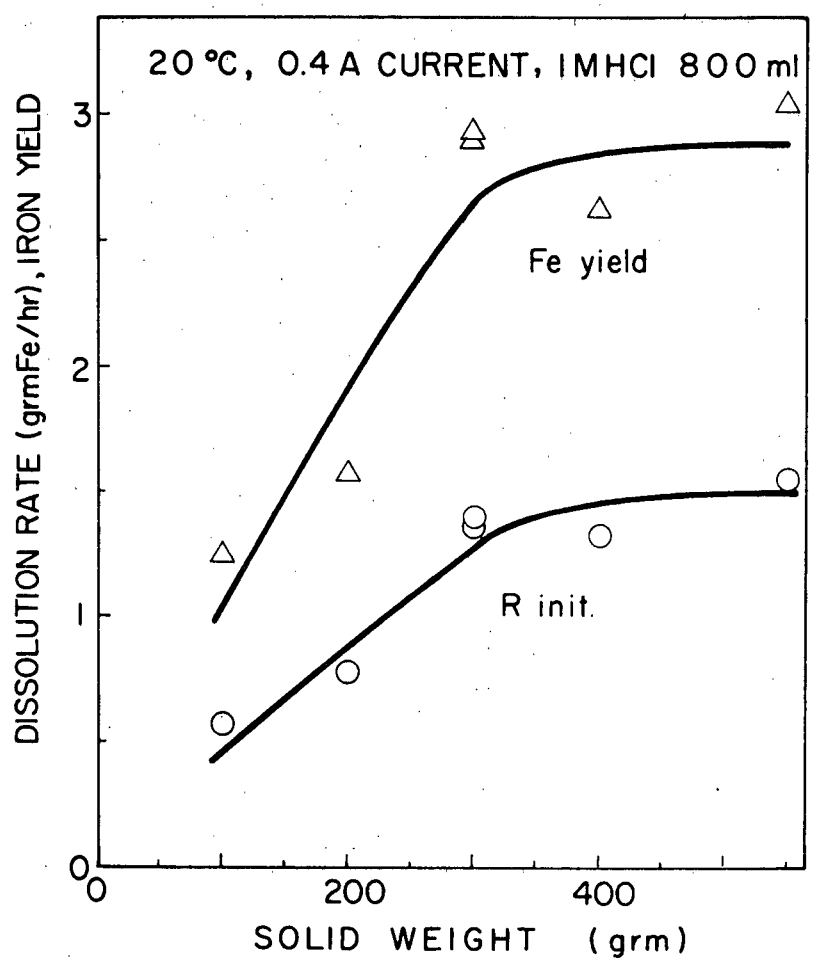

Figure 4-8. Effect of pulp density on the initial dissolution rate and iron yield.

1 M HCl at 20°C with 0.4 A cathodic current. The amount of solid was varied from 100 to 550 grms. According to the results, above 300 grms the pulp density does not influence the initial dissolution rate, which means that the Fe^{++} yield per coulomb for the reduction of the solid reaches a maximum at 300 grms of the solid charge under the experimental conditions.

Figure 4-9 shows the effect of the cathodic current on the initial and second dissolution rates in 0.9 M H_2SO_4 solution at 55°C with 300 grms of solid in 800 ml of electrolyte. As seen in this figure, the initial dissolution rate depends on the cathodic current up to 1.5 A, then becomes independent. Meanwhile, the second dissolution rate does not depend on the cathodic current, which is anticipated from the results in Figure 4-7.

In Figure 4-10, the initial and second dissolution rates are plotted against the sulphuric acid concentration at 55°C and 1A of cathodic current with 300 grms of solid. Both rates are influenced by the acid strength of the electrolyte according to these results.

In Figure 4-11, the dependence of the initial and second dissolution rates on temperature is shown in the temperature range between 40 and 85°C. Up to 55°C, the initial and second dissolution rates increase as temperature increases; however, above 55°C the fast second dissolution does not occur during 2 hours of electrolysis. The disappearance of the fast second dissolution at higher temperature is not understood; however, it is possible that at higher temperature

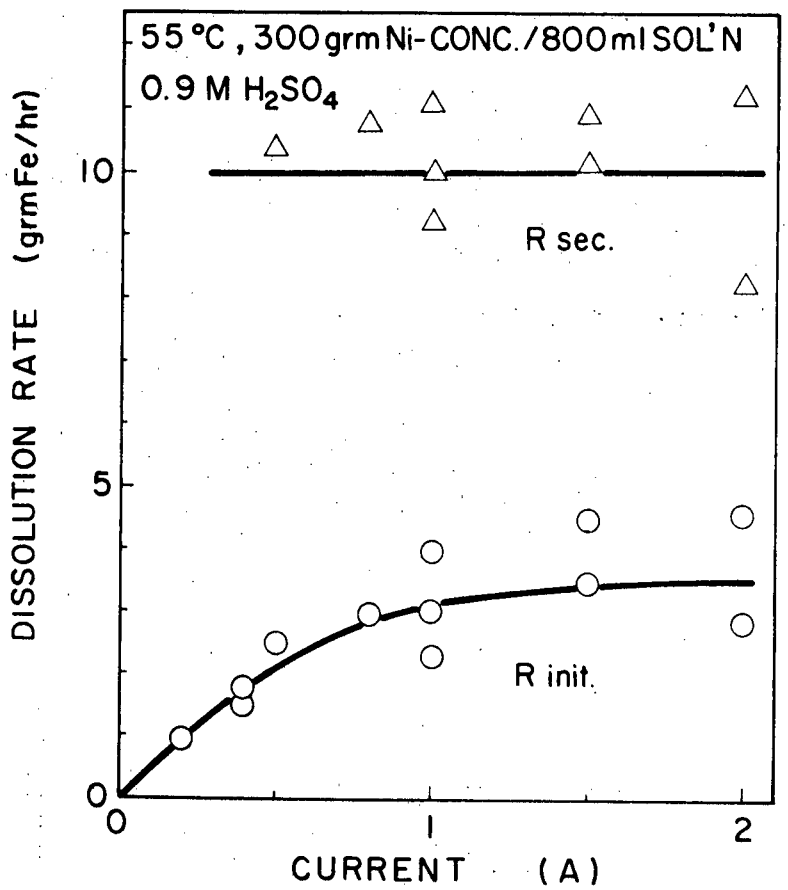

Figure 4-9. Effect of current on the initial and second dissolution rates.

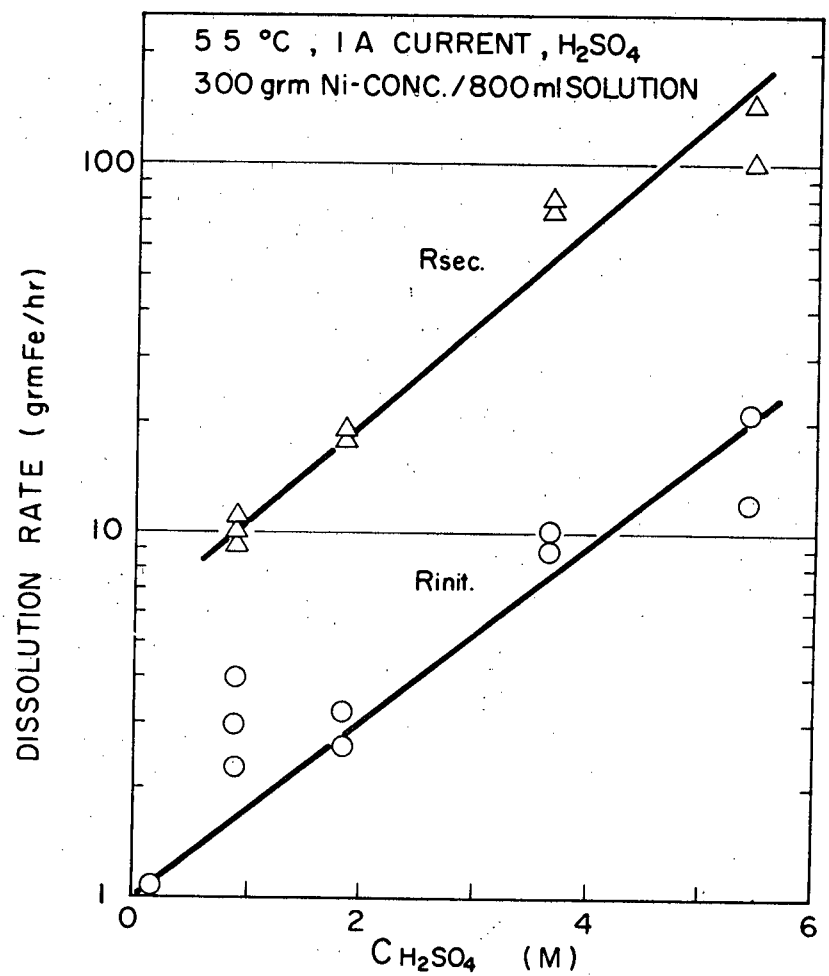

Figure 4-10. Effect of sulphuric acid concentration on the initial and second dissolution rates.

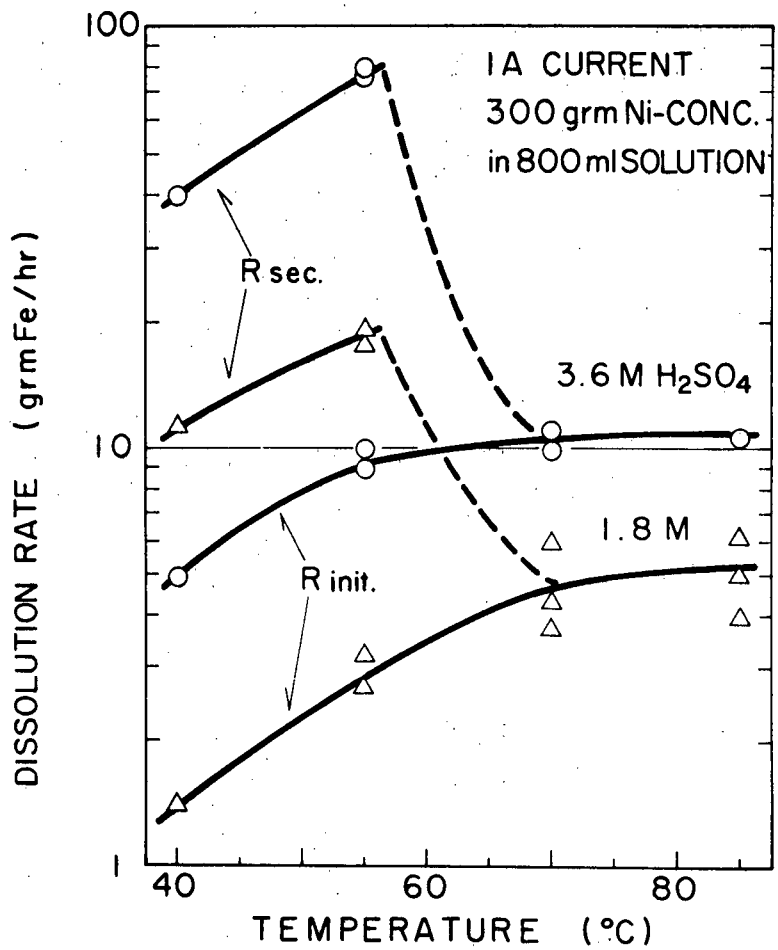

Figure 4-11. Effect of temperature on the initial and second dissolution rates.

reactions between oxidized surface and the pyrrhotite occur faster than the reduction of the oxidized surface by electrolysis with the consequence that only one stage of leaching is observed.

Through all experiments in the electrolytic dissolution of the Ni-concentrate, the amount of nickel dissolved was approximately one-hundredth of the total amount of iron dissolved, and this can be accounted for as nickel dissolution from the nickel bearing pyrrhotite phase. There is no need to assume any decomposition of pentlandite.

In the electrolytic dissolution of the Ni-concentrate, the selective dissolution of pyrrhotite from the concentrate could be initiated under suitable conditions of current, acid concentration, temperature and pulp density. The electrolytic cell designed in this work limits these conditions, because, at a pulp density of 300 grms of solid in 800 ml of electrolyte, where the maximum current efficiency and a reasonable dissolution rate were obtained, the minimum acid necessary to consume all the pyrrhotite in the concentrate is approximately 4 moles/800 ml or 5 M. As seen in Figure 4-7, the solubility of ferrous ion in 5.4 M H_2SO_4 solution is only about 50 grms/800 ml, and so the pyrrhotite separation from the Ni-concentrate will be limited to less than 50% of the amount present at the point where precipitation of ferrous sulphate in the electrolyte begins. Therefore, a commercial cell design must be based on a method of staying within the solubility limits of $FeSO_4$ by the time the pyrrhotite is completely dissolved.

2.4 Thermal reduction of Ni-concentrate

As noted above, it is essential to eliminate the air oxidized content to achieve the complete dissolution of the pyrrhotite from Ni-concentrate. This was accomplished by leaching in either strong hydrochloric acid, NaCl - containing mild acids, or leaching with the aid of cathodic electrolysis. It should also be possible to reduce the oxidized surface content by means of hydrogen at furnace temperatures prior to leaching. Hydrogen reduction was carried out, using a laboratory-scale fluid bed roaster with a charge of 200 grms under several controlled temperatures for $1 \sim 3$ hours. After hydrogen reduction, the Ni-concentrate was furnace cooled to room temperature under continuing hydrogen flow.

In Table 4-I, the chemical analyses of the Ni-concentrate before and after the hydrogen reduction are summarized for Fe, Ni and Cu.

According to these analyses of the Ni-concentrate, the metal content generally increases after H_2 reduction treatment; however, the increase is not significant. Thermodynamic calculations indicate that reduction of FeS, Ni_3S_2 and Cu_2S, in the concentrate to metals is unfavourable. However, H_2 reduction of the Ni-concentrate under the experimental conditions can reduce the excess sulphur content in the sulphides, if present, thereby accounting for small increases in metal content. Also, oxidized material on the particle surfaces would be reduced.

TABLE 4-I

CHEMICAL ANALYSES OF THE Ni-CONCENTRATE FOR Fe, Ni AND Cu

		Reduct. Temp.	500(°C)	600	700	700	800
%	Company Assay	Reduct. Time / Found	(hr) 1	1	1	3	1
Fe	37.9	35.6	35.7	36.5	36.4	37.9	36.9
Ni	5.92	5.69	6.15	6.00	5.88	6.00	6.00
Cu	2.41	2.40	2.42	2.56	2.42	2.57	2.57

The H_2 reduced Ni-concentrate was examined by means of leaching tests, which were carried out at 60°C and 300 ml of HCl or H_2SO_4 solution under a helium atmosphere.

In Figure 4-12, the extractions of Ni and Fe are plotted against leaching time for the reduced concentrate at different temperatures for 1 hour. The conditions of leaching (1 M HCl and 10% pulp density) correspond to approximate stoichiometry between hydrogen ions and all the pyrrhotite in the Ni-concentrate equivalent to about 85% of the iron. From all the results, except those for 500°C, the iron extraction from the pyrrhotite seems to be completed for all temperatures; however, the nickel extraction is a maximum for 600°C reduction.

Figure 4-13 represents the effect of the reduction time at 700°C on the extractions of Ni and Fe. The results suggest that in this

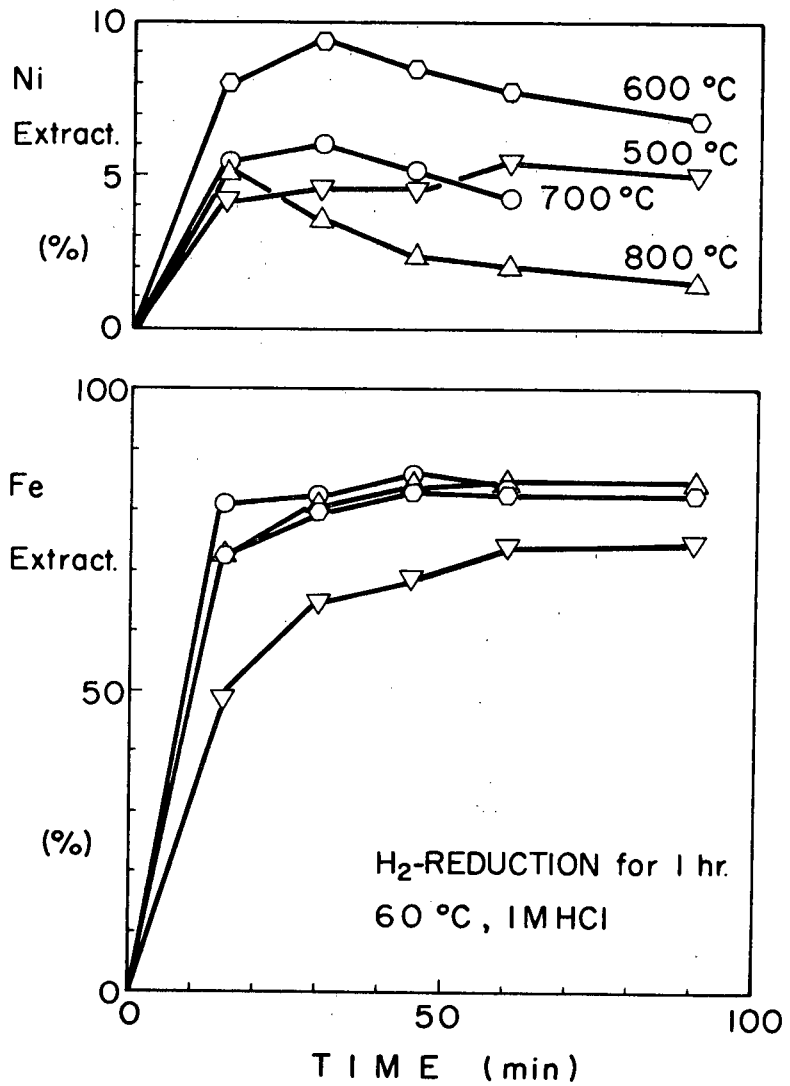

Figure 4-12. Iron and nickel extractions with different temperatures of hydrogen reduction. Pulp density = 10%.

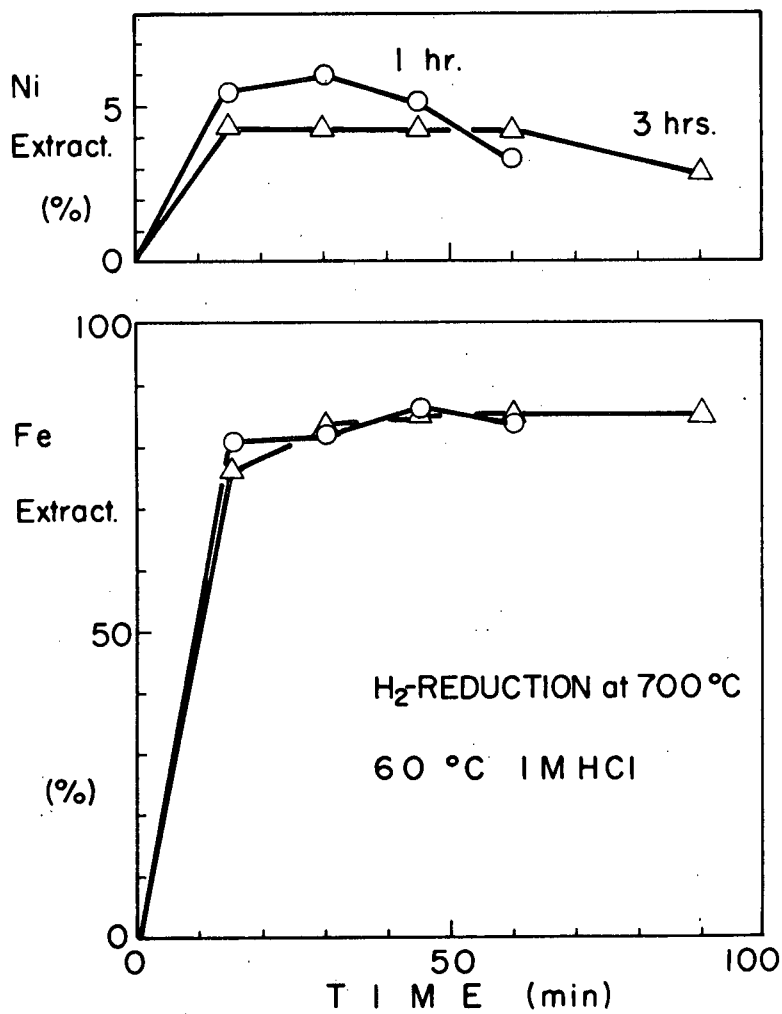

Figure 4-13. Iron and nickel extractions with different durations of hydrogen reduction at 700oC. Pulp density = 10%.

range there is no significant effect. This means that the reduction can be achieved in not more than 1 hour at this temperature.

Figure 4-14 shows the result of leaching with two different pulp densities and initial acid concentrations, maintaining the same acid-pyrrhotite stoichiometry. The iron extractions at the beginning are similar; however, at a later stage the iron extraction for the 30% pulp density decreases, possibly due to salt precipitation. Meanwhile, nickel extraction is much higher for 30% pulp density than for the 10% pulp density. This must be caused by partial dissolution of pentlandite in the charge at higher initial acid concentration.

In general, nickel extraction decreases in the later stages of leaching, as seen in the results shown in Figures 4-12~14. This may be caused by the precipitation of nickel sulphide with hydrogen sulphide remaining dissolved in the solution after depletion of acid.

In Figure 4-15, the results in sulphuric acid are shown for H_2 reduced Ni-concentrate at 700°C for 1 hour. The result in HCl solution is reproduced for comparison. In 0.5 M H_2SO_4 solution, the iron extraction reaches a maximum of 72% and the final nickel extraction is less than 1%. However, for 0.75 and 1.0 M H_2SO_4 solutions, the iron extraction and nickel extraction continuously increase, which suggests that dissolution of pentlandite is occurring. For the best separation of nickel from iron, therefore, acid concentration needs to be kept down to avoid dissolution of the pentlandite present in the concentrate.

As mentioned previously, the hydrogen reduction for

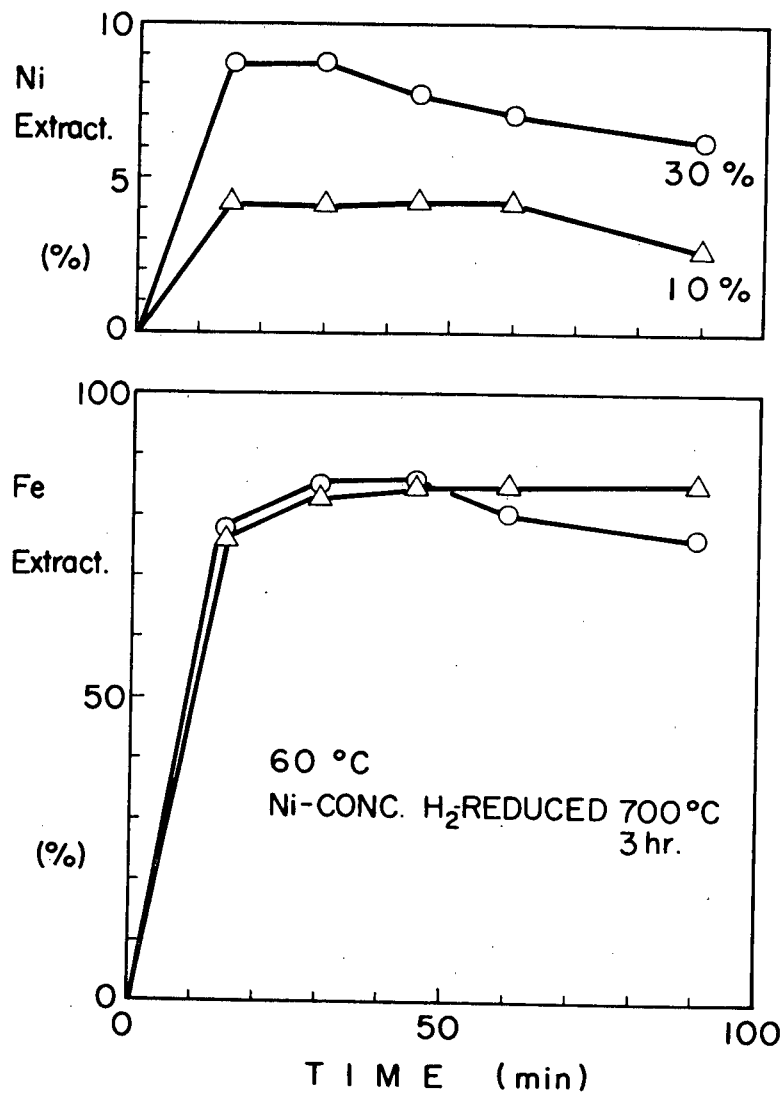

Figure 4-14. Iron and nickel extractions with different pulp densities. 30% = 30 grm solid/100 ml 3 MHCl, 10% = 30 grm solid/300 ml 1M HCl.

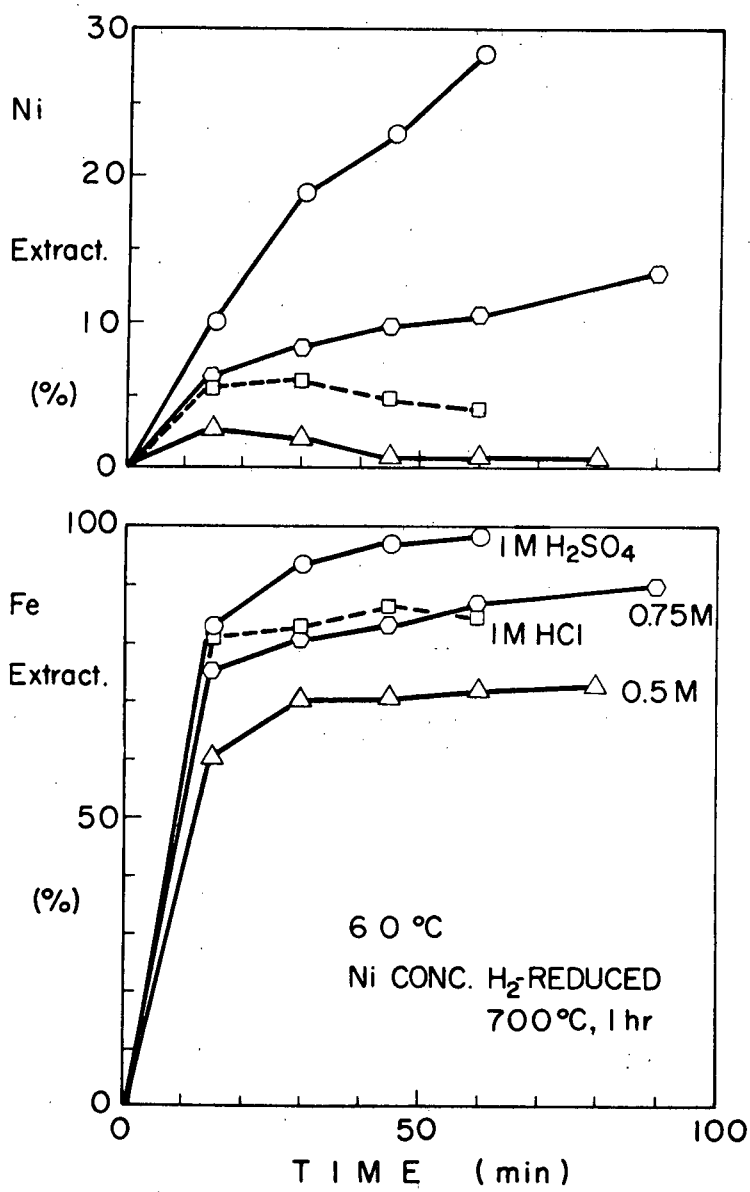

Figure 4-15. Iron and nickel extractions with different sulphuric acid concentrations. Pulp density = 10%.

Ni_3S_2, FeS and Cu_2S is an unfavourable reaction; therefore, a slight partial pressure of H_2S as a reaction product will affect the reduction reaction. An experiment was carried out to investigate the effect of partial pressure of H_2S in the hydrogen reducing gas. A mixture gas of H_2 + 1% H_2S was used for the hydrogen reduction of the Ni-concentrate at 600°C for 1 hour. After the reduction, the concentrate was leached in 0.75 and 4.5 M H_2SO_4 solutions under the same conditions as the previous experiments. The results are shown in Figure 4-16 with those of the pure hydrogen reduced concentrate at 700°C for 1 hour for comparison. From these results, the dissolution for the concentrate reduced with an H_2 + H_2S mixture spontaneously starts like that reduced with H_2 gas. In 0.75 M H_2SO_4 solution, the iron extraction for the former seems to be slightly smaller than that for the latter. In addition, the nickel extraction for the concentrate reduced with H_2 + H_2S gas mixture is about 6% and does not increase significantly after 30 minutes. Strong sulphuric acid (4.5 M) does not increase metal extractions greatly compared with 0.75 M H_2SO_4 solution. This differs from the result observed for the concentrate reduced with pure H_2 gas shown in Figure 4-15. From these data it may be concluded that a small amount of H_2S present in the reducing gas reduces the dissolution of the pentlandite in the concentrate although it does not seem to hinder the activation of the pyrrhotite. This conclusion is supported by the results shown in Figs. 3-2, and 3-4, which suggest that the dissolution rate of pentlandite is more sensitive to the PH_2S/PH_2 ratio in the range 0.01 ~ 0.001 than

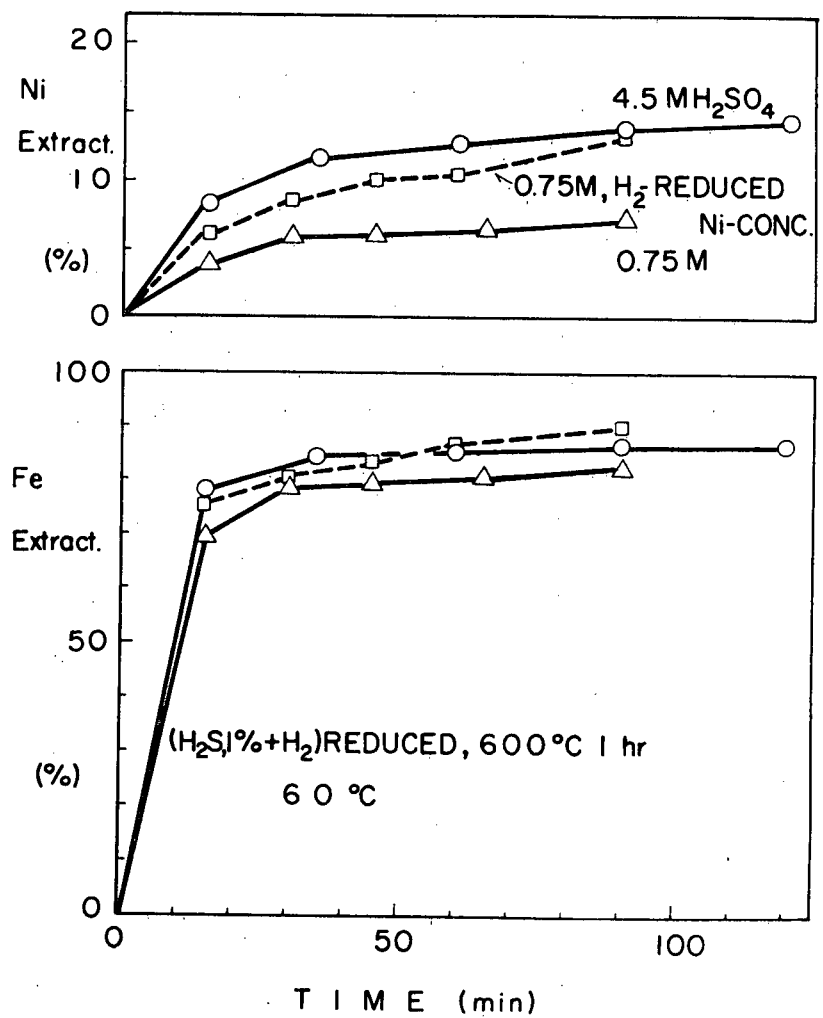

Figure 4-16. Effect of 1% H_2S in hydrogen on iron and nickel extractions. Pulp density = 10%.

that of pyrrhotite.

It is very important that the copper content in solution must be minimized to avoid loss of copper or an extra unit process to recover it. During the leaching of the H_2 reduced concentrate the copper content in the leach liquor was measured, and found to be usually less than 0.5% of the copper content in the concentrate, although occasionally a slightly higher value (1%) was observed, as in the leaching with 1 M H_2SO_4 solution. It can therefore, be concluded that copper dissolution into the leach liquor is sensitive to the presence of excess acid and when the excess acid is kept low, copper is not appreciably dissolved.

The results in Figure 4-15 indicate that when excess acid exists in the leach liquor, the dissolution of pentlandite in the concentrate reduced with H_2 gas may occur at a significant rate. Therefore, the leaching of pentlandite can be achieved by acid decomposition after the concentrate is reduced with hydrogen.

An attempt was made to dissolve nickel from a leach residue that had previously been hydrogen-reduced. A residue weighing 30 grms obtained from pyrrhotite leaching in 0.75 M H_2SO_4 solution at 60°C for 1 hr was charged into 300 ml of 1, 1.8 and 3.6 M H_2SO_4 solutions at 60°C. The amounts of nickel and copper dissolved were plotted against time in Figure 4-17. According to the leaching curves, 3.6 M H_2SO_4 solution seems to dissolve all the nickel after 140 minutes. The dissolution of copper starts after the nickel dissolution slows down and

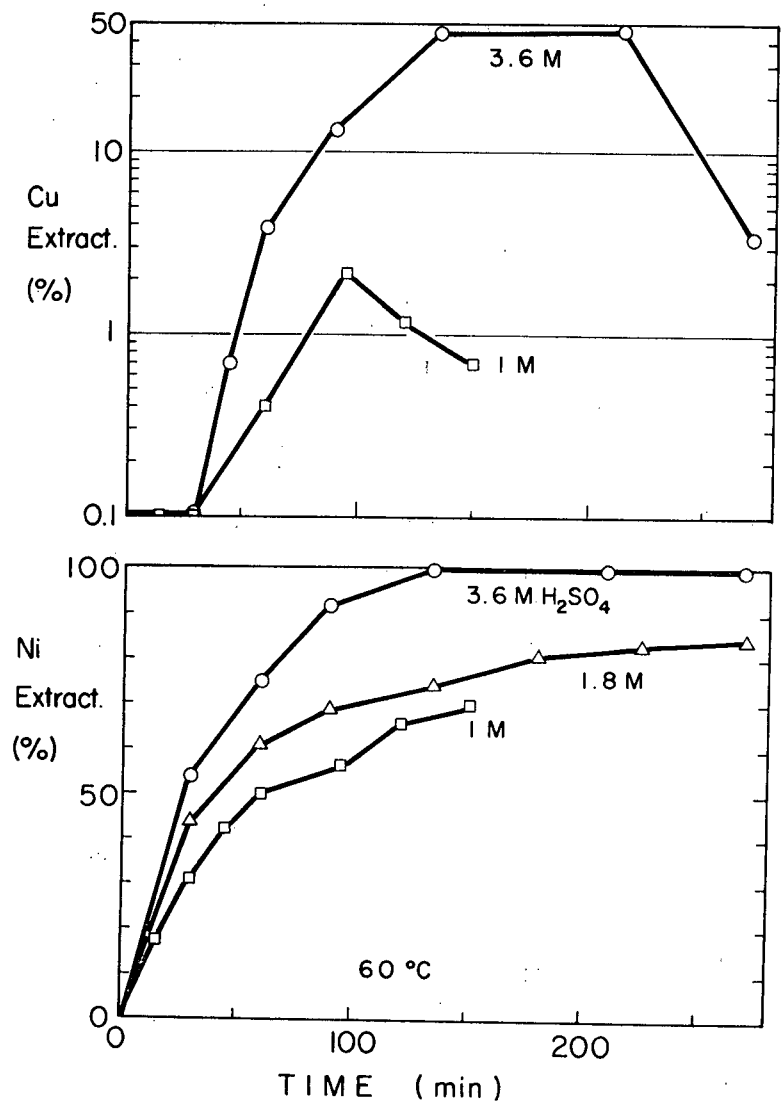

Figure 4-17. Nickel and copper extractions from the pyrrhotite-eliminated leach residue in different sulphuric acids. Pulp density = 10%.

the dissolved copper reprecipitates in the later stages of leaching. In Table 4-II, the chemical analyses for Fe, Ni and Cu in the leach residues are summarized.

TABLE 4-II

CHEMICAL ANALYSES FOR Fe, Ni AND Cu IN THE LEACH RESIDUES

%	H_2 reduced Ni conc.	1st leach residue $0.75M H_2SO_4$ 60°C, 60 min.	2nd leach residue 60°C		
			$1M H_2SO_4$ 150 min.	$1.8M H_2SO_4$ 270 min.	$3.6M H_2SO_4$ 270 min.
Fe	36.7	13.6	6.5	1.6	1.0
Ni	6.1	10.6	5.3	1.5	0.36
Cu	2.5	4.7	8.4	9.2	9.4
Solids	100	($\approx$ 52)			($\approx$ 30)

The percentage of solids in Table 4-II was calculated from the metallic ions dissolved in the leach liquors. The residue of the 1st leach probably consists mainly of pentlandite, chalcopyrite* and silicious material. The residue from the second leach probably consists of bornite and precipitated copper sulphides, such as covellite, as well as silicious material. The content of elemental sulphur in both residues was found

* Under H_2 treatment chalcopyrite would be expected to decompose to a two-phase mixture of bornite (Cu_5FeS_4) and pyrrhotite, according to a phase diagram published by Yund and Kullerud (70).

to be negiglibly small, i.e., about 0.1%. From the nickel contents of the initial concentrate and the residue of the second leach, the nickel recovery was calculated to be 98.2% provided that all dissolved nickel from both leaches could be recovered.

3. General Discussion

It is generally known that the nickel sulphide ores in the Sudbury district consist of pentlandite, chalcopyrite and nickel-bearing pyrrhotite. The stabilities of copper sulphides in acidic solution without oxidant are known to be high, and therefore would resist dissolution as was observed. In addition, the results shown in Chapter III anticipate that the dissolution rate of pyrrhotite may be much higher than that of pentlandite of equi-sulphur activity. Therefore, the separation of pyrrhotite from pentlandite and chalcopyrite may be achieved with the aid of the acid decomposition reaction. In practice, however, this anticipation was unrealized by the effect of oxidation on the pyrrhotite surface. The elimination of the passivated surface layer was essential in order to expose a fresh sulphide surface. During milling and flotation such oxidation of the sulphide surface is inevitable. A strong hydrochloric acid or chloride treatment, cathodic electrolysis, or hydrogen reduction at high temperature prior to the leaching were all successful in eliminating the oxidized surfaces and a reactive pyrrhotite was realized. The acid decomposition reaction on reactive pyrrhotite proceeds very fast in both dilute hydrochloric and sulphuric acids. All the

pyrrhotite in the concentrate dissolvesin the presence of slightly excess acid, provided ferrous salt solubilities are not exceeded.

From a practical point of view, the thermal reduction of the Ni-concentrate with hydrogen prior to leaching has the following advantages;

(1) sulphuric acid, which is more economical than hydrochloric acid, can be used,

(2) no chloride need be added to the leach liquor,

(3) the pentlandite in the leach residue can be subsequently leached by acid decomposition with strong sulphuric acid.

The third advantage is most interesting because the dissolution of pentlandite has been considered very difficult and requires very harsh leaching conditions for the completion of the reaction.

In Figure 4-18, a tentative conceptual flowsheet for the treatment of nickel concentrate or pyrrhotite concentrate incorporates a hydrogen reduction step prior to leaching.

Ni-concentrate or pyrrhotite concentrate is first reduced in the fluid bed roaster at about 800°C for 30~ 60 minutes, then leached in the first tank at 60°C under a non-oxidizing atmosphere in recycled solution with stoichiometric or slightly less sulphuric acid added for less than 2 hours to dissolve pyrrhotite and also precipitate excess nickel from the recycled solution. The residue from the first leach is sent to the second tank where strong sulphuric acid dissolves the remaining pyrrhotite and pentlandite in less than 4 hrs at 60 ~ 80°C under a non-

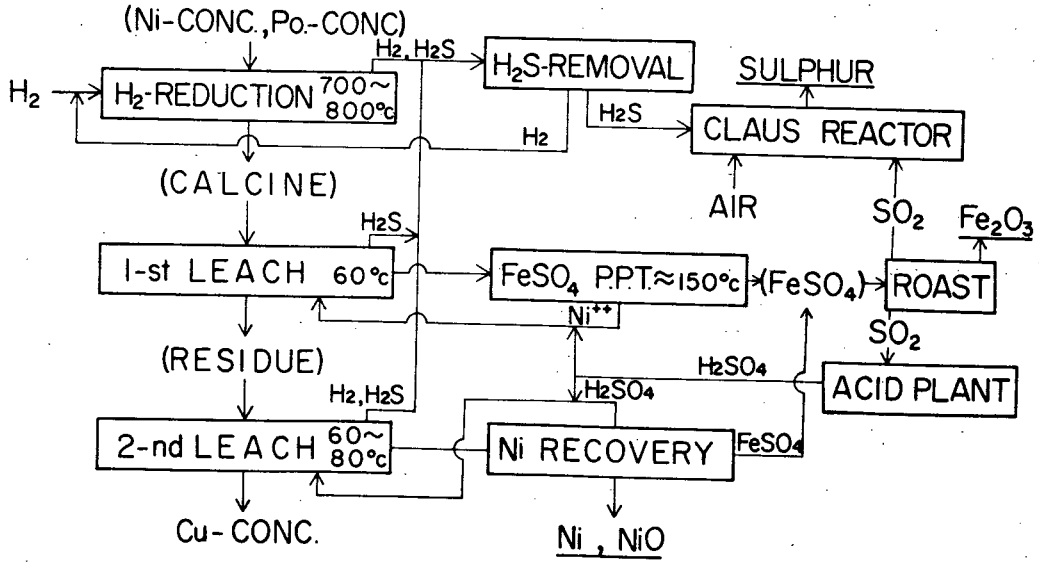

Figure 4-18. A tentative conceptual flowsheet for the treatment of nickel and pyrrhotite concentrates.

oxidizing atmosphere. The leach residue from the second tank is processed as a copper concentrate. H_2S gas in the exhaust gases from the fluid bed roaster and the leach tanks is stripped and sent to a Claus reactor to be recovered as elemental sulphur.

Ferrous ions in the leach liquor from the first tank is recovered as $FeSO_4$ or $FeSO_4 \cdot H_2O$ crystals in an autoclave at about 150°C, at which temperature the solubility of nickel sulphate is relatively high compared with that of ferrous sulphate. (71) The nickel remaining in the solution will be sent back to the first tank. The excess concentration of nickel in the first leach solution will be precipitated as nickel sulphide which will be leached in the second tank. The ferrous sulphate precipitate is passed to a rotary kiln to dry and decompose it to high grade iron oxide and sulphur dioxide. The former can be used as an iron ore depending on its purity.

A portion of sulphur dioxide gas can be sent to the Claus reactor to oxidize H_2S to yield elemental sulphur and the remainder to a sulphuric acid plant.

The leach liquor from the second tank is processed to recover nickel. This leach solution also contains ferrous ion and excess free sulphuric acid; therefore, by heating it to above 200°C under pressure ferrous and nickel sulphate are precipitated due to reduced salt solubilities. The precipitated sulphate mixture is then processed further to separate nickel from iron, while the residual sulphuric acid solution is sent to the second tank with further addition of sulphuric acid.

Oxidants in the leach solutions usually suppress the acid decomposition reaction and decrease the yield of H_2S; therefore, their contamination into the leach liquors must be minimized.

In this discussion, the behaviour of other metals in ore, i.e., cobalt, precious metals, was not discussed, because no analytical data dealing with their deportment was obtained in this work. It should be anticipated that the noble metals will not dissolve in sulphuric acid under the prevailing reducing conditions, and so can be expected to remain quantitatively in the final copper-rich residue.

CHAPTER V

CONCLUSIONS

1. Summary

(1) Acid decomposition of pyrrhotite is promoted by a low excess sulphur content in pyrrhotite, a high concentration of hydrogen ion, a high concentration of chloride ion at high acid concentration, and a low imposed potential by electrochemical means or chemical redox environments.

(2) Acid decomposition of pyrrhotite is suppressed by a high excess sulphur content in pyrrhotite, a high concentration of chloride ion at low acid concentration, the presence of cations forming sulphide precipitates less soluble than pyrrhotite, hydrogen sulphide in solution, and a high imposed potential or oxidizing environment.

(3) The acid decomposition reaction is highly selective towards the sulphide compounds with equi-sulphur activity in the Fe-Ni-S system. This is also true for the natural minerals in the Fe-Ni-S system.

(4) As found in the acid decomposition of pyrrhotite, the compounds in the Fe-Ni-S system are also susceptible to the inhibition in oxidizing environment. It was generally found that the higher the sulphur activity in the compounds, the more susceptible the compounds are to inhibition.

(5) It was concluded that the induction period which has been commonly observed in the acid decomposition of natural pyrrhotites is probably caused by air oxidation of the pyrrhotite surface. During the initial period of leaching, the slow dissolution of this air-oxidized pyrrhotite surface is occurring, followed by the rapid acid decomposition of the pyrrhotite bulk.

(6) The mild acid decomposition treatment of nickel concentrate (mainly pyrrhotite, pentlandite and chalcopyrite) was inhibited by the air-oxidized surface on the minerals. Treatment with strong hydrochloric acid or dilute acids with added chloride, cathodic reduction of the slurry, and reduction of the concentrate by hydrogen at high temperatures could expose the fresh pyrrhotite surface and lead to the quantitative separation of pentlandite and chalcopyrite from nickel concentrate by acid decomposition.

(7) The hydrogen reduction treatment of nickel concentrate could also activate even the pentlandite phase and make the acid decomposition applicable to it.

(8) Based on the acid decomposition reaction on hydrogen reduced nickel concentrate, a flowsheet of a process to recover elemental sulphur, possible iron ore, and nickel metal or compounds from nickel and pyrrhotite concentrates has been conceived.

2. Suggestions for future work

(1) For a more complete understanding of the mechanism of the acid decomposition reaction, further kinetic studies need to be carried out on pyrrhotite and other sulphides.

(2) The inhibition of the acid decomposition reaction by oxidants and by imposed higher potential, observed in the sulphides of the Fe-Ni-S system, should be looked at in more detail. If the formation of an oxide film on the sulphide surface is real, the oxidation leach decomposition of these sulphides proceeds through complicated steps and the nature of these oxide films will play a very important role in the reaction.

(3) For the cathodic reduction of a nickel concentrate slurry, the electrolytic cell design must be improved to yield a higher current efficiency and to prevent salt precipitation.

(4) To develop a practical industrial process for the acid decomposition treatment of pyrrhotite and nickel concentrates, further experiments and calculations must be carried out in order to determine many unknown factors, i.e., the behaviour of other minor sulphides and impurity elements, the recovery of metal values, the precipitation of salts at elevated temperatures, and the reactivities of minerals from other sources. Only after the above data are obtained can the process be scaled and optimized.

REFERENCES

(1) J.R. Boldt and P. Queneau, The Winning of Nickel, Longmans Canada Ltd. (1967).

(2) Engineering and Mining Journal, May, P. 80 (1973).

(3) K.W. Downes and R.W. Bruce, CIM Transactions, LVIII, p. 77 (1955).

(4) J. Gerlach, H. Hähne and F. Pawlek, Erzmetall, Bd. XVIII, p. 73 (1965).

(5) W. Kunda, B. Rudyk and V.N. Mackiw, CIM Bulletin, 61, p. 819 (1968).

(6) P.G. Thornhill, Canadian Met. Quarterly, V. 8, p. 219 (1969).

(7) J.A. Vezina, Mines Branch Technical Bulletin, TB129, 1970, and CIM Bulletin, V. 66, No. 733, P. 57 (1973).

(8) F. Habashi, Transactions of the Society of Mining Engineers, AIME, V. 254, p. 228 (1973).

(9) R.F. Pilgrim and T.R. Ingraham, Mines Branch Information Circular I.C. 243, 1970.

(10) W.M. Latimer, Oxidation Potentials, Prentice Hall Inc.

(11) E.T. Colson and C.S. Simons, Extractive metallurgy of copper, nickel and cobalt, by P. Queneau, Interscience Publisher, 1961.

(12) H.W. Parsons and T.R. Ingraham, Mines Branch Information Circular IC-242, 1970.

(13) R.G. Thornhill, E. Wigstol and G. Van Weert, J. Metals, V. 23, p. 13 (1971).

(14) K.N. Subramanian, E.S. Stratigakos and P.H. Jennings, Canadian Met. Quarterly, V. 11, p. 425 (1972).

(15) G. van Weert, CIM Bulletin, V. 67, p. 97 (1974).

(16) C.M. Criss and I.W. Cobble, J. Amer. Chem. Soc., V. 86, p. 5385, 5390, 5394 (1964).

(17) R.A. Robinson and R.H. Stokes, Electrolyte Solutions, Butterworths, London, p. 340 (1955).

(18) H.C. Helgeson, J. Phy. Chem., V. 71, p. 3121 (1967).

(19) P. Duby, Paper presented at International Conference of High Temp. and High Pressure Electrochemistry in Aqueous Solution, Jan. 1973, at Univ. of Surrey, England.

(20) H.C. Helgeson, Complexing and Hydrothermal Ore Deposition, Pergamon Press, 1964.

(21) L.P. Locker and P.L. deBruyn, J. Electrochem. Soc., V. 116, p. 1659 (1969).

(22) H.A. Pohl, J. Amer. Chem. Soc., V. 76, p. 2182 (1954).

(23) L.T. Romankiw and P.L. deBruyn, Unit Process in Hydrometallurgy, edited by H.E. Wadsworth and F.R. Davis, p. 45 (1963)

(24) K. Arai, J. Japn. Institute of Metal, V. 33, p. 965 (1969).

(25) T.R. Ingraham, H.W. Parsons and L.J. Cabri, Canadian Met. Quarterly, V. 11, p. 407 (1972).

(26) A. Yazawa and M. Eguchi, Bulletin of the Research Inst. of Mineral Dressing and Metallurgy, Tohoku Univ. Sendai, Japan, V. 23, p. 147 (1967).

(27) G. Kullerud, Research in geochemistry, V. II, edited by P.H. Abelson, John Wiley and Sons, Inc., p. 286 (1967).

(28) R.A. Yund and H.T. Hall, Material Research Bulletin, V. 3, p. 779 (1968).

(29) R.G. Arnold, Econ. Geology, V. 64, p. 405 (1969).

(30) R.G. Arnold, Canadian Mineralogist, V. 9, p. 31 (1967).

(31) R.G. Arnold, Econ. Geology, V. 57, p. 72 (1962).

(32) H. Haraldsen, Zeit. Anorg. und Allgem. Chem., V. 246, p. 195 (1941).

(33) L.A. Taylor, Carnegie Inst. Washington Year Book, No. 68, p. 1650 (1970).

(34) H.T. Hall and R.A. Yund, Program of Annual Meeting of Geological Society of America, (abstract), (1966).

(35) A.H. Clark, Trans. Inst. Min. and Met. Section B, V. 75, p. 232 (1966).

(36) F. Gronvold and H. Haraldsen, Acta. Chem. Scand. V. 6, p. 1452 (1952).

(37) K. Von Gehlen, Carnegie Inst. Washington Year Book, No. 62, p. 213 (1963).

(38) R.A. Yund and H.T. Hall, Econ. Geology, V. 64, p. 420 (1969).

(39) G. Kullerud, Carnegie Inst. Washington, Year Book No. 62, p. 82 (1963).

(40) R.C. Erd, H.T. Evans and D.H. Richter, Amer. Min., V. 42, p. 309 (1957).

(41) D.T. Richard, Nature, V. 218, p. 356 (1968).

(42) B.J. Skinner, R.C. Erd and F.S. Grimaldi, Amer. Min. V. 49, p. 543 (1964).

(43) M. Graterol and A.J. Naldrett, Econ. Geology, V. 66, p. 886 (1971).

(44) K.C. Micra and M.E. Fleet, Econ. Geology, V. 68, p. 518 (1973).

(45) R.W. Shewman and L.A. Clark, Canadian J. of Earth Science, V. 7, p. 67 (1970).

(46) A.J. Naldrett, J.R. Craig and G. Kullerud, Econ. Geology, V. 62, p. 826 (1967).

(47) L.F. Hamilton and S.G. Simpson, Quantitative Chemical Analysis, The Macmillan Company.

(48) H.S. Harned and B.B. Owen, The Physical Chemistry of Electrolytic Solutions, Reinhold Book Corp. (1958).

(49) L.T. Romankiw, S.M. Thesis, MIT (1962).

(50) I.N. Putilova, S.A. Balezin and V.P. Barannick, translated by G. Ryback, Metallic Corrosion Inhibitors, Pergamon Press (1960).

(51) M.M. Jones and B.D. Oakes, Material Protection, V. 7, August, p. 38 (1968).

(52) W.J. Lorenz, Corrosion Science, V. 5, p. 121 (1965).

(53) K. Schwabe and C. Voigt, Corrosion Science, V. 8, p. 853 (1968).

(54) K. Nobe and R.J. Chin, J. of Electrochem. Soc. V. 119, p. 1457 (1972).

(55) C.S. Simons, Unit Process in Hydrometallurgy, edited by M.E. Wadsworth and F.T. Davis, p. 592 (1963).

(56) A. Seidell, Solubilities, inorganic and metal organic compounds, American Chem. Soc., p. 1154 (1958).

(57) O.L. Riggs, Jr. and R.M. Hurd, Corrosion, V. 123, p. 252 (1967).

(58) E.B. Maxed, Trans. Faraday Soc., V. 41, p. 406 (1945).

(59) D.B. Maxed, K.L. Moon and E. Overgage, Disc. Faraday Soc., No. 8, p. 135 (1950).

(60) W.H. Cone, M.M. Renfrew and H.W. Edelblute, J. Amer. Chem. Soc., V. 57, p. 1434 (1935).

(61) W.E. Ewers, Proc. Australian Inst. Min. Met., No. 241, p. 19 (1972).

(62) V.R. Evans, The corrosion and oxidation of metals, Edward Arnold Ltd., p. 819 (1960).

(63) K.J. Vetter, Electrochemical Kinetics, Academic Press, p. 698 (1967).

(64) D.A. Vermilyea, J. Electrochem. Soc., V. 113, p. 1067 (1966).

(65) H.J. Engell, Z. Phy. Chem. Neue Folge, Bd. 7, p. 158 (1956).

(66) T. Rosenqvist, J. of the Iron and Steel Institute, V. 173, p. 37 (1954).

(67) P. Toulmin and P.B. Barton, Geochimica et Cosmochimica Acta. V. 28, p. 641 (1964).

(68) K. Niwa and T. Wada, Phy. Chemistry of Process Metallurgy, Metallurgy Soc. Conf. V. 8, p. 945 (1961).

(69) S.D. Scott, A.J. Naldrett and E. Gasparrini, Econ. Geology V. 67, p. 1010 (1972).

(70) R.A. Yund and G. Kullerud, J. of Petrology, V. 7, p. 454 (1966)

(71) G. Bruhn, J. Gerlach and F. Pawlek, Z. anorg und allgem. Chemie, Bd. 337, p. 68 (1965).

(72) A.I. Vogel, A Textbook of quantitative inorganic analysis, Longmans.

(73) P.J. McGauley, U.S. Patent, 3,053,651, Patented Sept. 11, (1962).

APPENDICES

APPENDIX I

The solubility of H_2S in aqueous solution can be calculated from the thermodynamic data for the reaction:

$$H_2S \text{ (gas)} \quad = \quad H_2S \text{ (aqueous)} \qquad \text{(I-1)}$$

According to Latimer (10);

$$H_2S \text{ (gas)}; \quad \Delta H^o = -4.815, \quad \Delta F^o = -7.892$$

$$H_2S \text{ (aqueous)}; \quad \Delta H^o = -9.4, \quad \Delta F^o = -6.54 \text{ Kcal.}$$

Using these values and the van't Hoff isochore; i.e.,

$$\log K_T = -\frac{\Delta H}{2.3R} \left(\frac{1}{T} - \frac{1}{298} \right) + \log K_{298}$$

where ΔH is assumed to be constant, the equilibrium constant for (I-1) can be calculated for each temperature. The calculated values for K are,

$$K_{293} = 1.03 \times 10^{-1}, \qquad K_{298} = 1.01 \times 10^{-1}$$

$$K_{303} = 0.890 \times 10^{-1}, \qquad K_{313} = 0.706 \times 10^{-1}$$

The solubility of H_2S in HCl was measured at 20, 30 and 40°C. An HCl solution was bubbled with H_2S for at least 30 minutes, then an aliquot was taken for analysis of H_2S by the standard iodimetric method. (72) Figure I-1 shows the results for the H_2S solubility under

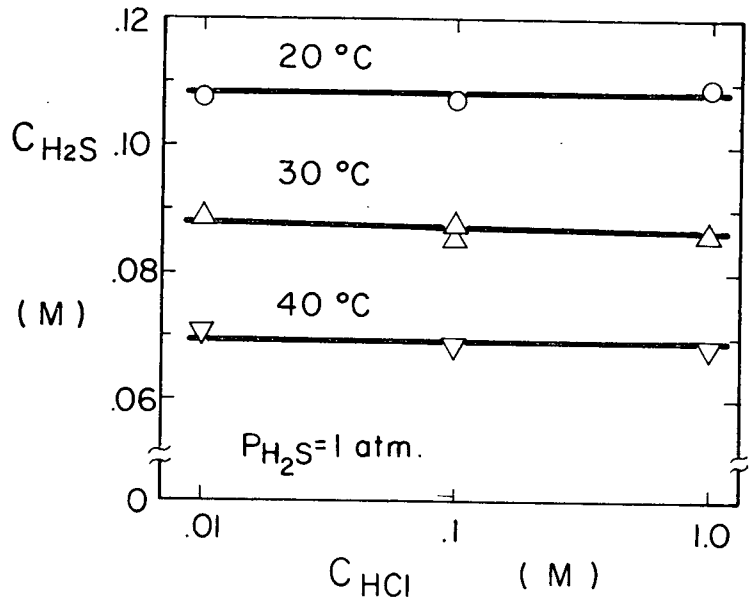

Figure I-1. Solubility of H_2S (1 atm.) in HCl at different concentrations temperatures.

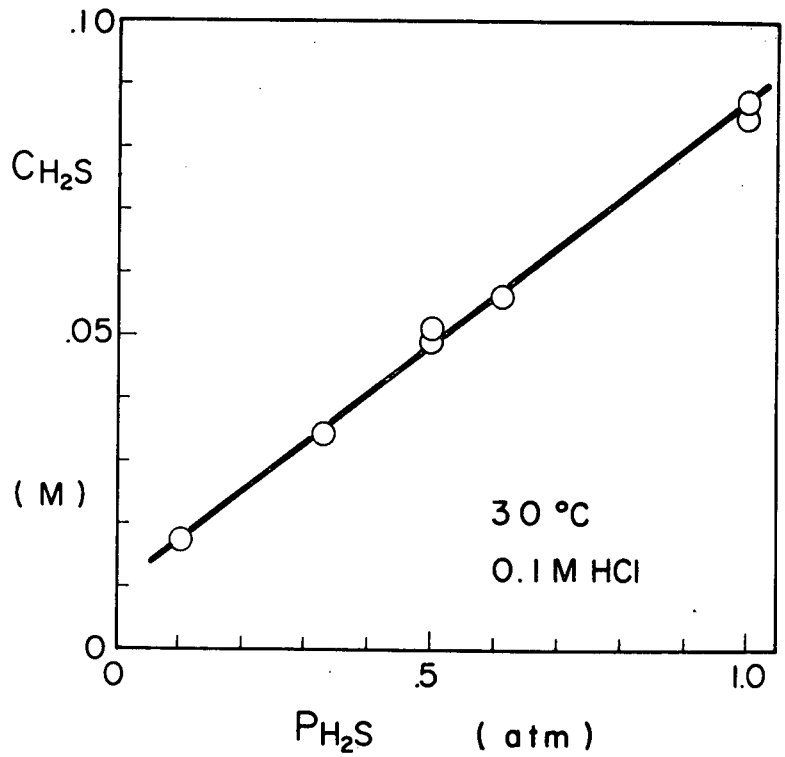

Figure I-2. Solubility of H_2S in 0.1 M HCl under different H_2S partial pressure at 30°C.

1 atmosphere pressure H_2S in HCl solution at those temperatures. The results indicate that the H_2S solubility does not change with the acid concentration in the range of 0.01 $\sim$ 1 M. The temperature dependence of the solubility is consistent with that obtained from the thermodynamic calculations.

In Figure I-2, the results on the H_2S solubility under different H_2S pressure are shown. The H_2S partial pressure was changed from 0.1 to 1 atm at 30°C by changing the fraction of H_2S in (H_2S + He) mixture. From this figure, it is evident that the H_2S solubility is directly proportional to the H_2S partial pressure in this range. The fact that the plot does not pass through the origin may be attributed to experimental error.

APPENDIX II

When we assume that the H_2S activity at the pyrrhotite surface is proportional to the surface coverage of H_2S, the Θ_{H_2S} term in equation (2.9);

$$\beta \Theta_{H_2S} = (Ro - R) / Ro$$

must have a linear relationship with aH_2S. In Figure II-1, the estimated log. aH_2S is plotted against log $\left\{ (Ro - R)/Ro \right\}$. Since Ro cannot be determined experimentally, the reaction rate under a helium atmosphere was taken as Ro. From this figure, it is evident that most of the slopes are approximately unity in the region of high values of (Ro - R)/Ro. In the low (Ro-R)/Ro region, the discrepancy can be attributed to the erroneous assumed Ro value. It can be concluded that the assumption for the linear relationship between aH_2S and ΘH_2S is reasonable in the experimental range.

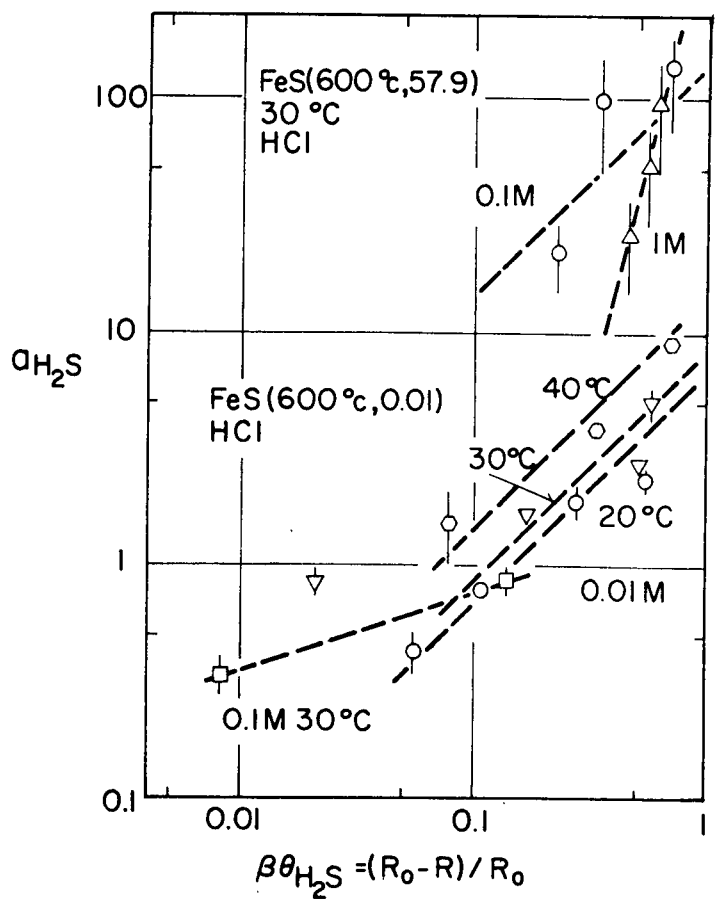

Figure II-1. Relation between log. aH_2S and log. (Ro-R)/Ro.

APPENDIX III

All binary sulphides treated by H_2S/H_2 mixtures have been subjected to sufficiently long residence times so that it is believed that they conform to the approximate compositions indicated by the data by T. Rosenqvist (66).

PH_2S/PH_2 at 600°C	Wt % S in $Fe_{1-x}S$	Wt % S in Ni sulphides
10^{-3}	$\approx$ 36.8	$\approx$ 24
10^{-2}	$\approx$ 37.2	$\approx$ 26
10^{-1}	$\approx$ 37.7	$\approx$ 28
1	$\approx$ 38	$\approx$ 35.5
10	$\approx$ 38.8	$\approx$ 36
57.9	$\approx$ 40	$\approx$ 37